The background of the cover is a high-resolution aerial photograph of a tropical forest. The forest is mostly green, but there are several large, irregular black rectangular areas scattered across the landscape, representing deforested regions. The text is overlaid on a dark grey rectangular background in the upper half of the image.

Assessing land use following tropical deforestation:

combining remote sensing and deep learning

Robert N. Masolele

Propositions

1. Land-use map generation requires more focus on improving annotated reference data than on creating new models.
(this thesis)
2. Earth observation will be the key data source for policies aimed at reducing commodity-driven deforestation.
(this thesis)
3. Heritage of colonial education is a barrier to the progress of science in Africa.
4. Data sources demanding personal information are not open-access.
5. Conflict between progressive and conservative ideas is an obstacle to climate change mitigation efforts.
6. Academic research is lagging behind industry research.
7. Derogatory expressions towards African countries have a negative impact on the development of children of African ascent.

Propositions belonging to the thesis, entitled

Assessing land use following tropical deforestation: combining remote sensing and deep learning.

Robert N. Masolele

Wageningen, 5 April 2023

**Assessing land use following tropical
deforestation:
combining remote sensing and deep
learning**

Robert N. Masolele

Thesis committee

Promotor

Prof. Dr M. Herold
Professor of Geo-information Science and Remote Sensing
Wageningen University & Research

Co-promotors

Dr V. De Sy
Assistant Professor of Geo-information Science and Remote Sensing
Wageningen University & Research

Dr D. Marcos
Junior Professor
Inria, University of Montpellier, France

Other members:

Prof.dr. R (Ricardo) da Silva Torres, Wageningen University and Research
Dr. Steffen Fritz, International Institute for Applied Systems Analysis, Austria
Dr. Alexandra (Sasha) Tyukavina, University of Maryland, United States of America
Dr. Sarah Carter, World Resources Institute Europe, The Netherlands

This research was conducted under the auspices of the C.T. de Wit Graduate School of Production Ecology & Resource Conservation (PE&RC)

Assessing land use following tropical deforestation: combining remote sensing and deep learning

Robert N. Masolele

Thesis

submitted in fulfilment of the requirements for the degree of doctor
at Wageningen University

by the authority of the Rector Magnificus

Prof. Dr A.P.J. Mol,

in the presence of the

Thesis Committee appointed by the Academic Board

to be defended in public

on Wednesday 5 April 2023

at 4 p.m. in the Omnia Auditorium.

Robert N. Masolele

Assessing land use following tropical deforestation:
combining remote sensing and deep learning

170 pages.

PhD thesis, Wageningen University, Wageningen, the Netherlands (2023)
With references, with summaries in English

ISBN 978-94-6447-539-5

DOI <https://doi.org/10.18174/583842>

For Hellen, Hendrick, Hollie, and Janeth

Summary

Forests are home to a vast variety species of plants and animals. They provide these species with vital ecosystem services such as fresh air, food, nutrients, and shade, essential for survival. They also help moderate the flow of freshwater and influence precipitation patterns on which humans depend for agriculture. Forests are also fundamental for removing carbon from the atmosphere through photosynthesis, and clearing them can also result in the emission of large amounts of carbon into the atmosphere. Thus, the protection and management of these forests are critical to maintaining a continual flow of these ecosystem services and supporting life on Earth.

However, over the centuries, forests have been facing threats from human activities. About 50% of the Earth's land was covered with forests a thousand decades ago, half of which have since been cleared. Today, less than 33% of the remaining forests are still intact, mostly due to deforestation and degradation. Despite the world's government's commitment to reduce or end forest loss, the trend is still increasing, specifically in the tropics, which holds 45% of the existing forest and nearly 50% of the Earth's biodiversity. The conversion of forests for food crops, commodity crops, mining, charcoal, and the need for building materials has been identified as the main leading driver of forest loss. A growing world population and increasing demand for agricultural products, especially those of commodity crops, are expected to increase demand for agricultural land and put additional pressure on forests, while changing climate patterns will aggravate this by affecting food production. Several actions, including improving farming practices (e.g. intensification), and buying only sustainable agricultural products, have been proposed to reduce pressure on forests. However, before any action is taken, the assessment of the origin, location and extent of forest loss and what drives it need to be identified.

One approach identified by the IPCC to estimate emissions from deforestation and forest degradation is through an estimate of activity data or areas of deforestation and degradation. The estimates of activity data are derived either from (1) the total area of forest loss without taking into account conversion of forest to other land uses, (2) identifying land-use after deforestation without taking into account their spatial information, (3) using spatially explicit information of land-use conversion obtained through sample-based or wall-to-wall mapping techniques. The approach (3), which requires the assessment of land use activities

related to forest change, is useful for countries to monitor and reduce their greenhouse gas (GHG) emissions from forest conversion. Specifically, to help track their location, extent, and trend, link emissions to specific land-uses, to plan and implement mitigation actions and assess their impact at the country level.

Recently, the European Union (EU) introduced a regulation with the objective of minimizing the consumption of products/commodity crops coming from supply chains associated with deforestation and forest degradation. This regulation is complemented by other measures such as (1) working with producer countries to help curb deforestation and promote sustainable forest management and (2) cooperation between consumer countries to minimize loopholes for products coming from a supply chain associated with deforestation and forest degradation entering the EU market. The success of these measures and regulations requires the availability of data and transparency for both parties in the supply chain of commodity crops. A particular focus should be put on companies sourcing commodity crops (for example, cacao, coffee, cashew, oil palm, rubber etc.) from deforestation hotspots.

Some of the world's largest companies have pledged to zero-deforestation (ZDCs) to eliminate deforestation from their supply chain by buying commodity crops only from sustainable producers. However, one important challenge is to figure out exactly the origin of the commodity crops by linking the users, suppliers, and farmers. Understanding the origin and type of the commodity crops in the supply chain is essential for assessing land-use associated with deforestation and is at the core of the entire EU regulatory process and zero-deforestation commitments by companies. Remote sensing, field surveys, and deep learning (DL) techniques are considered essential observation and analysis tools in monitoring and identifying land-use, land-use change activities associated with commodity crops in forest areas, in particular those that are linked to deforestation and forest degradation.

Thus, the objective of this thesis is to assess land use activities related to forest change using freely available remote sensing imagery and deep learning. This work contributes toward developing and applying novel methods for assessing land use after deforestation for different countries and regions to support their nationally determined contributions (NDCs), implementation strategies, and national targeting of mitigation activities.

In order to accomplish the above objective, three research questions are addressed in this thesis: (1) How can we use deep learning for assessing land-use following deforestation using remote sensing data? (2) How can these methods be applied to analyse land-use following deforestation in different national/regional context? (3) How can we leverage heterogeneous reference data to increase the thematic detail of land-use following deforestation mapping?

The thesis comprises four main chapters, each addressing one or more of the research questions presented above.

Chapter 2 focuses on developing and testing a reproducible method to assess land-use, moving beyond land-cover, using deep learning and open-source satellite images. In addition, in this chapter the performance of different spatial-temporal deep learning models at continental and pan-tropical scale are assessed to study the models performance variability in space and time. The developed methods provide an opportunity for frequent, consistent, and transparent monitoring and reporting of trends of forest resources by countries to provide spatial-temporal explicit information on the location and extent of direct drivers of forest loss.

Chapter 3 presents the development and application of deep learning method and high-resolution remote sensing data for automated wall-to-wall mapping of land use following deforestation in Ethiopia at national scale and in high thematic detail. The wall-to-wall mapping is essential to identify the key hotspots, spatial distribution, and variation of follow-up land use at a national scale. In addition, in this chapter, the relative performance of different satellite image modalities are assessed to study the effects of different satellite resolutions for land-use mapping in space and time.

Chapter 4 capitalised on newly developed deep learning method (Chapter 3) to map and assess land-use patterns after deforestation and regrowth in protected forests of Ivory Coast.

Chapter 5 leverages heterogeneous land-use data, newly available high-resolution satellite images, active learning, and a deep learning model (Chapters 3 and 4) to upscale the classification of land use following deforestation (wall-to-wall mapping) in Africa. This chapter presents land-use mapping with high spatial, temporal and thematic detail on a large scale.

Chapter 6 presents the main findings of this thesis and discusses the results with respect to the research questions. Chapter 6 further discusses the implication of these results and provides an outlook on the use of deep learning methods for assessing direct drivers of forest change, and the potential for use by countries in their forest monitoring systems.

In general, the research conducted in this thesis contributes to large-scale forest and land-use change monitoring in the context of REDD+, the global stocktake for the Paris Agreement, and the Sustainable Development Goals. This study is also useful for companies that want to measure their commitment to forest conservation initiatives to meet the climate action and net zero goals initiatives in a more transparent approach, in particular measuring the sustainability of these companies in their supply chain. In addition, this thesis's output information/maps can support further analysis of indirect drivers, policy formulation, and evaluation.

Contents

	Page
Summary	vii
Contents	xi
Chapter 1 Introduction	3
Chapter 2 Spatial and temporal deep learning methods for deriving land-use following deforestation: A pan-tropical case study using Landsat time series	13
Chapter 3 Using High-Resolution Imagery and Deep Learning to Classify Land-Use Following Deforestation: A Case Study in Ethiopia	45
Chapter 4 Deforestation, follow up land use and regrowth dynamics in Cote D'ivoire 2000-2019	77
Chapter 5 Mapping the diversity of land uses following deforestation across Africa	93
Chapter 6 Synthesis	117
Acknowledgements	151
About the author	153
PE&RC Training and Education Statement	155

CHAPTER 1



Introduction

1.1 Background

1.1.1 The importance of forests

Forests are home to diverse species of plants and animals. They provide these species with vital ecosystem services such as fresh air, food, nutrients, and shade essential for survival. They also help moderate the flow of freshwater and influence precipitation patterns on which humans depend for agriculture (FAO, 2014; IPCC, 2021; Koh et al., 2021). Forests are also essential in removing carbon from the atmosphere through the process of photosynthesis but can also emit carbon into the atmosphere when cleared. Thus, the protection and management of these forests are critical to maintaining a continual flow of these ecosystem services and supporting life on earth (IPCC, 2021).

However, over the centuries, forests have been facing threats from human activities. About 50% of the forests that covered half of the earth's land a thousand decades ago have since been cleared. Today, less than 33% of the remaining forests are still intact, mostly due to deforestation and degradation (Global Forest Review, 2022). Despite the world's government's commitment to reduce or end forest loss, the trend is still increasing, specifically in the pan-tropics, which holds 45% of the existing forest (FAO, 2020) and nearly 50% of the earth's biodiversity. The conversion of forests for food crops, commodity crops, mining, charcoal, and the need for building materials has been identified as the main leading driver of forest loss (Curtis et al., 2018; De Sy et al., 2019; FAO, 2020; Tyukavina et al., 2018). A growing world population and increasing demand for agricultural products, especially those of animal origin, are expected to increase demand for agricultural land and put additional pressure on forests while changing climate patterns will affect food production (Carter et al., 2017). Several actions, including improving farming practices(intensification), and buying only sustainable agricultural products, have been proposed to reduce pressure on forests. However, before any action is taken, the assessment of the origin/location and extent of forest loss and what's driving forest loss need to be identified (Bager and Lambin, 2022; Hansen et al., 2013; Hosonuma et al., 2012; Moran et al., 2020; World Resources Institute, 2016).

1.1.2 The need for assessing land use following deforestation

Human-related land-use conversions are the largest driver of forest loss and greenhouse gas (GHG) emissions, so their assessment is of importance for reducing emissions from deforestation and forest degradation (REDD+) (IPCC, 2013; IPCC, 2021). In part, 24% of global greenhouse gas emissions come from land use conversion for cultivation, livestock, and deforestation (FAO & JRC, 2012a). This situation is exacerbated by increasing demand for food crops, and commodity crops. In an effort to reduce carbon emissions, the United Nations Framework Convention on Climate Change (UNFCCC) established a framework to reduce emissions from deforestation and forest degradation and enhance

carbon stocks (REDD+). The framework aims to provide result-based payments for reduced emissions to developing countries (De Sy, 2016). However, countries are required to show that emissions were reduced before payments are made by developing a Measuring, Reporting, and Verification system (MRV) that follows key principles of the UNFCCC such as transparency, consistency, comparability, completeness, and accuracy (IPCC, 2013; UNFCCC, 2018), and abide by the international Good Practice Guidelines (GPG) set by the intergovernmental Panel on Climate Change (IPCC) (Grassi et al., 2008; UNFCCC, 2009b; (GOFC-GOLD, 2016)).

One approach identified by the IPCC to estimate emissions from deforestation and forest degradation is through an estimate of activity data or areas of deforestation and degradation (GOFC-GOLD, 2016). The estimates of activity data are derived either from (1) the total area of forest loss without taking into account conversion of forest to other land uses, (2) identifying land-use after deforestation without taking into account their spatial information, (3) use of spatial-explicit information of land-use conversion obtained through sample-based or wall-to-wall mapping techniques (GOFC-GOLD, 2016; Tyukavina et al., 2018). The approach (3) assessment of land use activities related to forest change is useful for countries to monitor and reduce their greenhouse gas (GHG) emissions from forest conversion (Hosonuma et al., 2012). Specifically, to help track their location, extent, and trend, link emissions to specific land-uses, to plan and implement mitigation actions and assess their impact at the country level (Hosonuma et al., 2012).

Besides the above REDD+, UNFCCC and IPCC initiatives for reducing emissions from deforestation and forest degradation. The European Union (EU) has also recently introduced a regulation with the objective of minimizing the consumption of products/commodity crops coming from supply chains associated with deforestation and forest degradation (EUROPEAN COMMISSION, 2022). This regulation is complemented by other measures such as (1) working with producer countries to help curb deforestation and promote sustainable forest management and (2) cooperation between consumer countries to minimize loopholes for products coming from the supply chain associated with deforestation and forest degradation entering the EU market. The success of these measures and regulations requires transparency for both parties in the supply chain of commodity crops (Lambin et al., 2018). Specifically, companies sourcing commodity crops (for example, cacao, coffee, cashew, oil palm, rubber e.tc.) from deforestation hotspots (Bager and Lambin, 2022).

Just, recently some of the world's largest companies have pledged to zero-deforestation (ZDCs) to eliminate deforestation from their supply chain by buying commodity crops only from sustainable producers (Bager and Lambin, 2022). However, one important challenge is to figure out exactly the origin of the commodity crops by linking the users, suppliers, and farmers (Bager and Lambin, 2022; Moran et al., 2020). Understanding the origin of the commodity crops in the supply chain is essential for assessing land-use associated with deforestation and is at the core of the entire EU regulatory process and zero-deforestation

commitments by companies (Bager and Lambin, 2022; EUROPEAN COMMISSION, 2022). Remote sensing, field surveys, and deep learning (DL) techniques are considered essential observation and analysis tools in monitoring and identifying land-use, land-use change activities associated with commodity crops in forest areas, in particular those that are linked to deforestation and forest degradation (GOFC-GOLD, 2016; Hosonuma et al., 2012; Moran et al., 2020; Tyukavina et al., 2018).

1.1.3 Use of remote sensing data to assess land-use following deforestation

Conventionally the task of identifying land-use following deforestation is based on field surveys, which are valuable but expensive and unrealistic to do at a large-scale. Satellite data or earth observation systems provide an opportunity to monitor the earth using spectral, spatial, and temporal information over a local to global scale. Contrary to the ground-based survey, satellite observation systems have the potential to monitor the earth at all places and more frequently. The latest advances and investments in earth observation programmes (EOP) for global environmental data acquisitions, such as the European Copernicus Earth Observation programme (Sentinel-1, Sentinel-2A, -2B) and joint NASA and U.S. Geological Survey programme (Landsat -1, 2, 3, 4, 5, 7, 8,9), have allowed the assessment of global forest cover change (Hansen et al., 2013; Reiche et al., 2021), classification of land cover (Balzter et al., 2015; Cole et al., 2018; Helber et al., 2017), and the analysis of time series of satellite data to study changes on the land surface (Arévalo et al., 2019; Kennedy et al., 2010; Pandey et al., 2018; Verbesselt et al., 2010a). The EOP's are accompanied by free data policies for data retrieval and use (i.e. Landsat, MODIS, Sentinel). The big data archives of EOP provide an opportunity to advance science in monitoring follow-up land use essential for reducing emissions from forest conversion (Boriah, 2010). On top of that, the increase in the spatial-temporal resolution of EO data enables the detection and follow-up of smaller and more subtle changes on the land surface with greater accuracy (Zhang et al., 2019). Yet, despite the increase in the availability of remote sensing data, information on land-use following deforestation is still limited. This is due to the fact that the identification of land use following deforestation on remote sensing images is made using visual interpretation over sample areas (Tyukavina et al., 2018), making it challenging to do it at scale and more frequent. The recent advance in deep learning (DL) and machine learning (ML) algorithms provide an opportunity for automated assessment of land use following deforestation more frequently and at a scale useful for decision-making and mitigation action (Moran et al., 2020).

1.1.4 Opportunities for mapping land-use following deforestation

As mentioned above, traditionally remote sensing images have been used to identify land-use following deforestation using human visual interpretation (De Sy et al., 2019; Fritz

et al., 2022; Fritz et al., 2017; Tyukavina et al., 2018). This is a valuable work, but it is intensive and requires a substantial investment of human resources to get the work done. It is slow for larger area applications and prone to human errors; for example- two experts might assign different labels of land use for the same location. The recent advance in deep learning methods provides an opportunity to complement visual interpretation for automated identification and mapping of the land use following deforestation and have become state-of-the-art in many tasks in fields such as computer vision, language, and signal processing (Lecun et al., 2015; Luus et al., 2015; Marmanis et al., 2016; Neagoe et al., 2012). The Deep learning algorithms are designed to reason based on the input data, in this case, remote sensing data. The algorithm can recognise the pattern on the data and compute the probability of part of the image data pattern belonging to a certain group of land use with a degree of certainty (Reichstein et al., 2019). This is similar to how the human brain works; we always give probability when assigning classes to certain objects, knowingly or unknowingly.

Deep learning (DL) aims to achieve the (same) identification of land-use following deforestation by automatic satellite image understanding as in human vision but much faster. Therefore it is essential the DL algorithms understand the indistinguishable spatial and/or temporal patterns of each type of land-uses and their relation to each other. To test this, the methods have been used to scale some visually interpreted samples up to large regions by interpolating to unobserved areas based on satellite imagery (Curtis et al., 2018; Descals et al., 2021a; Hansen et al., 2013; Irvin et al., 2020; Tracewski et al., 2017; Zhu et al., 2017). This can be done in cases where the relationship between the input data and the output is not too complex, such as using multi-spectral Sentinel, or Landsat imagery, with a moderate resolution of 10, 30 meters, to classify pixels into simple land-use classes, such as agriculture, natural forest, and build-up areas. However, this is not always the case; at such resolution, one pixel often contains the mixed spectral responses of multiple land-use features, with the effects of shadows, occlusions, and geometrical configurations averaged out. This invariance of the data to spatial and geometric details is not helpful when the aim is to classify into those land-use classes that are highly correlated with the spectral response.

Specifically, when dealing with more complex land-use classes such as tree crops (coffee, cashew, cacao, e.t.c), settlements, roads, and pastures, higher-resolution images are required. This is due to its richness in spatial resolution. The richness of spatial details of land-use in high-resolution images helps the deep-learning models highlight unique patterns that are essential for the classification task (Zhu et al., 2017). The unique patterns are enhanced by analyzing the geometry of the features and in relation to neighboring pixels. This is similar to how humans perform tasks. For instance, we might not be sure whether the land-use is large-scale cropland or not, but the presence of roads, irrigation infrastructure, size of the farm, and probably also the homogeneity of a crop, can help us with that decision. Depending on our experience, we might go a step further and infer

a crop type that it is a maize or wheat, or rice farm. Similarly, deep learning models apply the same principle by harnessing detailed spatial information from high-resolution images to generate features and analyze patterns before assigning a land-use label to an image (Reichstein et al., 2019). Thus the advance in deep learning algorithms and the recent availability of high spatial resolution images provide an opportunity to complement human visual interpretation by tracking land-use following deforestation in data-scarce regions, more frequently and on a large scale which otherwise would be difficult and expensive.

1.1.5 Use of deep learning for large-scale land-use mapping

Deep learning models are used to map land cover and land use with high accuracy, nonetheless at a small scale (Zhu et al., 2017). The high computational requirement, storage, and high requirement of training data hamper its application for larger scale mapping of follow-up land use (Reichstein et al., 2019). However, the emergence of open-source cloud-based computing, and storage, provides a huge potential in using even higher spatial-temporal resolution remote sensing data and deep learning algorithms to map land uses at different scales (local, national, regional, or global) (FAO, 2021). Harnessing the power of cloud computing technology to highly accurately detect and map the spatial and temporal distribution of land use following deforestation using open source tools is vital for the success of forest monitoring activities from country to global scale.

In this thesis, the focus is on the task of classifying direct drivers of deforestation or land-use following deforestation using deep learning (see Section 2 to Section 5), which consists of assigning a land-use class label to each pixel (location) in the satellite image, producing a land-use class map as a result. In the computer vision field, this task is often referred to as semantic segmentation.

1.2 Research Gaps

Existing assessment of land-use following deforestation are often rather generic and at coarse levels (Curtis et al., 2018) and does not fully differentiate land-use from land-cover. Land-use is much harder to assess with remote sensing. The assessment of land-use mostly relies on visual interpretation (Tyukavina et al., 2018). However, assessing land-use with the visual interpretation of high-resolution imagery is labor-intensive and time-consuming. We go a step further from existing studies that use visual interpretation to identify land-use following deforestation by showing that novel methods like deep learning methods are able to give satisfactory results, and can complement visual interpretation.

In particular, reducing the amount of time and resources invested in identifying land-use which would be advantageous, at this time when there is an ever-increasing demand for land-use data to be included in national estimates of deforestation-related emissions (BioCarbon

Fund, 2020; Curtis et al., 2018; De Sy et al., 2019; FAO, 2010; IPCC, 2021; UNFCCC, 2018), and in assessing companies commitment in eliminating deforestation in their supply chain (ZDCs) (Bager and Lambin, 2022; Lambin et al., 2018).

The use of satellite imagery offers promising potential to classify land-use following deforestation (De Sy et al., 2019; Hosonuma et al., 2012; Moran et al., 2020; Tyukavina et al., 2018) . However, for frequent, large-area applications, it is expensive and unrealistic to do through purely visual interpretation; specifically when the problem at hand has more thematic detail. Deep learning (DL) methods provide an answer to this challenge: they can process large amounts of data while extracting different patterns useful for solving complex tasks like detecting land-use following deforestation (Lecun et al., 2015; Marmanis et al., 2016; Tracewski et al., 2017). Unfortunately, in spite of its potential, currently, deep learning methods are used mostly to solve small-scale computer vision problems (Yuan et al., 2020; Zhu et al., 2017). Rarely have they been used to identify land use following deforestation; let alone on large-scale and complex forest landscapes (Reichstein et al., 2019). The current, spatial-explicit information on land-use changes is still coarse either in thematic, temporal, and/or spatial detail (Pendrill et al., 2022).

1.3 Research objectives

The objective of this thesis is to assess land use activities related to forest change using freely available remote sensing imagery and deep learning. This work contributes toward developing and applying novel methods for assessing land use after deforestation for different countries and regions to support their nationally determined contributions (NDCs), implementation strategies, and national targeting of mitigation activities.

In order to accomplish the above objective, three research questions are addressed in this thesis:

- A. How can we use deep learning for assessing land-use following deforestation using remote sensing data?
- B. How can these methods be applied to analyse land-use following deforestation in different national/regional context?
- C. How can we leverage heterogeneous reference data to increase the thematic detail of land-use following deforestation mapping?

1.4 Thesis outline

This thesis consists of four main chapters, each addressing one or more of the research questions presented in Section 1.3.

Chapter 2 focuses on developing and testing the reproducible method to assess land-use as opposed to land-cover using deep learning and open-source satellite images. In addition, in this chapter the performance of different spatial-temporal deep learning models at continental and pan-tropical scale are assessed to study the models performance variability in space and time. The developed methods provide an opportunity for frequent, consistent, and transparent monitoring and reporting of trends of forest resources by countries to provide spatial-temporal explicit information on the location and extent of direct drivers of forest loss.

Chapter 3 presents the development and application of deep learning method and high-resolution remote sensing data for automated wall-to-wall mapping of land use following deforestation in Ethiopia at national scale and in more thematic detail. The wall-to-wall mapping is essential to identify the key hotspots, spatial distribution, and variation of follow-up land use at a national scale. In addition, in this chapter the relative performance of different satellite image modalities are assessed to study the effects of different satellite resolutions for land-use mapping in space and time.

Chapter 4 capitalised on newly developed deep learning method (Chapter 3) to map and assess land-use patterns after deforestation and regrowth in protected forests of Ivory Coast.

Chapter 5 leverages heterogeneous land-use data, high resolution satellite images, active learning and deep learning model (Chapter 3 and 4) to upscale the classification of land use following deforestation (wall-to-wall mapping) in Africa. This chapter presents land-use mapping with more spatial, temporal and thematic detail on a large scale.

Chapter 6 presents the main findings of this thesis and discusses the results with respect to the research questions. Chapter 6 further discusses the implication of these results and provides an outlook on the use of deep learning methods for assessing direct drivers of forest change, and the potential for use by countries in their forest monitoring systems.

CHAPTER 2



Spatial and temporal deep learning methods for deriving land-use following deforestation: A pan-tropical case study using Landsat time series

This chapter is based on:

R. N. Masolele, V. De Sy, M. Herold, D. Marcos Gonzalez, J. Verbesselt, F. Gieseke, A. G. Mullissa, and C. Martius (2021). "Spatial and temporal deep learning methods for deriving land-use following deforestation: A pan-tropical case study using Landsat time series".

Remote Sensing of Environment 264, 112600.

Abstract

Assessing land-use following deforestation is vital for reducing emissions from deforestation and forest degradation. In this paper, for the first time, we assess the potential of spatial, temporal and spatio-temporal deep learning methods for large-scale classification of land-use following tropical deforestation using dense satellite time series over six years on the pan-tropical scale (incl. Latin America, Africa, and Asia). Based on an extensive reference database of six forest to land-use conversion types, we find that the spatio-temporal models achieved a substantially higher F1-score accuracies than models that account only for spatial or temporal patterns. Although all models performed better when the scope of the problem was limited to a single continent, the spatial models were more competitive than the temporal ones in this setting. These results suggest that the spatial patterns of land-use within a continent share more commonalities than the temporal patterns and the spatial patterns across continents. This work explores the feasibility of extending and complementing previous efforts for characterizing follow-up land-use after deforestation at a small-scale via human visual interpretation of high resolution RGB imagery. It supports the usage of fast and automated large-scale land-use classification and showcases the value of deep learning methods combined with spatio-temporal satellite data to effectively address the complex tasks of identifying land-use following deforestation in a scalable and cost effective manner.

2.1 Introduction

Land-use change is the second-largest contributor to greenhouse gas (GHG) emissions globally (IPCC, 2013), and in total, 24% of global greenhouse gas emissions come from deforestation activities (FAO, 2014). In response, the United Nations Framework Convention on Climate Change (UNFCCC) established a framework to reduce emissions from deforestation and forest degradation and enhance carbon stocks (REDD+) by result-based payments (UNFCCC, 2017). Before payments are made countries are required to show that emissions were reduced through a clear methodological and well-documented Measuring, Reporting, and Verification system (MRV) (IPCC, 2013; UNFCCC, 2018). A robust deforestation monitoring system can also support more informative and effective land-use policies and measures (UNFCCC, 2018) by monitoring what land-use activities drive deforestation. These land-use activities, *i.e.*, proximate or direct drivers of deforestation (Geist and Lambin, 2001), can be assessed using Earth Observation Technologies (EOT) to help provide spatially explicit and temporal information on land-use (Curtis et al., 2018; De Sy et al., 2019; De Sy et al., 2015). However, these studies detect land-use following deforestation at coarse thematic, spatial and temporal scales or use time-consuming methods (*i.e.*, visual interpretation of satellite imagery) which makes these approaches less suited for national level operational monitoring. Recent advances in Earth Observation (EO), computing technology and deep learning methods provide opportunities for automated large-scale assessment of land-use following tropical deforestation at more detailed spatial and temporal scales.

The latest advances and investments in Earth Observation Programmes (EOP) for global environmental data acquisitions, such as the European Copernicus EOP (Sentinel-1, Sentinel-2A, -2B) and joint NASA and U.S. Geological Survey program (Landsat 1-5, 7 & 8), have allowed the assessment of global forest cover change (Hansen et al., 2010a; Kim, 2010), classification of land cover (Balzter et al., 2015; Cole et al., 2018), and the analysis of time series of satellite data to study changes on the land surface (Arévalo et al., 2019; Pandey et al., 2018; Verbesselt et al., 2010a). The EOP's are accompanied by free data policies for data retrieval and use (*i.e.*, Landsat, MODIS, Sentinel). The EOP provides an opportunity to advance science in monitoring land-use essential for REDD+ (Boriah, 2010). On top of that, the increase in the spatio-temporal resolution of EO data enables the detection and classification of smaller and more subtle changes on the land surface with greater accuracy (Zhang et al., 2019).

Traditional land-use classification approaches with remote sensing images use the standard supervised/unsupervised machine learning methods such as K nearest neighbors, maximum likelihood estimators, support vector machines, or random forests. This is a mono-temporal approach exploiting the spectral aspect of land-use data (Curtis et al., 2018; Hansen et al., 2010a; Nguyen et al., 2018; Silva et al., 2018). However, these methods are not designed to work with time-series data nor with pattern recognition of land-use (Arévalo et al., 2019;

Comber et al., 2016; Curtis et al., 2018; Huang et al., 2018; Mas et al., 2017; Pelletier et al., 2019) and, therefore, ignore the temporal and spatial dependency which are essential in retaining information to differentiate land-uses (Castilla and Hay, 2007; Curtis et al., 2018; Pelletier et al., 2019).

Recently there have been advances in computing technology, cloud computing, and high-performance computing paralleled with those in advanced artificial intelligence (machine learning and, particularly, deep learning) algorithms (Helber et al., 2017; Lecun et al., 2015; Luus et al., 2015; Marmanis et al., 2016; Neagoe et al., 2012; Tracewski et al., 2017). Deep learning enables the automatic detection of complex spatial and temporal patterns in environmental data such as time series of satellite images based on training data (Hughes et al., 2018; Kit and Lüdeke, 2013; Minh et al., 2018; Pelletier et al., 2019). In contrast to the traditional focus on spectral information in remote sensing imagery, the ability to capture spatial-temporal patterns allows the detection and differentiation of types of land cover and land-use with closely resembling spectral signatures (Comber et al., 2016). Despite the success of machine learning and deep learning (Castelluccio et al., 2015; Rußwurm and Körner, 2018; Zhang et al., 2019; Zhu et al., 2017) in extracting spectral, spatial, and temporal features from remote sensing data, the methods are not widely used for large-scale remote sensing analyses. However, promising results have been reported on small-scale problem applications for satellite image classification, land-cover/land-use mapping and land cover/land-use change detection (Castelluccio et al., 2015; Helber et al., 2017; Interdonato et al., 2018; Kong et al., 2018; Liu et al., 2016; Song et al., 2018; Uba, 2016). Additional challenges arise when extrapolating results to a large-scale, as models trained on small areas and evaluated over large areas will often not perform satisfactorily (Kellenberger et al., 2018; Yuan et al., 2020; Zhu et al., 2017).

Furthermore, the assessment of land-use is often rather generic and at coarse levels (Curtis et al., 2018; Hansen et al., 2010b), and does not fully differentiate land-use from land-cover (Bp et al., 2015; Campbell et al., 2005; Fritz et al., 2017; Mas et al., 2017; Zhao et al., 2012). The lack of land-use/cover differentiation generates confusion when forest cover change statistics derived from satellite imagery are compared directly against land-use statistics reported by governments in their national statistics (Curtis et al., 2018). In fact, they are used interchangeably in many land-cover/use maps. However, land-use describes how the land is used in a given location, such as forestry, residential, agricultural, industrial, forestry, and recreational, while land-cover refers to what is physically on the earth surface such as forests, grasslands, or water (Castilla and Hay, 2007). In other words, land-use can contain multiple land-covers (Fritz et al., 2017; Herold et al., 2003). Identifying land-use with remote sensing is challenging (IPCC, 2013) because we measure vegetation indices (VI) for land-cover and greenness and not directly use (Asselen and Verburg, 2012; Hansen et al., 2010b; Mas et al., 2017; Nguyen et al., 2018; Verbesselt et al., 2010b; Vogelmann et al., 2012). The assessment of land-use can be done via visual interpretation, but this is subjective and time-consuming.

In addition, land-use assessment approaches over regional or global scales are still problematic because they do not capture spatial heterogeneity (Curtis et al., 2018; FAO & JRC, 2012b; Hansen et al., 2010b; Pandey et al., 2018; Pelletier et al., 2019). Here, the spatial heterogeneity refers to the variation in the patterns of land-use classes in spatial, spectral and spatial domains within and between regions. The heterogeneity of land-use may be observed as both the intra-regional variability (*e.g.*, diverse patterns of same land-use, *i.e.* small-scale agricultural practice within the country) and the inter-regional variability (*e.g.*, diverse patterns of same land-use *i.e.* small-scale agricultural practice, between the countries or regions) as observed in Figure 2.1. In land-use classification, this heterogeneity of land-use patterns can result in the inability of the training data to represent the diversity of each class of the land-use. Not taking into account spatial heterogeneity introduces uncertainties and sources of error when evaluating the methods over different geographical locations, even if they present similar land-use. This results in an increase in uncertainty of the accuracy of land-use maps to estimate and measure the national forest emission reductions contributions for REDD+ (World Resources Institute, 2016). The critical question is whether integrating spatial-temporal information of land-use can achieve a reproducible large-scale land-use classification based on the diverse geographically sampled data as opposed to traditional approaches, where the sampled data are either relatively small (Olofsson et al., 2012), sampled in a non systematic way (Descals et al., 2021a; Fritz et al., 2017; Pengra et al., 2015), sampled from a one time step (Fritz et al., 2017; Irvin et al., 2020), contain relatively few land-use classes (Descals et al., 2021a; Irvin et al., 2020) or are sampled from small regions (Doggart et al., 2020; Irvin et al., 2020).

While recent advances in EOT, computing technology and deep learning methods hold promise for large-scale assessment of land-use following deforestation, or Follow-up Land-use (FLU), in the tropics, there is a need for new approaches that integrate the spatio-temporal information in dense satellite time series with deep learning methods. In this work, we therefore assess the potential of several deep learning methods for identifying FLU in the tropics using dense satellite time series. Specifically, the following two objectives are addressed:

1. We assess the performance of multiple deep learning approaches on a held out test dataset for classifying FLU after tropical deforestation using the spatial and temporal information from dense time series of satellite imagery.
2. We use the same procedure to assess the classification performance of continental models versus a pan-tropical model.

2.2 Method and materials

The study focuses in the tropical regions of Latin America, Africa, and Asia (Figure 2.2). The heterogeneity of land-use following deforestation or follow-up land-use (FLU) on

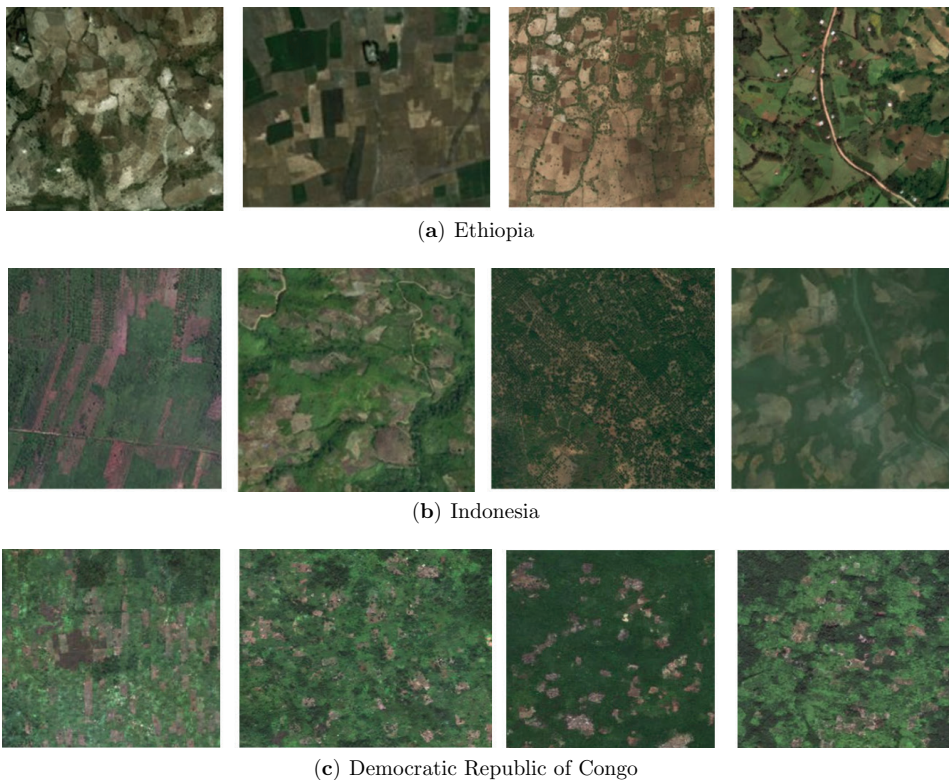


Figure 2.1: Spatial heterogeneity of small-scale cropland land-use pattern within and between countries of (a) Ethiopia, (b) Indonesia and (c) the Democratic Republic of Congo - DRC, respectively. The heterogeneity is observed as both intra-variability (e.g., diverse patterns of small-scale agriculture within the country) and the inter-variability (e.g., diverse patterns of small scale agriculture between the countries or regions). Example imagery retrieved from Google Earth Engine.

these continents makes these regions suitable for methodological research on large-scale assessment of land-use following deforestation (Müller et al., 2015).

2.2.1 Data

In this study we used two data sources: 1) the ground truth/reference data, manually annotated using very high resolution imagery and provided by De Sy et al., 2019, containing the land-use following deforestation classes and 2) Landsat satellite time series data cubes over the same geographical extent.

Reference data

We used a large reference dataset containing land-use following deforestation from 1990–2005 in tropical regions of Latin America, Africa and Asia (De Sy et al., 2019). From the reference dataset, only the land-use data from 2000–2005 were used in this study to match with deforested areas from Hansen et al. (2013). The basis for the reference dataset is the FAO 2010 global Remote Sensing Survey (FAO FRA-2010 RSS) which used a systematic sampling design with sampling units spaced in a 10km by 10km grid on each degree latitude-longitude confluence point (FAO & JRC, 2012a) to assess forest (change). This dataset consists of three main land-use classes, which are: forest, other wooded land, and other land (FAO & JRC, 2012a). De Sy et al. (2015) further classified land-use following deforestation into more detailed land-use classes (Table 2.1), through expert knowledge and visual interpretation of land-use using publicly available medium to high resolution satellite imagery. The definition of each of the FLU classes can be found in (De Sy et al., 2019). For this study we focus on 6 land-uses as the dominant drivers of deforestation, as indicated in (Table 2.1), *i.e.*, large-scale and small-scale cropland, pasture, mining, tree-crops and other land with tree cover. The six selected land-use classes cover 95.0%, 97.2%, and 93.2% of the total reference dataset for Latin America, Africa and Asia respectively. In Figure 2.2, we show the spatial distribution of reference/ground data used in this study. The reference data are based on the forest area loss per follow-up land-use in the pan-tropics for the six selected follow-up land-use classes.

Satellite data

For this study, we used Landsat 5 and 7 satellite imagery. This imagery has a spatial resolution of 30m and a temporal resolution of 16 days. The Landsat data was chosen as it is the only satellite dataset with sufficient spatial and temporal coverage for the entire study period of 2000 to 2005. Two median composite images (January-June, July-December) were collected for each sample location from dense Landsat image time series for each year from 2000 to 2005 using Google Earth Engine. The collected dataset was filtered for clouds using the quality assessment band of Landsat SR data (Google Earth Engine, 2020). Only images which contained cloud cover less than 50% were used to create a composite, this made sure we obtained enough images as possible but also we didn't lose more images. For each median composite in the time series, the normalized vegetation index (NDVI) and the normalized difference moisture index (NDMI), were computed. For each year, we collected at least 2 median composite images showing different phenological stages and texture, which contributes to differentiate FLU. Each composite image consisted of 7 spectral bands (Blue, Green, Red, Near-Infrared, Shortwave infrared 1, Thermal-infrared and shortwave infrared 2) and two vegetation indices (NDVI and NDMI), making a total of 9 bands for each Landsat based image composite in a time series collection. Overall every collected dataset from all sampled locations in the study area consist of a time series

Table 2.1: land-use classes contained in the reference data. The land-use with * symbol denotes the land-use selected for our study.

Main classes	subclasses	Description
Agriculture	Mixed agriculture	<ul style="list-style-type: none"> Mix of agricultural land-uses
	Small-scale crop-land*	<ul style="list-style-type: none"> Land under cultivation for crops, characterized by very small (< 0.5 ha) to small field sizes (0.5–2 ha)
	Large-scale crop-land*	<ul style="list-style-type: none"> Land under cultivation for crops, characterized by medium (2–20 ha) to large (> 20 ha) field sizes
	Tree-crops*	<ul style="list-style-type: none"> Miscellaneous tree-crops (e.g. coffee, palm trees), orchards and groves
	Pasture (grazing land)*	<ul style="list-style-type: none"> Land used predominantly for grazing; in either managed/cultivated (pastures) or natural (grazing land) setting; includes grazed woodlands
Infrastructure	Urban, settlements	<ul style="list-style-type: none"> Residential areas
	Roads, built-up areas	<ul style="list-style-type: none"> Transport, industrial and commercial infrastructures
Mining*		<ul style="list-style-type: none"> Land used for extractive subsurface and surface mining activities (e.g. underground and strip mines, quarries and gravel pits), including all associated surface infrastructure
Water		<ul style="list-style-type: none"> Natural (river, lake etc) or man-made water bodies (e.g. reservoirs)
Other	Bare land	<ul style="list-style-type: none"> Exposed soil, sand, or rocks
	Other land with tree cover*	<ul style="list-style-type: none"> Land not classified as forest, spanning more than 0.5 ha; with trees higher than 5 metres and canopy cover of 5%–10%, or trees able to reach these thresholds in situ, or with a combined cover of shrubs, bushes and trees above 10 percent. It does not include land that is predominantly under agricultural or urban land-use.
	Grass and herbaceous	<ul style="list-style-type: none"> Land covered with (natural) herbaceous vegetation or grasses
	Wetlands	<ul style="list-style-type: none"> Areas of natural vegetation growing in shallow water or seasonally flooded environments. This category includes Marshes, swamps, and bogs.
Unknown land-use		<ul style="list-style-type: none"> All land that cannot be classified (e.g. due to low resolution imagery)

of 12 composites with 7 spectral bands (plus 2 vegetation indices) from 12-time steps from 2000 to 2005.



Figure 2.2: Shows the spatial distribution of the reference data on land-use following deforestation across the pan-tropics for the six selected FLU classes. The size of each circle represents the forest loss area (in ha), and the colored pies within the circle represent the proportion of land-use following deforestation. The grey-lined countries are study area countries.

2.2.2 Deep learning models for FLU classification

Six neural network architectures with varying focus on spatial and/or temporal features were tested to characterise FLU using dense time series of Landsat imagery:

1. A two-dimensional convolution neural network (2D CNN), which exploits the spatial spectral-correlations of neighboring pixels of each image in the time series data (Castelluccio et al., 2015; Huang et al., 2018).
2. A long short-term memory neural network (LSTM), a type of recurrent neural network (RNN) which focuses on the temporal dynamics of the time series data by explicitly controlling the flow of information through time (Wang et al., 2019; Zhong et al., 2019).
3. A three-dimensional convolutional neural network (3D CNN), which treats the time dimension as an additional spatial dimension and can thus exploit spatial-temporal-spectral correlations in the data (Kumar et al., 2019; Li et al., 2017; Xu et al., 2018).
4. A hybrid of 2D-CNN and LSTM, which aims to benefit from the exploitation of spatial information by using a 2D-CNN and controlling the temporal information flow with an LSTM (Hu et al., 2018; Yang et al., 2020; Zhu et al., 2020).
5. A convolutional long short-term memory neural network (ConvLSTM), a type of recurrent neural network with internal matrix multiplications replaced by convolution operations that can thus simultaneously exploit spatial-temporal correlations in the data (Shi et al., 2015).
6. A CNN+Multi-Head Self-Attention model (CNN-MHSA) or CNN-Transformer, an attention mechanism which focuses on certain parts of the input sequences of images to allow for more flexible interactions between the different time steps, applied in conjunction with a CNN feature extractor (Bazi et al., 2021; Rußwurm and Körner, 2020).

Implementation details for each model are discussed in the following section and summarized in Table. 2.2. The diagrams of individual model architectures are provided in appendix 2.6.1.

2.2.3 Implementation details

The hyper-parameters used in these models were chosen based on the F1-score performance on a randomly chosen validation set consisting of 10% of the data. The dataset for each continent was split three times into training 75%, validation 10%, and 15% testing subsets for 3-fold cross-validation (Figure 2.3). In order to select the model parameters (see below Table 2.2), we use Bayesian optimization using one of the folds (see details in Appendix 2.6.2), in which the models have been trained on the training set and the

best-performing parameters for each model type (2D-CNN, LSTM, CNN-LSTM, 3D-CNN, ConvLSTM, and CNN-MHSA) have been selected based on the accuracy achieved on the validation set. For each run, the final model was then evaluated on the held-out test set. The accuracies reported in this article are the averages and standard deviations on the test sets over the three folds. The final assignments of best parameters are reported in Table 2.2 (the same assignment was used for each of the three runs mentioned above).

All models were implemented by using the Keras library and TensorFlow as back-end. All network architectures were trained for 30 epochs with a batch size of 512. All convolutional layers were preceded by a padding operation that ensured that the spatial extent of the output stayed the same as the input and followed by a ReLU non-linearity (Table 2.2). Batch normalization was used to normalize the features in the second convolutional and the following two dense layers, while a dropout rate of 0.1 was used to regularize the second convolutional layer and third dense layer. All models were optimized by using Stochastic Gradient Descent (SGD) with a learning rate of 10^{-4} , learning rate decay of $3.3 \cdot 10^{-6}$ at each iteration, and momentum of 0.9. The optimized loss was a multi-class cross-entropy between the post-softmax scores and the one-hot label corresponding to the class of the central pixel of the patch. All models are designed to receive input tensors of shape (12 time steps \times 9 width \times 9 height \times 9 bands) and to predict the FLU class of the central pixel of every data cube, such that the output is always a vector with the six scores, one per FLU class, followed by a softmax activation function.

2D Convolutional Neural Network (2D-CNN) We use a six-layer 2D-CNN classification architecture applied to each (9 width \times 9 height \times 9 bands) temporal slice of the input tensor, with shared weights. The six layers of the 2D-CNN consists of 32, 32, 64, 64, 128, 128 filters respectively, all with kernel size 3×3 and a stride of 1. A 2×2 max-pooling operation is applied on the second and fourth convolution layers. Each convolution operation is followed by a rectified linear unit (ReLU) activation function and batch normalization. These CNNs are wrapped inside a TimeDistributed layer in Keras that allows for sequential operations to every 9 width \times 9 height \times 9 bands image in a time series. The resulting feature maps are concatenated and then flattened into a vector of size 6144, followed by three linear layers with 1024, 512, and 6 neurons to provide FLU class predictions.

Long Short-Term Memory Recurrent Neural Network (LSTM) Designed to control the flow of time-series information over arbitrarily long or short time intervals in sequential data, the LSTM model was used to leverage the temporal patterns in the time series input that are relevant to produce the final labels of FLU. The LSTM model was optimized by using two LSTM layers with 32, and 128 units respectively, to extract relevant non-linear temporal dependencies present in the remote sensing time series. The input shape for the LSTM layer was (12 time steps \times 729 pixels) feature vectors flattened

over $9 \text{ width} \times 9 \text{ height} \times 9 \text{ bands}$ images. The LSTM layer was used jointly with three fully connected layers of size 1024, 512 and 6, batch normalization, and dropout of 0.1.

3D Convolutional Neural Network (3D-CNN) The 3D-CNN model treats the time series data as volumetric data by extracting features in three dimensions, one temporal and two spatial. We used an input image patches of size ($12 \text{ time steps} \times 9 \text{ width} \times 9 \text{ height} \times 9 \text{ bands}$). The filter size of ($3 \times 3 \times 3$) was used to convolve in all spatial and temporal dimensions in all convolution layers. The resulting feature maps from the convolution layers are concatenated and then flattened into a vector of size 1536, followed by three linear layers with 1024, 512 and 6 neurons.

Hybrid CNN-LSTM As an alternative to the 3D-CNN to account for spatial-temporal patterns in the imagery, we used an LSTM that resorts to convolutional filters in order to also account for spatial patterns. At each of the 12 time steps, a 2D-CNN is used to extract a feature vector of size 32, 64, 128 from the corresponding $9 \text{ width} \times 9 \text{ height} \times 9 \text{ bands}$ image patch. A two-layer LSTM module then receives these vectors sequentially, keeping a state vector of size 12. This architecture enabled our model to extract spatial features associated with each FLU from CNN layers, then cascading the features into the LSTM layer, which extracted the non-linear temporal dependencies present in the remote sensing time series. Similarly to the 2D-CNN and LSTM methods, after the LSTM layer, a fully connected layer, dropout and batch normalization.

ConvLSTM We use a ConvLSTM network to map FLU using spatial-temporal features from the input sequence of satellite images of size $12 \text{ time steps} \times 9 \text{ width} \times 9 \text{ height} \times 9 \text{ bands}$. The first part of the network includes three ConvLSTM layers followed by batch normalization and max pooling layers. The ConvLSTM layers include 32, 64, and 128 filters, respectively, with a kernel size of 3×3 used to perform convolutions. Finally, max-pooling with pooling window size of 2×2 is used to reduce the size of the output ConvLSTM features. The output of the last ConvLSTM layer is followed by three fully-connected layers with 128, 64, and 6 neurons, respectively.

CNN Multi-Head Self-Attention Is another spatial-temporal model comprising a hybrid network of CNN and Multi Head self-attention block. The CNN block is used to determine spatial features and the self-attention block to determine temporal features from the CNN layer. The input data has a sequence of image of size $12 \text{ time steps} \times 9 \text{ width} \times 9 \text{ height} \times 9 \text{ bands}$. The first block of the network includes six convolutional layers of filter size 32, 32, 64, 64, 128, and 128 followed by ReLU activation function, and batch normalization. Max pooling layers of pool size 2×2 is applied on the second and fourth convolution. The kernel size of 3×3 used to perform convolution operation to

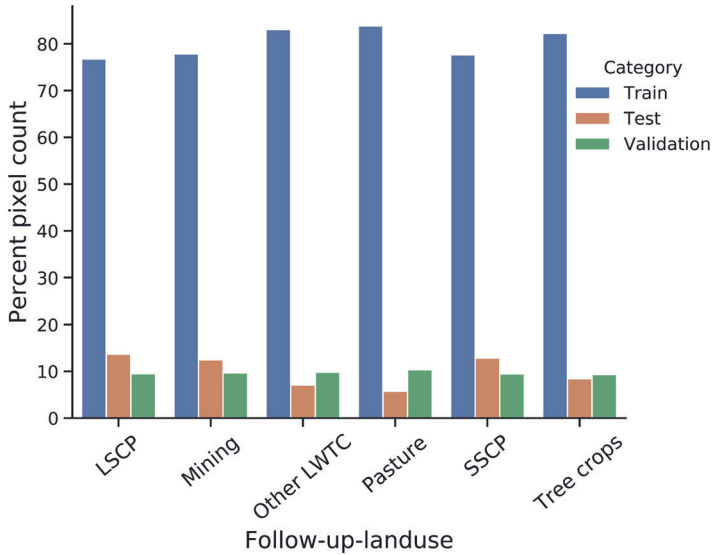


Figure 2.3: The percentage of pixels per FLU for the training, validation, and test sets of one of the random splits over the full tropical dataset. Where LSCP, other LWTC, and SSCP stands for large-scale cropland, Other land with tree cover, and small-scale cropland, respectively.

determine spatial features respectively. Finally the convolution operation is followed by the global average pooling operation.

The second block of the network includes the transformer block which encodes features from the CNN block with 4 attention heads, 128 hidden dimension, and 32 hidden layer size in the feed forward inside the transformer. The transformer block is followed by global average pooling which takes the mean across all time steps and feed into 2 dense layers.

2.2.4 Evaluation of performance deep learning models

The performance of the deep learning models in classifying the FLU was evaluated using a held out test set and following a 3-fold strategy. The standard error of the F1-score on test set was computed as $\sigma_{\bar{x}} = \sigma/\sqrt{n}$, where $\sigma_{\bar{x}}$ is the standard error, σ standard deviation and $n = 3$ is the number of test F1-scores. The evaluation metrics computed were the classwise F1-scores, micro-average of F1-scores and macro-average of F1-scores. The F1-score is the harmonic mean of precision and recall, $F1 = 2(P * R)/(P + R)$ (Rußwurm and Körner, 2017). The precision, $P = TP/(TP + FP)$, is a measure of result relevancy, while recall, $R = TP/(TP + FN)$, is a measure of how many relevant results are returned. . TP, FP, and FN stands for the number of true positives, false positives, and false negatives of each

Table 2.2: Architecture of 2D-CNN, LSTM, 3D-CNN, 2D-CNN-LSTM, ConvLSTM, and CNN-MHSA model

Parameters	Model Type and Dimensions					
	2D-CNN	LSTM	3D-CNN	2D-CNN-LSTM	ConvLSTM	CNN-MHSA
Input shape	12 x 9 x 9 x 9	12 x 729	12 x 9 x 9 x 9	12 x 9 x 9 x 9	12 x 9 x 9 x 9	12 x 9 x 9 x 9
No. Conv layers	6	-	6	6	6	6
No. filter	32, 32, 64, 64, 128, 128	-	32, 32, 64, 64, 128, 128	32, 32, 64, 64, 128, 128	32, 64, 128	32, 32, 64, 64, 128, 128
Filter size	3 x 3	-	3 x 3 x 3	3 x 3	3 x 3	3 x 3
Padding	same	-	same	same	same	same
Pool size	2 x 2	-	2 x 2 x 2	2 x 2	1 x 2 x 2	2 x 2
Strides	1 x 1	-	1 x 1 x 1	1 x 1	1 x 1	1 x 1
LSTM Units	-	32, 128	-	32, 128	-	-
No. Dense layer	2	2	2	2	2	2
Learning rate	0.0001	0.0001	0.0001	0.0001	0.0001	0.0001
Hidden dims	-	-	-	-	-	128
Hidden layer	-	-	-	-	-	32
No. of heads	-	-	-	-	-	4
No. Classes	-	-	-	-	-	6

of the predicted FLU classes. In addition, the confusion matrix of the predicted samples and true samples were computed using the unseen test set. We used the F1-score of each class as an indicator of the model’s capability to identify each single class of FLU. At the same time, the micro-average and macro-average of F1-score was used as an indicator of the general classification capability of the model (Pan et al., 2017; Zhang et al., 2019). The macro-average of the F1-score is the average of all classwise F1-scores and covers class imbalance of each class, giving more importance to rare classes (Johnson and Khoshgoftaar, 2019; Pan et al., 2017). The micro-average F1-score computes the aggregated contribution of all classes by using precision and recall values averaged across all samples. This puts emphasis on the more abundant classes in the data, since it gives each sample the same importance (Pan et al., 2017).

2.3 Results

In this chapter, we present the classification results using spatial, temporal, and spatio-temporal models for identifying the FLU in the pan-tropics (namely 2D-CNN, LSTM, 3D-CNN, Hybrid CNN-LSTM, ConvLSTM, and CNN-MHSA). In the following sections we present the FLU classification results for the continental models (Section 2.3.1) and for the pan-tropical models (Section 2.3.2). Finally, in Section 2.3.3 we present a spatial comparison of predicted versus reference dominant FLU per sample location using the best continental models and pan-tropical model from section 2.3.1, and 2.3.2.

2.3.1 Classification results – continental models.

The results in Figure 2.4 show the per-class F1-scores, micro-averaged F1-score and macro-averaged F1-score for the six deep learning methods, both for the continental and pan-tropical models. All methods obtain comparable levels of accuracy in the continental setting except for the LSTM, which tends to trail the other methods by a large margin.

The 2D-CNN performs almost as well as the hybrid spatio-temporal methods (Figure 2.4).

In Figure 2.5a, 2.5b, 2.5c and 2.5d we show the confusion matrix for the FLU’s classification of one of the best performing model (Hybrid CNN-LSTM) over Latin America, Africa, Asia and for full pan-tropical test datasets, respectively. For Latin America, there is high recall rate of over 78% for large-scale cropland, 90% pasture, and 91% mining. Other classes such as small-scale cropland, tree-crops and other land with tree cover attained low recall rate of over 45%, 24%, 26% respectively. Most of the small-scale cropland and other land with tree cover tends to be confused with the pasture while tree-crops tend to be confused with other land with tree cover as in Figure 2.5a. In Africa (Figure 2.5b), pasture and tree-crops tend to be confused with small-scale cropland (55%, 38%). In Asia (Figure 2.5c), almost every FLU class has a recall rate higher than 80% with the exception of tree-crops (54%) which tends to be confused with SSCP (26%) and other land with tree cover (19%).

2.3.2 Classification result – pan-tropical model.

Unlike in the continental setting, the Hybrid CNN-LSTM, ConvLSTM and CNN-MHSA outperform all the other methods in the pan-tropical setting by a substantial margin, as shown in Figure 2.4. The pan-tropical Hybrid CNN-LSTM, and CNN-MHSA model reached a micro-average F1-score of (58%, 66%) and a macro-average F1-score of (53%, 61%). Among all the follow-up land-use types, larger-scale cropland (42%), mining (96%), small-scale cropland (95%) and other land with tree cover (75%) are the most distinguishable FLUs (Figure 2.5d). Larger-scale cropland, pasture, tree-crops and other land with tree cover are some likely to be confused with small-scale cropland by (30%, 62%, 87%, 24%), respectively. Larger-scale cropland is also confused with pasture (22%), while pasture is confused with other land with tree cover (11%). The pan-tropical model’s confusions are similar to the continental models confusion, where tree-crops in Latin America and Asia is the most misclassified follow-up land-use class, reaching the F1-score of (10%) (Figure 2.5d). Similarly, the tree-crops is the follow-up land-use class with the lowest recall rate in both continental and pan-tropical models. This can be attributed to the spatial scale and spectral similarity of tree-crops with small-scale cropland and large-scale cropland across the tropics.

2.3.3 Comparison of dominant FLU per sample location using the Hybrid CNN-LSTM method.

Using one of the best performing spatio-temporal methods in the pan-tropical setting (Hybrid CNN-LSTM), we compare the most dominant FLU per sample location for the predicted and reference FLU dataset, for both the continental (Figures 2.6a and pan-tropical models (Figures 2.6b. In Latin America, for the continental models’ predictions (Figure

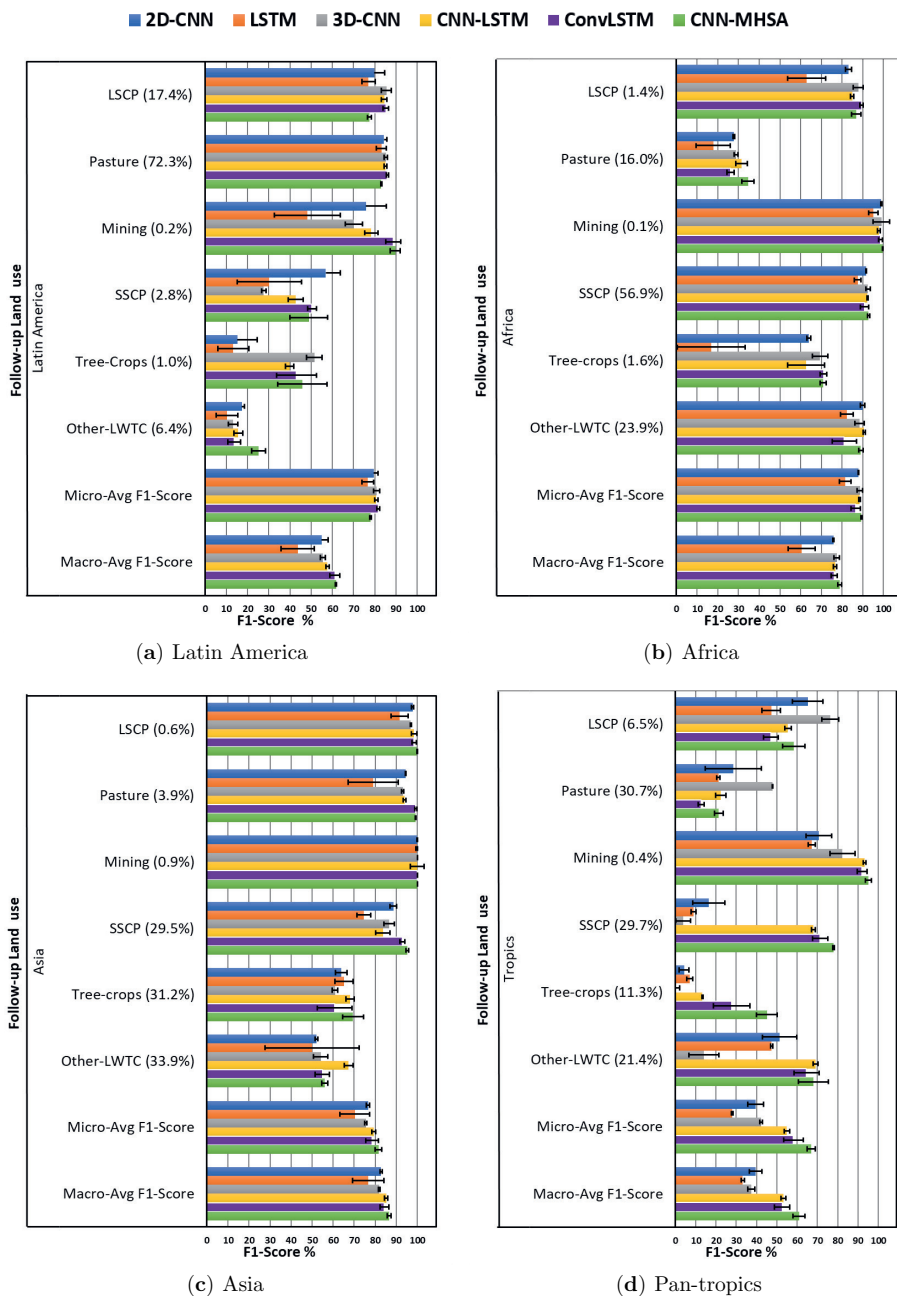


Figure 2.4: F1-scores of FLU classification (in percentages) for deep learning methods for continental and pan-tropical models for (a) Latin America, (b) Africa, (c) Asia, and (d) pan-tropics, respectively. LSCP stands for large-scale cropland, SSCP for small-scale cropland, and Other LWTC for other land with tree cover. In brackets are the percentages of each FLU class present on each continent. The error bars are the standard deviation on F1-scores.

6a), pasture and large-scale cropland are the most dominant FLUs in both prediction and reference datasets. For sample locations in Brazil, Paraguay, Bolivia, and Uruguay these two dominant FLUs are mostly similar for predicted and reference FLU. However, we also observe that large-scale cropland tends to be confused with pasture, particularly in Argentina, Paraguay, northern Mexico, and eastern Brazil (mainly in the state of Bahia). Other confusions are also observed in Mexico between other land with tree cover and small-scale cropland as well as other land with tree cover and pasture (Figures 2.6a).

In Africa, small-scale cropland is the most dominant driver in both prediction versus reference dataset (Figure 2.6a). For small-scale cropland, predicted dominant FLU matches well in parts of central Africa (i.e., Democratic Republic of Congo -DRC, Congo), southern Zimbabwe and Mozambique, Ethiopia, and parts of West Africa (i.e., Nigeria, Cameroon, and Cote d'Ivoire). Nevertheless, we also observe confusion between other land with tree cover and small-scale cropland in central Mozambique, northern Zambia, and Angola. Another notable confusion is between pasture and other land with tree cover as well as small-scale cropland and pasture in Tanzania, Kenya, and some parts of West Africa.

In Asia, tree-crops and small-scale cropland tend to be the most dominant driver in both prediction versus reference dataset (Figures 2.6a). Tree-crops are predicted well as dominant FLU in Malaysia and Indonesia. Small-scale cropland are predicted well as dominant FLU in central parts of Myanmar, some parts of Thailand, Laos, and Vietnam. On the other hand, in parts of Thailand, Cambodia, India, and Indonesia there is mismatch between predicted and reference dominant FLU as small-scale cropland, pasture, and tree-crops tend to be confused with other land with tree cover.

For the pan-tropical model similar spatial patterns of the reference versus predicted dominant FLU could be observed as in the continental models' prediction results (Figures 2.6a for Latin America and Asia. In Africa, larger-scale cropland was over-predicted as dominant FLU at the expense of small-scale cropland, especially in parts of west and east Africa.

2.3.4 Computational considerations

In terms of computation time, the optimal architectures for LSTM and ConvLSTM resulted in more computationally intensive models at training time compared to the other four models (Table 2.3). This can be due to the sequential feed forward and back propagation between hidden vectors of each timesteps, since the subsequent steps in LSTM and ConvLSTM cells depends on previous ones resulting in more time and computational resource demand. This is different from other models such as 2D-CNN, 3D-CNN and CNN-MHSA where the feature computations happen in parallel. In the CNN-LSTM the CNN part is also computed in parallel, providing a better image representation than the LSTM without a CNN feature extractor, resulting in a more efficient architecture. There were only marginal differences in testing time between the models. This is useful, as, in

Table 2.3: The training time and test time in minutes (m) for Latin America, Africa, and Asia datasets using 2D-CNN, LSTM, 3D-CNN, ConvLSTM, 2D-CNN-LSTM and 2D-CNN-Multi-Head Self-Attention methods.

Study Regions	2D-CNN		LSTM		3D-CNN		ConvLSTM		CNN-LSTM		CNN-MHSA	
	Train(m)	Test(m)										
Latin America	113.13	3.26	212.58	1.45	115.39	4.55	433.23	24.50	112.30	3.37	108.43	3.29
Africa	62.5	3.52	149.72	1.56	66.5	5.32	346.5	26.51	66.17	4.5	152.5	3.44
Asia	67.5	1.18	212.5	0.84	84.5	1.52	343.33	9.26	86.1	1.23	175.55	1.16

the future, we can re-use the saved deep learning models when making predictions of FLU on recent deforested locations. Thus, there will be no need to re-train the model from scratch (Castelluccio et al., 2015). All experiments were completed in a secured cloud-based computing environment (SEPAL 2.0) that is part of the Amazon cloud with instance type g8, NVIDIA Tesla M60 GPU 32GB RAM.

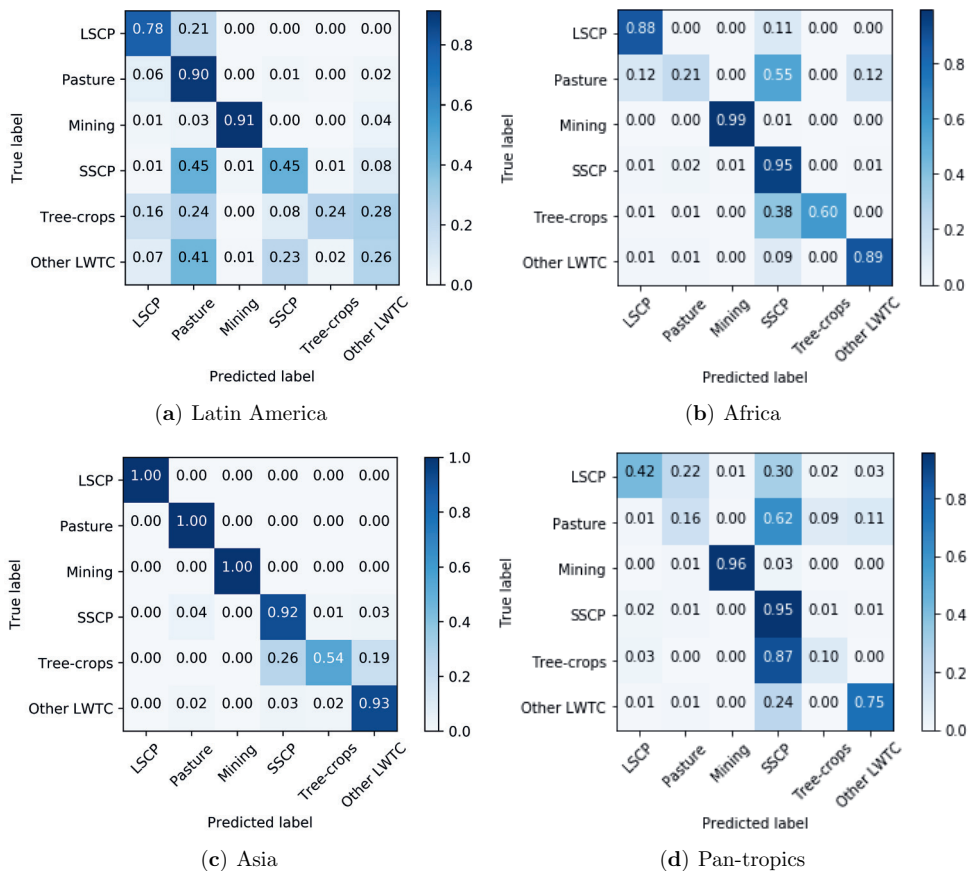
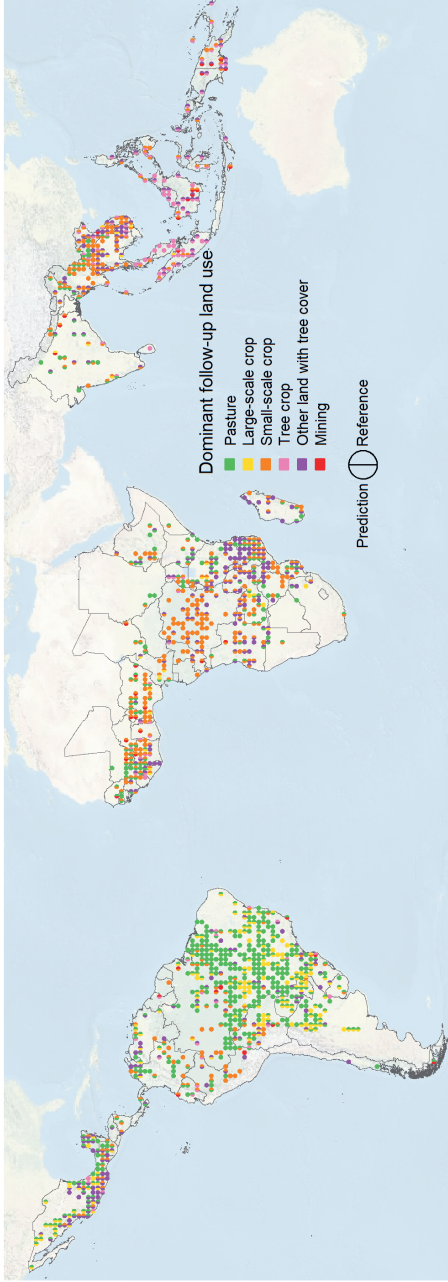
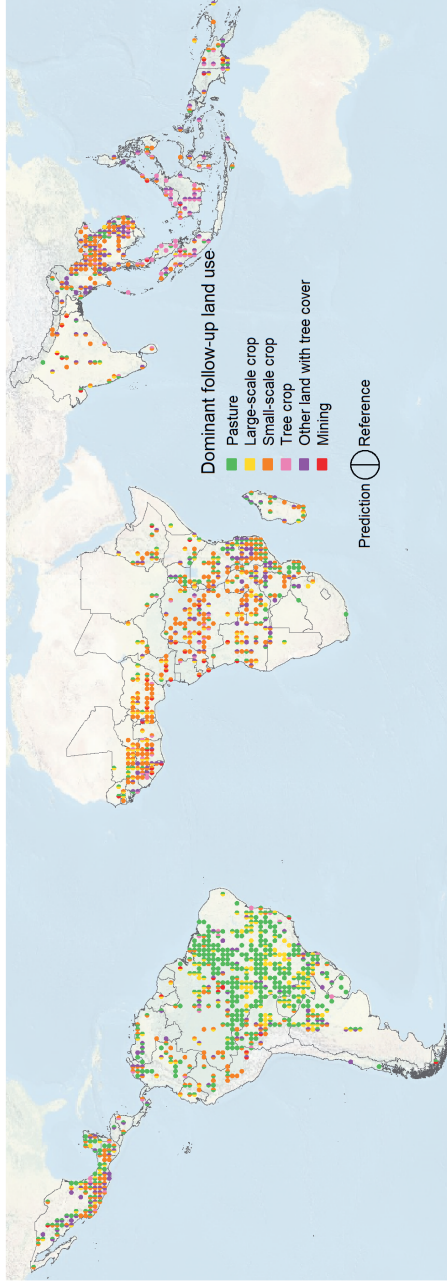


Figure 2.5: The confusion matrix showing the percentage of correct predicted and false predicted FLU's using one of the spatio-temporal deep learning method with highest score (CNN-LSTM) for (a) Latin America, (b) Africa, (c) Asia, and (d) pan-tropics, respectively. LSCP stands for large-scale cropland, SSCP for small-scale cropland, and Other LWTC for other land with tree cover.



(a) Continental FLU predictions



(b) Pan-tropical FLU predictions

Figure 2.6: Dominant follow-up land-use for each sample location for prediction and reference FLU dataset for (a) continental models (CNN-LSTM), and (b) pan-tropical model (CNN-LSTM). Each circle represents the dominant FLU for a sample location, with the left half of the circle showing the predicted dominant FLU and the right half showing the reference dominant FLU. Best viewed in the digital version and by zooming in.

2.4 Discussion

The scope of this work was designed to evaluate the use of different spatio-temporal deep learning models for classifying land-use following deforestation at a large scale in continental Latin America, Africa, and Asia. Large-scale experiments were conducted on a real-world dataset acquired from freely available time series of Landsat satellite data (2000-2005) together with reference data provided by FAO 2010 global Remote Sensing Survey (FAO & JRC, 2012a). The results from our experiments (in Sections. 2.3.1, 2.3.2) have shown that simultaneously accounting for spatial and temporal patterns in the model design decisions results in better performances compared to models which by design can solely rely only on spectral, spatial (2D-CNN) or temporal information (LSTM) (Zhang et al., 2019). The higher accuracies attained by the spatio-temporal methods confirms that 2D-CNN (spatial), LSTM (temporal), methods alone are less able to differentiate the FLUs. We also observed that the 2D-CNN achieved higher classification performance on the continental scale compared to the LSTM, as seen in Figure 2.4a, 2.4b and 2.4c. This shows that spatial patterns of land-use are more useful for land-use characterization than temporal ones when considering the problem at the regional level. This may indicate a higher level of heterogeneity in terms of the temporal patterns that characterize each FLU, possibly due to regional differences in seasonality and land-use practices. The performance of all models in identifying tree-crops and other land with tree cover in Latin America and Asia, as well as pasture in Africa, is relatively low compared to other FLU classes, also suggesting a more heterogeneous spatio-temporal pattern in these cases. On the other hand, pasture achieves above average performance in Latin America and Asia, even though in the latter it is a minority class, suggesting that more homogeneous spatial patterns are associated with pasture in these continents than in Africa.

Looking at predicted versus reference dominant follow-up land-use (Figures 2.6a and 2.6b), some spatial patterns could be observed. In Latin America, we do not see as much confusion in the so-called arc of deforestation (edge of Amazon forest) compared to the region more to the south, where the dominant FLUs (pasture and large-scale cropland) are more established. This might be related to the fact that, over time, the extensively managed large-scale cropland tends to be used as pastures during one or two rotational cycles, thus exhibiting a similar texture and spatial arrangement compared to newly established pasture/large-scale cropland in the arc of deforestation (Müller et al., 2015). Another spatial pattern of confusion is observed in eastern and mid-southern Africa, where most small-scale cropland and pasture tend to be confused with other land with tree cover. The confusion may arise from the fact that both pasture, small-scale cropland, and other land with tree cover are characterized by savanna and shrubland vegetation types and have no clear distinct spatial and temporal patterns to make them distinguishable, making it even challenging with visual identification (Müller et al., 2015). Another reason for this confusion can be attributed to the confidence in reference data, *i.e.*, some samples of

reference data used in our study from visual interpretation had low confidence level of belonging to the referenced class, which might have contributed to low performance of the model (De Sy et al., 2019) in these areas.

Overall, the Hybrid CNN-LSTM, ConvLSTM and CNN-MHSA models achieved better classification accuracies compared to the 2D-CNN, LSTM and 3D-CNN in the pan-tropical setting. This is in spite of the cloud cover affecting parts of the data. While other studies focus on filtering out cloudy data (Zhang et al., 2019) or on exploiting partly cloudy images (Oehmecke et al., 2019), our results suggest that models making explicit use of spatio-temporal patterns, in particular those using attention-based mechanisms such as CNN-MHSA, are able to cope with these high levels of cloud coverage. The observation that explicitly accounting for both spatial and temporal patterns in the data boosts the generalization performance is in line with the results of Zhong et al. (2019), who use a multi-temporal deep neural network for a classification task, and the Joint Deep Learning (JDL) model of Zhang et al. (2019), which incorporates a multilayer perceptron (MLP) and convolutional neural network (CNN) for land cover and land-use classification. The approaches in the Zhang et al. (2019) are methodologically closest to the Hybrid CNN-LSTM and CNN-MHSA models used in this study and are comparable with our setting in terms of the type of land-use data used. However, their relatively small study area (Southampton and Manchester), together with their image data type (aerial photos), hinders a direct comparison. Indeed, one of the main contributions of this work is going beyond small-scale benchmarking tasks (Castelluccio et al., 2015; Doggart et al., 2020; Irvin et al., 2020; Li et al., 2018; Zhang et al., 2019). Also (Descals et al., 2021a; Doggart et al., 2020; Irvin et al., 2020) achieved relatively higher accuracies compared to our study, although their studies were country based or covered fewer FLU classes. Overall, in all three study areas (Latin America, Africa, and Asia), the hybrid CNN-LSTM, ConvLSTM and CNN-MHSA models yielded the best results, thus making the use of these models for identifying the FLU in the pan-tropical more promising by reducing the work of using human interpreters in identifying land-use over large areas.

It is also important to note that the deep learning approaches in this study were tested and evaluated on data limited to the sample locations and dates in De Sy et al., 2019. Nevertheless, the deep learning model evaluated in this study could be applied to monitor land-use following deforestation wall-to-wall and for more recent time periods. Given the current and expected future availability of high resolution and accurate global deforestation data, these methods could be applied following open-source global deforestation data such as the Hansen et al., 2013 global forest loss and RADD alerts (Reiche et al., 2021) or to national deforestation data in the context of national forest monitoring systems. These provide an opportunity to implement the proposed methods to identify the land-use following deforestation in deforested areas while masking out non-deforestation areas using the updated forest loss layers. Relying on existing deforestation data makes the

task of detecting land-use following deforestation at large-scale more tractable without compromising its applicability.

In addition, this study further validates that large-scale land-use classification tasks can be accomplished without the necessity of using spatio-temporal handcrafted features (expert knowledge) to account for spatio-temporal dependencies of land-use as in traditional machine learning models, *i.e.*, random forests or support vector machines (Ma et al., 2019; Reichstein et al., 2019; Zhang et al., 2019; Zhu et al., 2017). Better classification results of deep learning versus traditional machine learning in terms of classification accuracy have also been obtained in (Huang et al., 2018; Zhang et al., 2019). Besides its success, technical challenges remain, such as (1) limited model interpretability due to lack of direct causal relationship between inputs and outputs, *i.e.*, in identifying important and most useful variable for the classification problem (2) high computational requirements due to an increase in data volume as a result of an increase in the number of features and dimensions extracted by the models during the computational stage, resulting to higher training time and RAM requirement or usage, (3) high demand of reference data, caused by intraclass variability (heterogeneity) (Reichstein et al., 2019; Zhu et al., 2017). According to Reichstein et al. (2019), the possible challenge of deep learning models when working with heterogeneous data is that they may work well during training and on test datasets but perform poorer when extrapolating to other regions outside their valid domain. Despite these challenges, the deep learning field is still growing and has achieved better classification accuracies when compared to other traditional models (Zhang et al., 2019; Zhao and Du, 2016). Swift advancement are expected in the near future in the field of remote sensing, especially through the use of transfer learning and self-supervised learning (Zhu et al., 2017) for large-scale classification problems. For future work, we plan to expand our analysis to predict, validate, and monitor changes in land-use at the continental level while leveraging the pan-tropical data through meta-learning (Rußwurm et al., 2020; Tseng et al., 2021).

2.5 Conclusion

We have explored the potential of using spatio-temporal deep learning models for large-scale classification of land-use following deforestation using time series of satellite (Landsat) images. Six deep learning models were considered in this study, the 2D-CNN, LSTM, 3D-CNN, Hybrid CNN-LSTM, ConvLSTM, and CNN-MHSA. The models were evaluated in the tropical regions of Latin America, Africa, and Asia as continental models and pan-tropical model. We found that, for most land-use classes, the complementary spatio-temporal information extracted by the spatial-temporal models (Hybrid CNN-LSTM, 3D-CNN, ConvLSTM, CNN-MHSA) from the time series of Landsat images improved the accuracy of the model in classifying the FLU by a significant margin compared to the

2D-CNN and LSTM, which are designed to focus only on spatial or temporal features, respectively.

Nevertheless, the FLU classification from Landsat satellite imagery remains a challenging task due to the existence of spatial heterogeneity and spatio-temporal variability of the FLU over large-scale assessments. In some areas, the classification challenges were particularly caused by clouds and shadows that cover most tropical areas of Africa and Asia. Yet, the evaluated spatio-temporal models, were able to distinguish the FLU in most of these areas, particularly when trained on regional data. We also found that models focusing on spatial patterns only performed competitively in the continental setting but not in the pan-tropical one, suggesting that land-use types within a region are more readily characterized by their spatial patterns than their temporal signature. This effect disappears at the pan-tropical level, pointing at different spatial patterns across the tropics. Indeed, this is the setting where it was most advantageous to use spatio-temporal models and, particularly, the attention-based CNN-MHSA. We hypothesize that the arbitrary temporal interactions allowed by attention-based models provide an edge against the noise derived from the high cloud cover characteristic of the tropics.

Therefore, given the size and coverage of this study, this work could be particularly useful for large-scale forest and land-use change monitoring in the context of REDD+, the global stocktake for the Paris Agreement and the Sustainable Development Goals. In this paper we address challenges associated with large-scale FLU assessments in the pan-tropics such as the heterogeneity of land-uses, and identifying land-use instead of just land cover. Our methodology can support a more detailed spatial and temporal assessment of where forests are lost, and the land-use activities driving it. This will allow targeting of REDD+ mitigation efforts towards specific proximate deforestation drivers in order to achieve more impact. Our approach could also be adopted for national forest monitoring systems as it uses open-source data and platforms, and can be calibrated with local or national data. Our method could be further developed toward more frequent and wall-to-wall monitoring of land-use following deforestation to identify hotspots and local patterns of land-use change. Other data source such as recent forest loss data and other satellite sources (e.g. high resolution imagery, radar data) could be included.

2.6 Appendix

2.6.1 Diagrams of individual deep learning model architectures

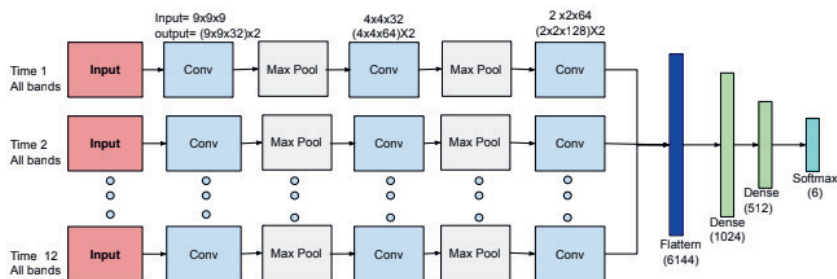


Figure 2.7: Schematic view of our convolution network. Time 1 to Time 12 are the tensors input along the temporal dimension each of size $9 \times 9 \times 9$. The colors represents, light red = Input images, light blue = Convolution operations, light grey = MaxPooling operation, blue = flatten operation, light green = feed forward network and cyan = output layer.

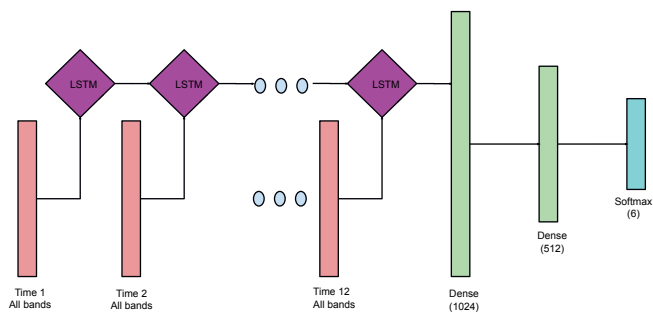


Figure 2.8: Schematic view of our long-short term memory network. The colors represents, light red = Input array, magenta = LSTM cells, light green = feed forward network and cyan = output layer.

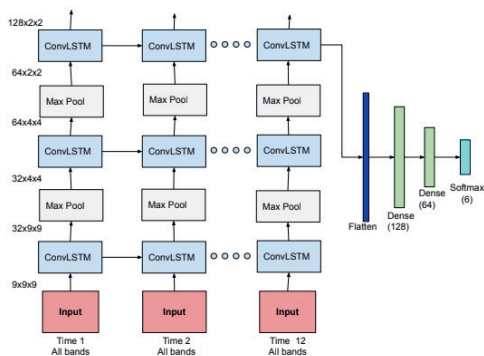


Figure 2.9: Schematic view of our ConvLSTM network. The colors represents, light red = Input images, light blue = Convolution operations, light grey = MaxPooling operation, blue = flatten operation, light green = feed forward network and cyan = output layer.

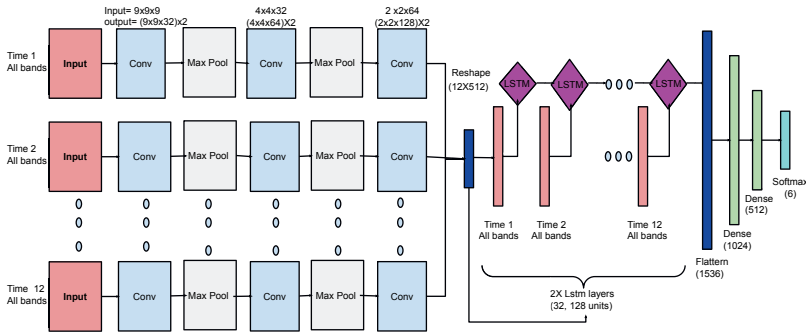


Figure 2.10: Schematic view of our convolution+long-short term-memory network. Time 1 to Time 12 are the tensors input along the temporal dimension each of size $9 \times 9 \times 9$. The colors represents, light red = Input arrays, light blue = Convolution operations, light grey = MaxPooling operation, magenta = LTM cells, blue = reshape operation, light green = feed forward network and cyan = output layer.

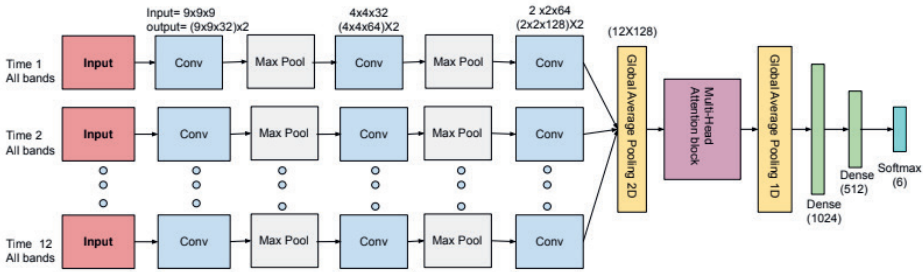


Figure 2.11: Schematic view of our convolution+Multi-head Self-attention model. Time 1 to Time 12 are the tensors input along the temporal dimension each of size $9 \times 9 \times 9$. The colors represents, light red = Input images, light blue = Convolution operations, light grey = MaxPooling operation, light magenta = Attention layer, light yellow = Average pooling operation, light green = feed forward network and cyan = output layer.

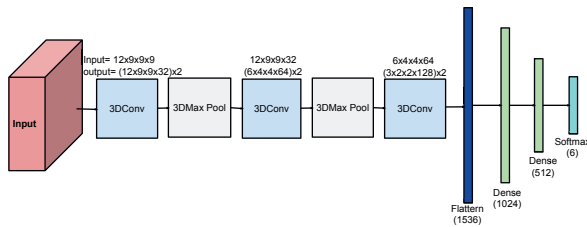


Figure 2.12: Schematic view of our 3D convolution network. The input tensors along the spatial and temporal dimension are of size $12 \times 9 \times 9 \times 9$. The colors represents, light red = Input images, light blue = Convolution operations, light grey = MaxPooling operation, blue = flatten operation, light green = feed forward network and cyan = output layer.

2.6.2 Hyper-parameter optimization using Bayesian optimization

We used Bayesian optimization from the scikit-optimize package (Gilles and Manoj, n.d.) to find the best possible set of hyper-parameters that gives us high performance of the model on validation data. A total of 20 calls or runs was used to optimize the hyper-parameters Figure 2.13. For most of the involved model hyper-parameters, a search space of parameters ranging from learning rate ($\{2^{-6}, \dots, 2^{-2}\}$), number of filters ($\{16, \dots, 128\}$), number of dense layers ($\{1, \dots, 3\}$), number of dense nodes ($\{64, \dots, 1024\}$), number of LSTM units ($\{32, \dots, 128\}$), number of heads ($\{3, \dots, 8\}$) have been used. However, as expected, the learning rate had significant impact on the validation accuracies compared to other hyper-parameters, refer to Figure 2.14. In Figure 2.15 we also show the sample distributions for each of the hyper-parameters during the Bayesian optimization and the order in which the samples were taken.

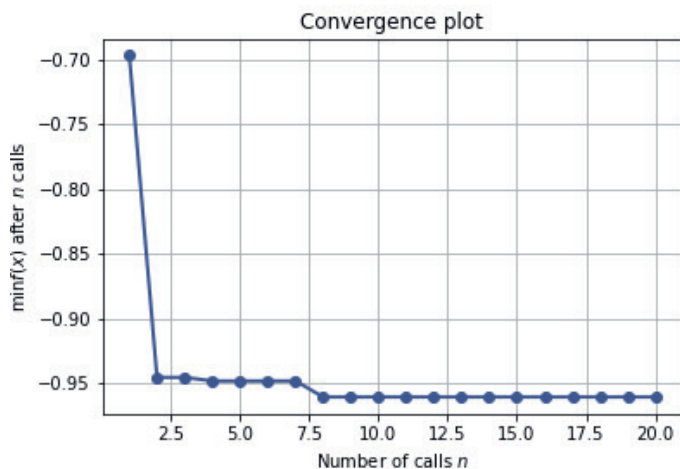


Figure 2.13: The view of the progress of the hyper-parameter optimization on the validation data over 20 calls. The X-axis shows the number of calls and y-axis the minimization, or the convergence trace over n calls.

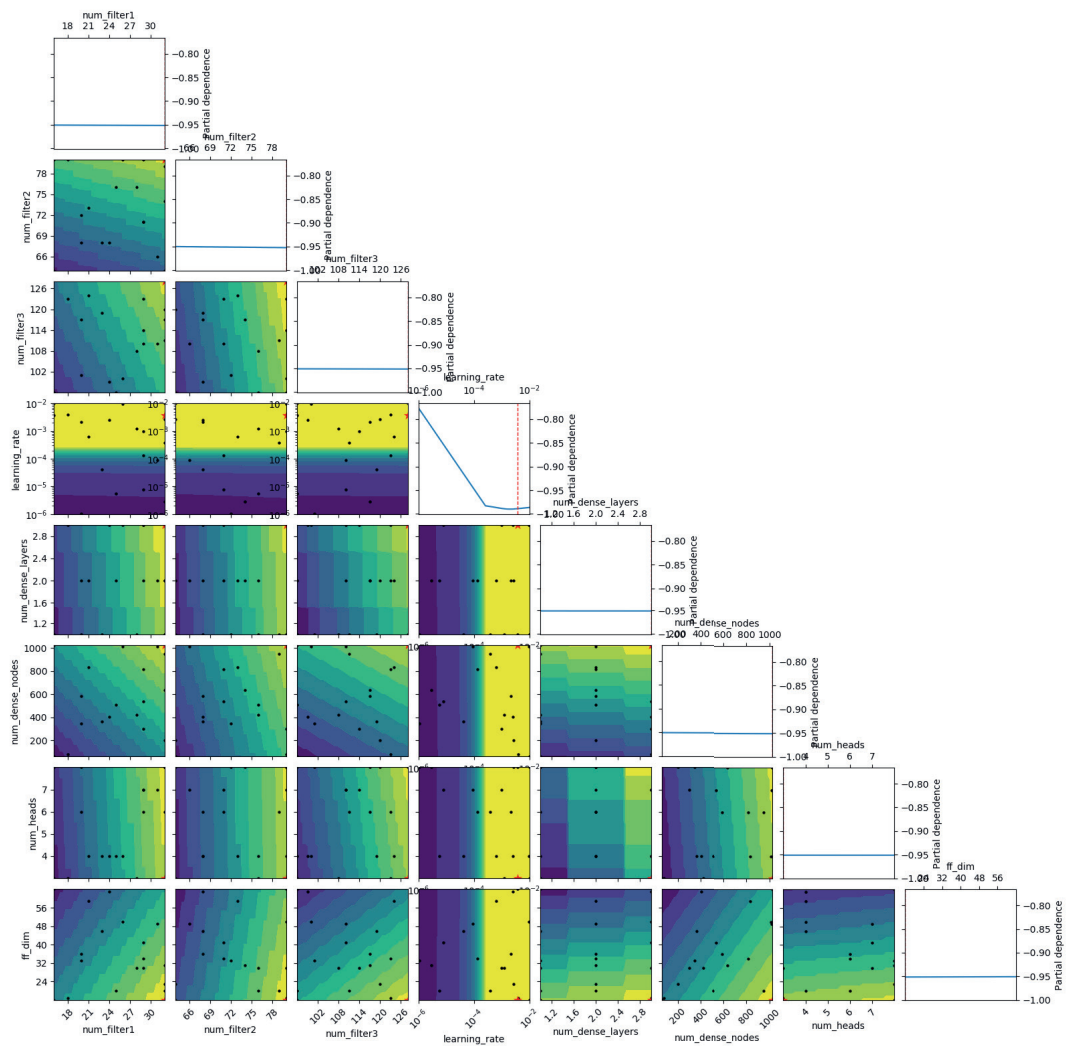


Figure 2.14: The Partial Dependence plot showing a matrix-plot of all combinations of searched hyper-parameters during Bayesian optimization. This shows how the approximated fitness value changes when we are varying two dimensions simultaneously. The top diagonal subplots shows the influence of a single dimension on the accuracy. For each sub-plot the blue and yellow regions shows areas that gives us low and high performance hyper-parameters. The black dots show where the optimizer has sampled the hyper-parameter and the red dot shows the best hyper-parameters found.

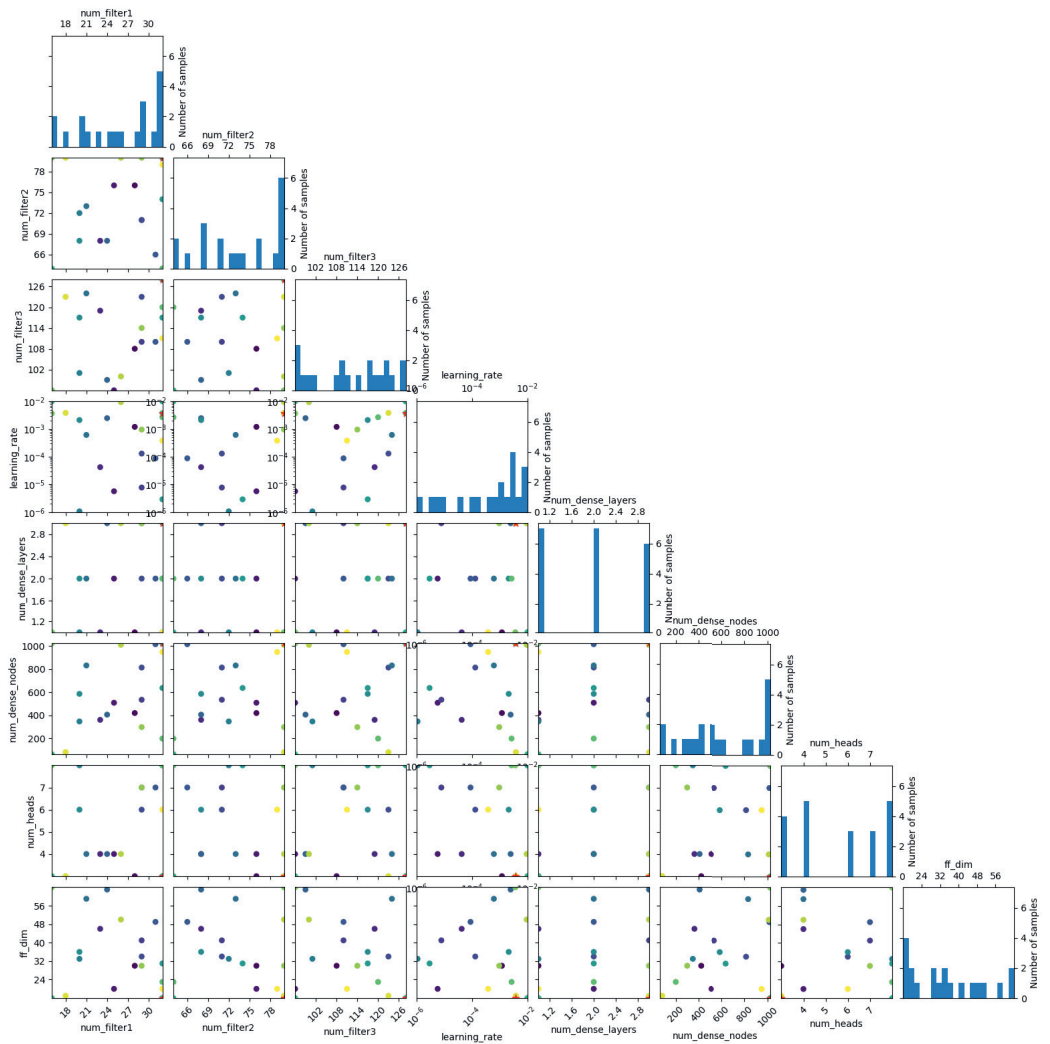


Figure 2.15: The Matrix-plot. The top diagonal plots shows histograms of the sample distributions for each of the hyper-parameters during the Bayesian optimization. The plots below the top diagonal show the location of hyper-parameters in the search-space and the colour-coding shows the order in which the hyper-parameters were taken. The points in dark-purple corresponds to earlier hyper-parameters and lighter-yellow to later hyper-parameters. The points in red shows the location of the minimum or best hyper-parameter found by the Bayesian optimization process(Gilles and Manoj, n.d.).

CHAPTER 3

3

Using High-Resolution Imagery and Deep Learning to Classify Land-Use Following Deforestation: A Case Study in Ethiopia

This chapter is based on:

R. N. Masolele, V. D. Sy, D. Marcos, J. Verbesselt, F. Gieseke, K. A. Mulatu, Y. Moges, H. Sebrala, C. Martius, and M. Herold (2022). "Using high-resolution imagery and deep learning to classify land-use following deforestation: a case study in Ethiopia". *GIScience & Remote Sensing* 59.1, 1446–1472.

Abstract

National-scale assessments of post-deforestation land-use are crucial for decreasing deforestation and forest degradation-related emissions. In this research, we assess the potential of different satellite data modalities (single-date, multi-date, multi-resolution, and an ensemble of multi-sensor images) for classifying land-use following deforestation in Ethiopia using the U-Net deep neural network architecture enhanced with attention. We performed the analysis on satellite image data retrieved across Ethiopia from freely available Landsat-8, Sentinel-2 and Planet-NICFI satellite data. The experiments aimed at an analysis of (a) single-date images from individual sensors to account for the differences in spatial resolution between image sensors in detecting land-uses, (b) ensembles of multiple images from different sensors (Planet-NICFI/Sentinel-2/Landsat-8) with different spatial resolutions, (c) the use of multi-date data to account for the contribution of temporal information in detecting land-uses, and, finally, (d) the identification of regional differences in terms of land-use following deforestation in Ethiopia. We hypothesize that choosing the right satellite imagery (sensor) type is crucial for the task. Based on a comprehensive visually interpreted reference dataset of eleven types of post-deforestation land-uses, we find that either detailed spatial patterns (single-date Planet-NICFI) or detailed temporal patterns (multi-date Sentinel-2, Landsat-8) are required for identifying land-use following deforestation, while medium-resolution single-date imagery is not sufficient to achieve high classification accuracy. We also find that adding soft-attention to the standard U-Net improved the classification accuracy, especially for small-scale land-uses. The models and products presented in this work can be used as a powerful data resource for governmental and forest monitoring agencies to design and monitor deforestation mitigation measures and data-driven land-use policy.

3.1 Introduction

The recent Intergovernmental Panel on Climate Change (IPCC) report highlights that human activities are the unequivocal cause of climate change. It further accentuates that human activities are accountable for an increase in greenhouse gases emissions henceforth an increase of 1.1°C of warming since 1850–1900 (IPCC, 2021). Tropical forests are essential in mitigating the impact of climate change through provision of clean air, contributing to the biodiversity, regulating water cycle, preventing erosion, and mitigating climate change (FAO, 2014; IPCC, 2021; Koh et al., 2021; Nowak et al., 2014). However, the increasing global trend of forest loss and degradation risks losing the continual supply of these ecosystem services provided by forests (Hansen et al., 2013; IPCC, 2021). Providing information on the human activities (direct drivers) causing forest loss (Finer et al., 2018; Geist and Lambin, 2001) and its coverage will enable governments, and national forest monitoring systems to concentrate on forest emissions reduction and on mitigation efforts (REDD+) towards specific proximate deforestation drivers, where they will have the greatest impact (BioCarbon Fund, 2020; Curtis et al., 2018; De Sy et al., 2019; FAO, 2010; IPCC, 2021; UNFCCC, 2018).

Currently, there are several global initiatives for the assessment and monitoring of deforestation and its proximate drivers (Curtis et al., 2018; Hansen et al., 2014; Hansen et al., 2013). However, these global assessments often differ from national assessments in terms of reported forest extent, drivers and trends of deforestation (Nomura et al., 2019; Sandker et al., 2021). The difference is due to the fact that these initiatives often require a similar definition of forest and method to ensure consistency on large area, which usually entails a choice in precision and accuracy at local level (Hansen et al., 2014; Latawiec and Agol, 2015; Lu, 2007; Yanai et al., 2020). In addition, global assessments often differ from national assessments due to either one or the other assessment being poorly analyzed or inaccurate, but also by decisions relating to the included land-use types and the choice of minimum mapping unit (Nomura et al., 2019). Furthermore, global scale assessment of direct deforestation drivers are prone to lack of diverse representation of land-use classes due to spatial heterogeneity (Masolele et al., 2021), thus causing more uncertainties when comparing global versus national land-use change data (Curtis et al., 2018). In the present work we aim at a method that is locally suited for developing a national forest monitoring system for REDD+ reporting, and thus informing the local and national decision-making processes (CIFOR, 2021). Having an open, accessible, transparent, reliable, credible, and relevant national forest monitoring system can result in better decision making for forests and can contribute to driving down deforestation and attain nationally determined contributions (NDCs) (Sandker et al., 2021; UNFCCC, 2021).

In spite of the increasing demand and technical capacity for national based forest monitoring system, the assessment of proximate causes of forest loss in the tropical countries remain limited (De Sy et al., 2015; FAO, 2010; FAO, 2016; Hansen et al., 2013). Specifically, the

limitation of data, location, spatial extent, and type of human activities causing forest loss (FAO, 2010). The limitation is due to a lack of a robust system that can monitor forest loss to provide up-to-date information on drivers and data driven land-use policies and actions (FAO, 2010; Nomura et al., 2019; UNFCCC, 2018) through identifying the land-use activities that cause forest loss and help mitigate its effects (Finer et al., 2018). In this paper, we explore the analysis of drivers of forest loss at the national scale by focusing on Ethiopia, where the vast majority of the original forests are long gone (FAO, 2010; Hansen et al., 2013). As a proxy for the deforestation drivers, we use the follow-up land-use (FLU) after a forest loss event.

The recent advances and availability of free and open-source remote sensing satellite imagery like Landsat 1–5, 7, 8 & 9 and Sentinel-1, 2A, 2B have extensively enabled the assessment of changes in land-use (Curtis et al., 2018; De Sy et al., 2019; Masolele et al., 2021), changes in land-cover (Brown et al., 2022; Tsendbazar et al., 2021), forest characteristics (Lu et al., 2004; Mutanga et al., 2012; Potapov et al., 2021), and in forest disturbances monitoring (Decuyper et al., 2022; Reiche et al., 2021; Ye et al., 2021). The policy of free and open data with respect to the Landsat and Sentinel satellites means increased accessibility of moderate resolution images to commercial and non-commercial players, that is essentially relevant to the assessment of land-use changes over the pan-tropics in a medium spatial and high temporal detail (Curtis et al., 2018; Hansen et al., 2013; Schepaschenko et al., 2019). Nevertheless, the moderate spatial resolution limit its use in identifying the land-use following deforestation in much subtle and fine detail (Irvin et al., 2020; Masolele et al., 2021). The considerable increase in the capacity of new generation sensors to detect subtle change has opened new opportunities for ecological monitoring with higher accuracy (Finer et al., 2018; Gallwey et al., 2020; Masolele et al., 2021; Meng et al., 2017; Zhang et al., 2019).

One example of this is the privately owned PlanetScope constellation, which aims at providing under 5 m spatial resolution daily imagery with four bands, RGB and NIR. Recently, thanks to Norway’s International Climate & Forests Initiative (NICFI) program, tri-monthly composites with a 4.77 m spatial resolution and very low cloud cover, thanks to the daily acquisition frequency, have been made available to initiatives that help protect forest and biodiversity and reduce the impact of climate change (NICFI, 2021). This imagery has already proven useful for mapping forest loss accross the tropics (Zeng et al., 2018). The availability of this imagery, in conjunction with the forest loss dataset in Hansen et al., 2013, provides an opportunity to characterise the direct drivers of forest loss in Ethiopia. Together with Deep Learning (DL) approaches, these data can be utilized to automate the classification of deforestation drivers, which, in turn, would allow to locate hotspots and spatial patterns of land-use changes at local level (Finer et al., 2018; Irvin et al., 2020; Masolele et al., 2021).

DL methods for computer vision, based on convolutional neural networks (CNN), are designed to automatically learn to extract useful spatial or spatio-temporal patterns in images, often leading to substantially better performances than traditional machine learning approaches (Gallwey et al., 2020; Rousset et al., 2021; Verma and Jana, 2020; Wang et al., 2021; Zhang et al., 2021; Zhao et al., 2017). These methods have recently demonstrated capabilities in an extensive range of satellite image analysis tasks (Irvin et al., 2020; Masolele et al., 2021; Reichstein et al., 2019; Rußwurm and Körner, 2020), including for FLU detection (Descals et al., 2021a; Irvin et al., 2020; Masolele et al., 2021).

However, these approaches either require substantial computational resources (on dense time series analysis) (Masolele et al., 2021; Rußwurm and Körner, 2018; Rußwurm and Körner, 2020), are not aimed towards wall-to-wall land-use classification (Descals et al., 2021a), assess somewhat smaller number of land-use classes (Irvin et al., 2020) or only use medium resolution (10-30 m) images (Landsat or Sentinel) (Curtis et al., 2018; Geist and Lambin, 2001; Silva et al., 2018). Integrating DL algorithms with HRSI provides an opportunity to map and analyse FLU at the national scale with higher accuracy and spatial resolution than alternative approaches (Finer et al., 2018).

Unfortunately, despite the recent advancements in remote sensing, and computational capabilities for the assessment of land-use, or direct drivers of forest loss (Irvin et al., 2020; Masolele et al., 2021), we still lack the capacity to frequently monitor land-use characteristics (De Sy et al., 2019; De Sy et al., 2015; Schepaschenko et al., 2019). Field assessments or surveys are valuable to have an accurate information of the types of deforestation drivers, locations, and extent. However, they are challenging and expensive to implement at an administrative or decision making level (FAO, 2010; Gibbs et al., 2007; Harfoot et al., 2021). Existing efforts to assess land-use change and causes of forest loss in Ethiopia based on medium resolution remote sensing imagery have thus far been performed at the subnational scale (e.g., (Habte et al., 2021; Tadese et al., 2021; Tewabe et al., 2020; Zewdie and Csaplovics, 2017).

The government of Ethiopia is currently starting to pilot the use of high resolution Planet-NICFI for land-use change detection (Ethiopian Forest Division, 2022). Nevertheless, these studies were conducted on a few isolated study areas (local scale) and do not provide detailed identification of the drivers of forest loss (few classes). There is a need for national or sub-national-based approaches that can integrate the available land-use data and high-resolution Planet-NICFI imagery (NICFI, 2021) with DL methods to identify the direct drivers of deforestation. Therefore, in this work, we apply state-of-the-art DL approaches for monitoring land-use that can assist in detecting land-use following deforestation in Ethiopia. Particularly, we address the following two objectives:

1. We develop, validate and apply a segmentation method to predict the deforestation drivers in Ethiopia based on open-source satellite data (Planet-NICFI/Sentinel-2/Landsat-8) at multiple spatio-temporal resolutions and assess its performance.

2. We use the same procedure to produce a country scale map of post-deforestation land-use, and assess the proportionality (%) of each land-use based on region and forest types in Ethiopia.

To achieve these objectives, we explore the use of models specifically designed for mapping tasks, inspired by U-Net (Ronneberger et al., 2015), in contrast to the patched-based approaches used in (Masolele et al., 2021), in order to allow for efficient inference of large-scale wall-to-wall FLU maps. We also extend the application of attention gates (Oktay et al., 2018) to the multi-class setting.

3.2 Method and Materials

Our methodology follows six consecutive steps: (i) data extraction, which includes using a map of forest loss Hansen et al., 2013, reference land-use and satellite data (Planet-NICFI, Sentinel-2, and Landsat-8, refer to Subsection 3.2.2), (ii) data pre-processing (refer to Subsection 3.2.2), (iii) DL method design for land-use classification (refer to Subsection 5.2.5), (iv) technical implementation details of the methods for classifying land-use, refer Subsection 3.2.4, (v) evaluation of the performance of DL models, refer to Subsection 3.2.5, and finally (vi) wall-to-wall prediction of FLU over Ethiopia, refer to Subsection 3.2.6. These steps are discussed in detail below.

3.2.1 Study Area

We have selected Ethiopia, a country in East Africa, as the study area for this work (Figure 3.1). Ethiopia has a diverse climate and geography with yearly rainfall in a range of below 200 mm to over 2400 mm and altitudes ranging from 125 metres below sea level to 4533 metres above sea level (Friis Ib et al., 2010). The rainfall for most parts of the country occurs in two seasons, between March to April and June to September. Ethiopia possesses high forest biodiversity consisting about 7000 higher plant species. 12% of plant species are endemic to Ethiopia (Berhan and Egziabher, 1991). Due to its long history of high deforestation rate caused by increasing population and hence increased clearing for agriculture, grazing, and settlements (Bishaw, 2001; FAO, 2010; Getahun et al., 2017), 64 species are identified as threatened in 2018, and 21 species are identified as endangered in the IUCN Red List (Stévant et al., 2019). Over 50 years ago, Ethiopia had about 40% of the forest. At present, that number is close to 15% (BBC, 2019), mostly in the south-west of the country. Efforts have been initiated to preserve these remaining forests because of its richness in plant species, for instance, hosting most of the world’s coffee diversity (Lemenih and Kassa, 2014). The country has been praised in its effort to reduce deforestation through forest restoration and regeneration (BBC, 2019; UN-REDD, 2017). However, in-spite of the said effort, the speed of forest loss is still high (Hansen et al., 2013), specifically deforestation related to small-scale and large-scale cropland

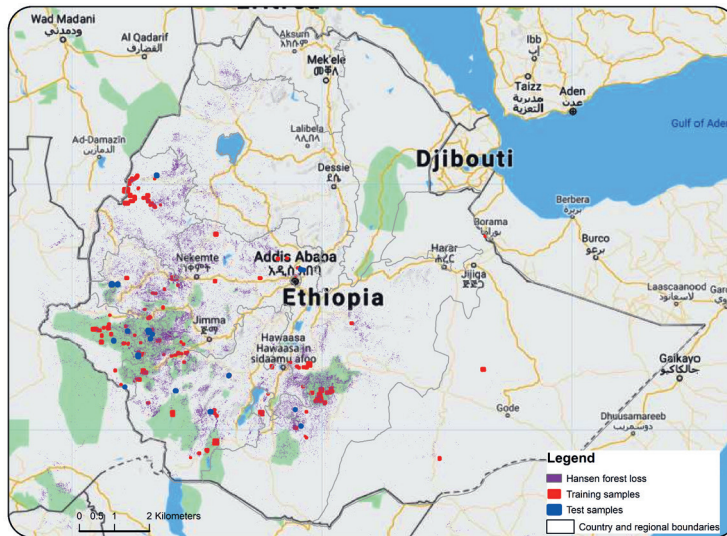


Figure 3.1: Map showing the spatial distribution of forest loss locations, training and test data across Ethiopia. The colors represent training and testing samples of one of the train-test split. The grey-lines are the boundaries of the study area, regions, and country.

expansion (Lemenih and Kassa, 2014). This work aims at improving the tool-set for data driven forest management and policy towards sustainable and actionable conservation of Ethiopian forests.

3.2.2 Data

Three data sources acquired within Ethiopian boundaries were used in this study: 1) the Hansen forest loss, to identify areas of forest loss 2) Manually annotated reference data, using very high resolution imagery, containing eleven land-use following deforestation or follow-up land-use (FLU) classes and 3) satellite imagery data (Planet-NICFI, Sentinel-2, and Landsat-8).

Forest Loss Data

We made use of the Hansen forest loss data (Hansen et al., 2013) as an interim step in identifying training labels of land-use following deforestation. Hansen forest loss data is a global forest product that has been extensively used to evaluate forest loss. The data provides useful annual spatial and temporal forest loss information on global scale for as much as 2000 (Zeng et al., 2018). A total of 300 forest loss locations were randomly sampled using Hansen forest loss in Google Earth Engine (GEE) with a buffer of 5km. However, 5 were rejected due to cloud cover. The 5km spacing or buffer ensured that samples are sufficiently spaced to avoid the risk of spatial auto-correlation. The sampled

locations were used as priors to visually create or identify FLU training and validation labels.

Reference Data

Using seasoned experts and manual interpretation of HRSI from the Planet-NICFI, GEE and Hansen forest loss data, we visually interpreted the randomly collected reference sample data specifically for classifying FLU in Ethiopia (Figure 3.1). The task of interpreting and collecting the reference FLU was conducted during July and August, 2021. The Hansen-derived forest loss from 2010 to 2014 (Hansen et al., 2013) was used as a baseline for identifying the forest loss areas while the HRSI from the Planet-NICFI for 2016 and GEE was used for identifying and digitizing the FLU as polygons (Figure 3.2). In addition, other data sources such as the Ethiopia Sentinel-2 Land-Use Land-Cover 2016 map, forest cover change map for year 2000 – 2013 based on Landsat images and the Ethiopia Mining Cadastre were also helpful to aid in interpreting and digitizing the FLU classes (Ministry of Mines and Petroleum, 2021; RCMRD, 2018; UN-REDD, 2017). Here we adopt the definitions of FLU presented in Masolele et al., (2021), corresponding to IPCC main FLU classes (IPCC, 2013). The FLU classes were identified in consultation with representative stakeholders from Ethiopia such as the National REDD+ Secretariat, Environment, Forest and Climate Change Commission (EFCCC), Oromia REDD+ Coordination Unit, FAO - Ethiopia, Ethiowetlands, International Center for Tropical Agriculture (CIAT), Ethiopian Geospatial Information Agency, Ethiopian Environment and Forest Research Institute (EEFRI), Farm Africa, and Center for International Forestry Research-World Agroforestry (CIFOR-ICRAF).

The collected labels consist of six main land-use classes, namely: Agriculture, Infrastructure, Mining, Water, Tree plantations, and Other. The main land-use classes were further divided into 11 more detailed FLU classes (see details as provided by Masolele et al., 2021), *i.e.*, large-scale cropland (20.0%), small-scale cropland (30.2%), pasture or free grazing (6.5%), roads (3.0%), tree plantation (3.5%), coffee crops (10.5%), tea plantation (10.0%), mining (7.0%), buildings and dams (2.3%), other land with tree cover (1.2%) and water (5.8%). In Figure 3.1, we present the reference data showing the spatial distribution of FLU used in this research. The ground-truth data are polygons relative to the forest loss per FLU in Ethiopia for the eleven selected FLU classes. It is important to note that the tree plantation class is often not related to the loss of natural forest. Tree plantations are often cleared for sustainable forestry management and typically grow back over time between rotational periods. This class was included in this study to avoid confusion with other FLU, since the harvested patches from forest plantations are shown in the Hansen data as forest loss.

In total, we annotated 237 tiles used for model training and an additional set of 28 and 30 images as test sets stemming from disjoint locations for the years 2016 and 2020 based

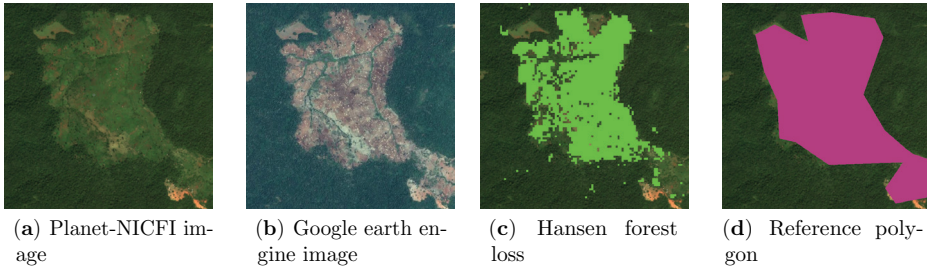


Figure 3.2: For the same location in Ethiopia, (a) Planet-NICFI image, (b) Google earth engine image used for visual interpretation, (c) Hansen forest loss and, (d) manually annotated reference polygon. Example imagery and polygon were retrieved from Google Earth Engine.

on forest loss from 2010 to 2014 and 2015 to 2019, respectively. This was important to evaluate the spatial and temporal robustness of our model Figure 3.1.

Satellite Data

We used Planet-NICFI, Sentinel-2, and Landsat-8 satellite imagery to classify land-use following deforestation. The imageries have a spatial resolution of 4.77m, 10m, 30m, and a maximal temporal resolution of bi-annual, five, and sixteen days, respectively. For this study, we used bi-annual images to match the temporal resolution of Planet-NICFI images. We selected these satellite images to assess for usefulness of different spatial resolutions for characterising FLU. For Planet-NICFI imagery, we used analysis-ready, PlanetScope Surface Reflectance Mosaics¹ covering a period from December 2015 to May 2016. The Planet-NICFI images are a product of KSAT and Airbus. They are HRSI made open-source (non-commercial) by Planet Lab through NICFI in order to assist protect forest and biodiversity and reduce the impact of climate change (NICFI, 2021). The images come with four spectral bands, specifically - Blue, Green, Red, and Near-Infrared (NICFI, 2021), plus 3-vegetation indices (NDWI - the normalized difference water index, SAVI - the soil-adjusted vegetation index, and NDVI - the normalized difference vegetation index), resulting in 7 bands in total.

Median composite images (December 2015 - May 2016) for Sentinel-2, and Landsat-8 images were also collected for each sample location using GEE. The images cloud filtering was performed by use of the quality assessment band of Sentinel-2, and Landsat-8 (Cook et al., 2014). The final image composite was created using images with less than fifty percent of cloud cover. For each median composite, the NDVI, the SAVI, the normalized build-up index (NDBI), and the normalized difference moisture index (NDMI) were computed. Each composite image for Landsat-8 included seven spectral bands e.g., (Blue, Green, Red, Near-Infrared, Shortwave infrared-1, Thermal-infrared, and shortwave infrared-2) and

¹planet_medres_normalized_analytic.2015-12.2016-05.mosaic

four vegetation indices (SAVI, NDVI, NDMI, and NDBI), resulting in a total of 11 bands. On the other hand, the composite image for Sentinel-2 consisted of 10 spectral bands (Blue, Green, Red, 3-Vegetation red edge bands (B5, B6, B7), Near-Infrared, Narrow Near-Infrared, Shortwave infrared-1, and shortwave infrared-2), plus four indices (SAVI, NDVI, NDMI, and NDBI), resulting in a total of 14 bands. All sentinel-2 bands were resampled to 10 m. Overall, the satellite data collected comprises of 4, 7, 10 spectral bands (plus 3,4,4 vegetation indices each for Planet-NICFI, Landsat-8, and Sentinel-2, respectively) from 2016.

Additionally, four composite images, each with the same number of bands as the above images, were collected from four different time steps for multi-date image analysis. The composite images were acquired from (December 2015 - May 2016, June 2016 - November 2016, December 2016 - May 2017, and June 2017 - November 2017). The multi-date images were essential to add the temporal dimension in classifying the FLU.

Data Preprocessing

Using 295 sampled forest loss location across the country, we manually delineated rectangular polygons around sampled locations to download images (tiles) from GEE for each data source (Planet-NICFI, Sentinel-2, and Landsat-8). From each downloaded image tile, patches of dimensions $x_i \in \mathbb{R}^{w \times h \times d}$ and the corresponding FLU labels $y_i \in \mathbb{R}^{w \times h \times c}$ were extracted, where w , h and d specifies the width, height and number of bands of an image patch and c specifies the number of classes. The patch dimensions for each modality were, respectively 128×128 , 64×64 , 32×32 pixels, to account for the different resolutions. Patches were extracted such that each would have a 3/4 overlap with others, in an effort to decrease the loss of data used for training due to border effects. Each band $j \in \{1, \dots, d\}$ of a given image patch x_i was normalized via min-max scaling by resorting to the minimum and maximum pixel value for that band across all the training-images such that the resulting pixel values were in the range from 0 to 1.

3.2.3 Deep Learning Models For FLU Classification

Two semantic segmentation DL architecture, inspired by U-Net (Ronneberger et al., 2015), were tested to characterise FLU using Planet-NICFI, Sentinel-2 and, Landsat-8 satellite imagery. The U-Net architecture was chosen as starting point due to its efficiency in extracting features and spatial patterns from satellite data, even in the case of limited training data (Gallwey et al., 2020; Zhao et al., 2022). In particular, we consider the following two variants:

1. A standard U-Net architecture, which uses convolution operations to retrieve spatial features from images at different scales of an image. The coarse activation maps highlight contextual-rich information and underscore the type and position of global descriptors. The activation maps retrieved along different scales are subsequently

combined via shortcut connections to join coarse and higher-level predictions (Descals et al., 2021b; Irvin et al., 2020; Ronneberger et al., 2015). Refer to the architecture details in the Appendix 3.9

2. Attention U-Net, which integrate attention gates into the standard U-Net architecture to accentuate important descriptors that are passed via the shortcut connections. This is important as pieces of information retrieved from lower layers are used in the attention gate layer to amplify unimportant and noisy features in shortcut connections (Oktay et al., 2018; Schlemper et al., 2019). We adapted the design of the attention module to the multi-class setting by learning one attention map per feature map. Without this adaptation, the models in (Oktay et al., 2018; Schlemper et al., 2019), developed to remove the background information in foreground/background segmentation tasks, tend to completely remove information from some of the image areas, negatively affecting performance.

The details for implementation of each model are described in the subsequent section and its summary in Appendix 3.6.2. The computational consideration are described in Appendix 3.6.6. The figures of individual model designs in Appendix 3.6.1. We also provide the flowchart showing the workflow of this research in Appendix 3.6.3.

3.2.4 Implementation Details

In this section we talk about hyperparameter optimisation and model implementation. We split the training dataset 3-times in a ratio of 90% and 10% for training and validation important for three-fold cross-validation (Figure 3.3). We use Bayesian optimization to choose the model parameters (see below Appendix 3.6.2) based on one of the folds (see details as provided by Masolele et al., 2021), in which the best model parameter for U-Net and Attention U-Net models are chosen on the basis of accuracy attained on the validation data. The ultimate model architecture was then evaluated on the held-out test data for each run. Thus, in this paper, we report the mean and standard deviations of the accuracies on the test data over the 3-folds (Masolele et al., 2021). We describe the final allocation of best parameters in Appendix 3.6.2.

Both models were created using the Keras library (Chollet et al., 2015) and TensorFlow (Abadi et al., 2015) as backend. All models were trained for 100 epochs using a batch size of 64. For every convolutional layer we added a padding operation to ensure that the size of the last layer stays comparable to the input layer and followed by a non-linearity function-ReLU (Appendix 3.2). The features in the convolution layers were normalized using Batch normalization followed by a regularization dropout rate of 0.1. All models were optimized by using Adam optimizer with a learning rate (lr) of 10^{-3} . The optimized loss was a sum of multi-class categorical Focal Loss and Dice Loss of the post-softmax probability and the one-hot label analogous to the land-use class of the pixels of the

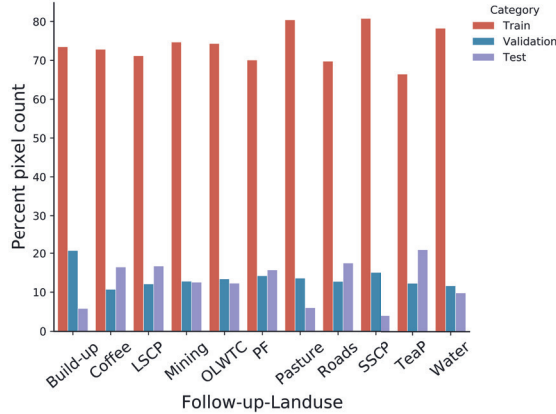


Figure 3.3: The training, validation, and test data showing the number of pixels per FLU (in %) of one of the random splits. Where SSCP, OLWTC, PF, LSCP, and TeaP corresponds to small-scale cropland, Other land with tree cover, tree plantation, large-scale cropland, and tea plantation, respectively.

image patch. Every one of the associated tasks were performed using Python in the Sepal geospatial analysis platform FAO, 2021.

U-Net.

This is a direct adaptation of the standard U-Net architecture (Ronneberger et al., 2015) that receives images from a single timestep of shape (width x height x bands), along with the corresponding label maps. The model architecture is made up of an encoding followed by a decoding section. For the encoder we have used four successive convolution layers with 3x3 filters, each followed by a pooling layer, resulting in a set of 512 feature maps. The encoder section is designed such that at each block the number of feature maps is increased by a factor of 2 while its spatial size is decreased by a factor 2. This is useful to increase the receptive field during the convolution operation. It also allows the model to increasingly retrieve semantic-contextual information. The decoder is the reverse of the encoder, by which the convolution layer is followed by upsampling layers instead of the pooling layers. The output maps of the decoders have the same spatial dimensions as the input data. The coarse and fine feature maps extracted at various blocks of the encoder and decoder section are combined through shortcut connections as shown in (Appendix 3.9). Finally, the softmax activation functions was used to obtain the final segmentation results.

Attention U-Net.

As an improvement to the standard U-Net we incorporated attention gates, in fashion similar to those proposed by Oktay et al., 2018, into the standard U-Net architecture to accentuate predominant descriptors that are passed via the shortcut connections, see (Appendix 3.10). Unlike in Oktay et al., 2018, we compute one attention map per feature, instead of all features sharing the same attention map in each attention gate, in order to adapt the method to the multi-class setting. In this way, the attention gates learn features passed through the skip connections to model location and relationship between FLU at local scale thus improving the detection of small scale and complex FLU *i.e.*, *roads, settlement, small-scale cropland*. This is important as pieces of information retrieved from lower layers are used in the attention gate layer to amplify unimportant and noisy features in shortcut connections. The gating operation is done prior to the concatenation step to combine only important activations. In addition, in both forward-and backward pass the neuron activations are filtered (Schlemper et al., 2019). This enables the parameters in lower layers to be updated largely in the context of spatial locations that are important to a specific class Oktay et al., 2018.

Ensemble of Attention U-Nets.

Finally, we consider an ensemble of different models trained on single-date Planet-NICFI, Sentinel-2, and Landsat-8 data, respectively. The ensemble is based on the late fusion of probability maps of the output of the three attention U-Net models from single-date Planet-NICFI, Sentinel-2, and Landsat-8. Since the satellite data and, hence, the prediction maps are available in different spatial resolutions (there are three resolutions in our scenario; “Planet-NICFI model”, “Sentinel-2 model”, and “Landsat-8 model”, equivalent to images patches with a resolution of 4.77 m, 10 m, and 30 m, respectively), we first upscale the prediction maps that stem from the Sentinel-2 and Landsat-8 data to match the resolution of the Planet-NICFI model (via nearest neighbor upscaling). The output of the ensemble is then based on the average probabilities induced by these three Attention U-Net models, where the final prediction per pixel is the class with the highest mean value.

3.2.5 Evaluation of Models

Typically, land-use classification and related tasks are evaluated based on spatially sampled data acquired at the same time step. For this study, however, the same model is validated two times on spatial and temporal test datasets to predict the FLU for other years. Thus, we evaluated the performance of our DL models in identifying the FLU (1) by use of a held-out test data for 2016 (the same year as training data) and applying a three-fold approach, and (2) using the test dataset of FLU for 2020 (Section. 3.3.4). For each model, we used Precision $P = TP/(TP + TN)$, Recall $R = TP/(TP + FN)$, F1-scores $F1 = 2 \cdot P/(P + R)$, micro-and macro average of F1-scores as the evaluation metrics, where

TP , TN and FN stand for true positives, true negatives and false negatives, respectively. More details can be seen in (Masolele et al., 2021).

3.2.6 Wall to Wall Prediction

Once the best-performing satellite imagery and DL model was identified using the F1-score Section 3.2.5, we then used this satellite imagery and model to predict land-use following deforestation in Ethiopia for the study period of 2016 using the areas known to be covered by tropical forest in 2010 (FAO, 2010) and forest loss data in 2010-2014 as a mask (Hansen et al., 2013).

After land-use were classified we estimated the proportions of each of land-use following deforestation per loss area based on Ethiopian regions (Abebe et al., 2019; FAO, 2010) and forest type (Dinerstein et al., 2017). This is important to show the patterns and dominance of different deforestation drivers for each regions and forest type for better conservation actions and data-driven land-use policy decisions.

3.2.7 Accuracy assessment of the Wall-to-Wall Product

To evaluate the accuracy of the final wall-to-wall land-use product, we conducted independent assessments based on the visual interpretation of bi-annual Planet images. We used stratified estimation of area, and accuracy Olofsson et al., 2014 to estimate the number of samples required to assess the output map of direct drivers of forest loss. First, the area of each land-use class was estimated from the map product, followed by calculating the proportion of each class of drivers of forest loss. For each class, sample estimation weights were calculated. The resulting weights were used to calculate the number of samples required to assess the accuracy of the map for each land-use class. In total, 770 samples were collected and interpreted (Figure 3.17). Following these, the accuracy of the map was calculated using the F1-score, user's and producer's accuracies.

3.3 Results

We start by presenting the results of classification of FLU for single-date, multi-date and an ensemble of Planet-NICFI, Sentinel-2 and Landsat-8 images using deep learning model (namely Attention U-Net), for identifying the FLU in Ethiopia. In Section 3.3.1 we present the FLU classification results comparing the performance of U-Net and Attention U-Net models. We then explore the classification results of FLU based on single-date Planet-NICFI, Sentinel-2, and Landsat-8 data using the attention U-Net model (Section 3.3.2). In Section 3.3.3 we report the performance of FLU classifications from single-date image prediction, multi-date image prediction, and ensemble of multi-sensor image prediction, using test data from same year as training data (2016). In Section 3.3.4 we compare the accuracy score of FLU prediction using forest loss test data from year 2016 and year 2020.

Eventually, in section 3.3.6, we show the spatial pattern & proportions (%) of land-use following deforestation per region and forest type in Ethiopia.

3.3.1 Model Comparison

In this section we highlights the advantage of adding the attention mechanisms to the standard U-Net model using Planet-NICFI data. The Attention U-Net model achieved relatively higher accuracy than the standard U-Net model (Figure 3.4). For most FLU classes both models obtain near similar levels of accuracy except for FLUs with smaller footprints such as small-scale agriculture, settlement, and Roads where the standard U-Net, tends to lag behind the Attention U-Net by a large margin (Figure 3.4).

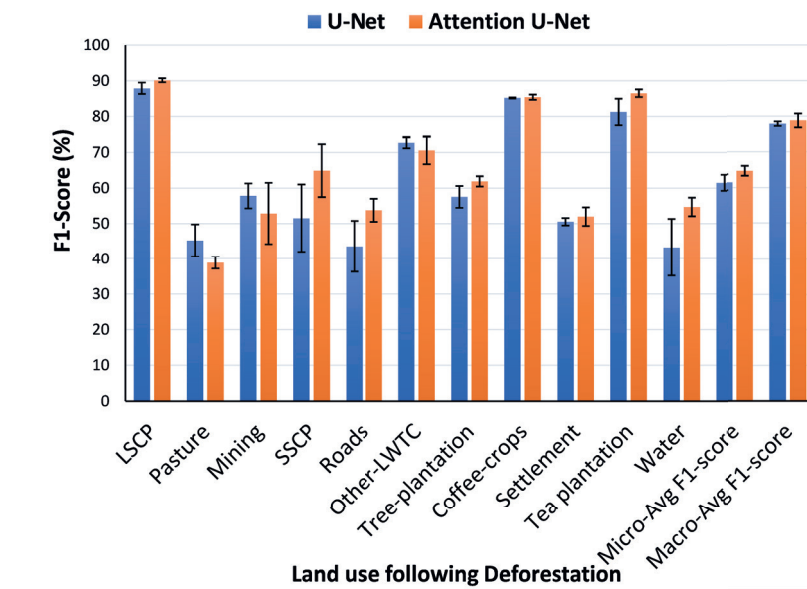


Figure 3.4: The classification F1-scores of FLU using standard U-Net, and Attention U-Net models in Ethiopia. SSCP and LSCP correspond to small-scale cropland and large-scale cropland, while Other-LWTC correspond to other land with tree cover. For each F1-score, we show the standard deviation represented as error bars.

3.3.2 Performance of single-date Planet-NICFI, Sentinel-2 and Landsat-8 satellite imagery.

The FLU classification model based on single-date Planet-NICFI data outperformed the models based on single-date Sentinel-2, and Landsat-8 data, as shown in Figure 3.5. The Planet-NICFI model attained a macro and micro-average F1-score of 79%, 65% compared to 70%, 59% for Sentinel-2, and 70%, 54% for Landsat-8 model.

The higher score by planet-NICFI model is particularly observed for the FLU type, large-scale cropland (90%), mining (53%), small-scale cropland (72%), roads (54%), coffee crops (86%), settlement (52%) and tea plantation (85%). The exception is water where Sentinel-2 and landsat-8 based models outperformed Planet-NICFI based model, possibly due to additional spectral bands in the short-wave region of the spectrum useful for monitoring water variability (Figure 3.5). On the other hand pasture, and small-scale cropland are likely to be incorrectly predicted as other land with tree cover by (27%, 12%), respectively. Settlements and tree plantations are often misclassified as other land with tree cover, 31% and 43% of the test samples respectively. (Figure 3.16). This results are based on image acquired on a single time-step.

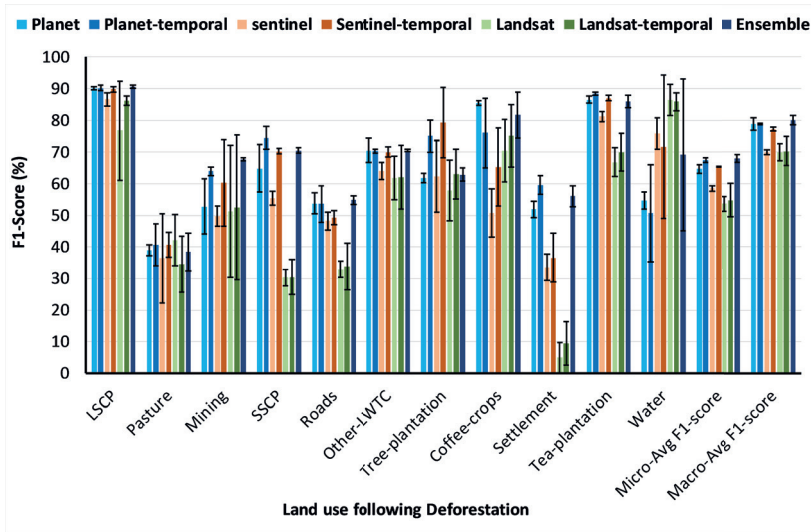


Figure 3.5: The classification F1-scores of FLU using Attention U-Net models in Ethiopia. The F1-scores are based on single-date, multi-date, and an ensemble of image predictions for Planet-NICFI, Sentinel-2 and Landsat-8 data. SSCP and LSCP correspond to small-scale cropland and large-scale cropland, while Other-LWTC correspond to other land with tree cover. The error bars are the standard deviation on F1-scores.

3.3.3 Performance of single-date image predictions, multi-date image predictions, and ensemble prediction.

As we expected, the F1-classification scores were higher for the single-date planet-NICFI, ensemble and multi-date medium resolution image predictions compared to the single-date medium resolution images predictions (Figure 3.5).

Interestingly, the increase in F1-score when moving to multi-date imagery is only consistent in the case of Sentinel-2 imagery, where it improves for all classes and for the overall FI-scores. For example, prediction accuracies increased for large-scale croplands (from 87%

to 90%), coffee crops (from 51% to 66%), mining (from 50% to 52%), Roads (from 48% to 50%), and tea Plantation (from 81% to 87%). Also, higher micro (59% to 66%) and macro (70% to 77%) average F1-scores were obtained. In the case of Landsat-8, improvement in F1-score is observed mostly for large-scale land-uses such as large-scale cropland (from 77% to 86%), tree-plantation (from 58% to 63%), coffee-crops (from 71% to 75%), and tea-plantation (from 67% to 70%). For planet-NICFI improvement in F1-score is observed for small scale land-uses such as mining (from 53% to 64%), small-scale croplands (from 65% to 74%) and settlement (from 52% to 60%) (Figure 3.5).

3.3.4 Temporal robustness

We further analysed the robustness of our approach over independent data (Planet-NICFI) from different time step (2020), based on forest loss from 2015 to 2019. The earlier FLU predictions using Planet-NICFI images of 2016 (Figure 3.5) are based on forest loss from 2010 to 2014. The 2016 FLU prediction results are compared with FLU prediction results from 2020 test data. This step is necessary to investigate the capability of our approach in generalizing across spatial locations and time. As indicated in Figure 3.6 relatively similar micro and macro average F1-scores (65%, 64% and 79%, 79%) were obtained when predictions are made for year 2016 and 2020.

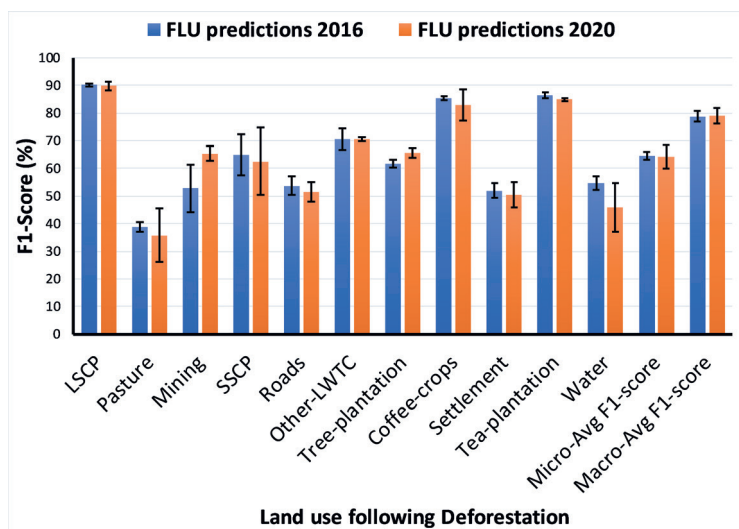


Figure 3.6: The classification F1-scores of FLU using for planet-NICFI images acquired in year 2016 and 2020. SSCP and LSCP correspond to small-scale cropland and large-scale cropland, while Other-LWTC correspond to other land with tree cover. The error bars are the standard deviation on F1-scores.

3.3.5 Wall-to-wall product

The accuracy assessment of wall-to-wall map using stratified estimation of area and accuracy using planet-NICFI showed the reliability of the final land-use following deforestation product produced by the attention U-Net model. Most validated FLU had an accuracy higher than 0.8% (Table 3.1), with the exception of mining (0.73%). These accuracy results are consistent with the model performance accuracies obtained in Section 3.3.3, which further proves the robustness of our proposed method for mapping land-use following deforestation.

Table 3.1: Accuracy metrics of the wall-to-wall map from independent sampled validation data. SSCP and LSCP correspond to small-scale and large-scale cropland and PF for plantation forests. The \pm are the 95% confidence intervals for each class.

FLU	User’s accuracy (%)	Producer’s accuracy (%)	F1 (%)
LSCP	95 \pm 3.6	92 \pm 4.5	94 \pm 3.9
Pasture	84 \pm 10.2	88 \pm 9.0	86 \pm 9.6
Mining	100 \pm 0.0	57 \pm 13.7	73 \pm 12.3
SSCP	90 \pm 8.3	94 \pm 6.5	92 \pm 7.5
Roads	96 \pm 5.4	100 \pm 0.0	98 \pm 3.8
PF	86 \pm 9.6	88 \pm 9.0	87 \pm 9.3
Coffee	97 \pm 4.7	92 \pm 7.5	94 \pm 6.6
Settlement	94 \pm 6.6	96 \pm 5.4	95 \pm 6.1
Tea	96 \pm 5.4	100 \pm 0.0	98 \pm 3.9
Water	100 \pm 0.0	80 \pm 11.1	88 \pm 9.0

3.3.6 Regional patterns of land-use following deforestation.

Using the HRSI and attention U-Net, we classify and map the FLU per forest loss location in Ethiopia based in regions and forest types were forest loss occur. The map in Figure 3.7 shows forest being heavily cleared for the establishment of small-scale croplands in regions like SNNPR², Oromia, Gambela and Benishangul Gumuz Figure 3.8a. Small tract of forest have also been cleared for small-scale croplands in Amhara region. Bright hotspots of forest loss for coffee crops are most prevalent in the north west and east of SNNPR and Gambela region respectively, while large-scale croplands is most prevalent in Gambela, Benishangul Gumuz, SNNPR and Oromia regions respectively. Nevertheless, we can also see a confusion between small-scale cropland with pasture and other land with tree cover, particularly in Gambela and Benishangul Gumuz. Another confusion can be seen in SNNPR between other land with tree cover and coffee crops (mainly in the district of Guraferda) Figure 3.13. In (Figure 3.7), we show detail maps (zoomed in) of some of the areas indicated by B, C, D, E, F, and G. Detail maps shows the local patterns exhibited

²Since 2020 SNNPR has ‘split off’ into two regions, Sidama & South West Ethiopia Peoples’ regions. Here we are referring to the region before the split.

by each type of land-use following deforestation including, (B) Coffee crops (teal), (C) Small-scale cropland (orange) and settlement (pink) (D) Roads (red), settlement (pink) and dam construction in the woodlands of Benishangul Gumuz (E) Large-scale croplands (yellow) (F) small-scale croplands and (G) Tea plantations (cyan). New roads (red), as detected in (D), (E), (F), and (G), provide accessibility to patches of land-use.

Likewise, the results of FLU prediction based on forest types (Figure 3.8b) follows similar spatial patterns to predictions based on regions (Figure 3.13, Figure 3.7). Small-scale cropland is the dominant FLU observed in all Ethiopian forest types.

Croplands (SSCP, LSCP, coffee and tea plantations) dominate the FLU in all of the regions and all of the forest types (73%, 15%, 0.75%, 0.21%), with the majority of small-scale croplands establishments being observed in the Ethiopian montane forests, especially on forest edges, while large-scale croplands are observed in montane grasslands and shrublands, deserts and xeric shrublands, as well as tropical and subtropical grasslands, savannas and shrublands (Figure 3.8b).

3.4 Discussion

Our results confirm the usability of U-Net Ronneberger et al., 2015 style CNN architectures for large scale FLU mapping using either Landsat-8, Sentinel-2 or Planet-NICFI imagery. They also show that it is advantageous to use a multi-class version of Attention U-Net Oktay et al., 2018.

As expected, we observed a strong correlation between spatial resolution and FLU classification performance, with Planet-NICFI imagery resulting in the best overall results even if it provides less spectral resolution than the other sources (Section. 3.3.2). This confirms that more detailed spatial features are vital to differentiate the FLUs, especially the FLUs with smaller footprints such as settlement, roads and small-scale cropland. Visually, this is also true as small features are easily identifiable with high resolution images at local level, as opposed to coarser resolutions, possibly due to mix of different land-use practices at a coarser spatial scale i.e., new roads passing through forest, or new village settlements.

Additionally, we also observed that the use of multi-date data for medium resolution images allows to close the accuracy gap with high-resolution imagery, at least for Sentinel-2 data (Figure 3.5). This shows that for medium resolution images, temporal patterns of land-use can compensate from the loss of spatial information stemming from the coarser spatial resolution with respect to the Planet-NICFI imagery, particularly when the problem includes small-scale agriculture and coffee crops. On the other hand this might suggest a higher level of the temporal variability that distinguish every land-use, probably because of variation in seasonality and land-use practices in Ethiopia (Masolele et al., 2021).

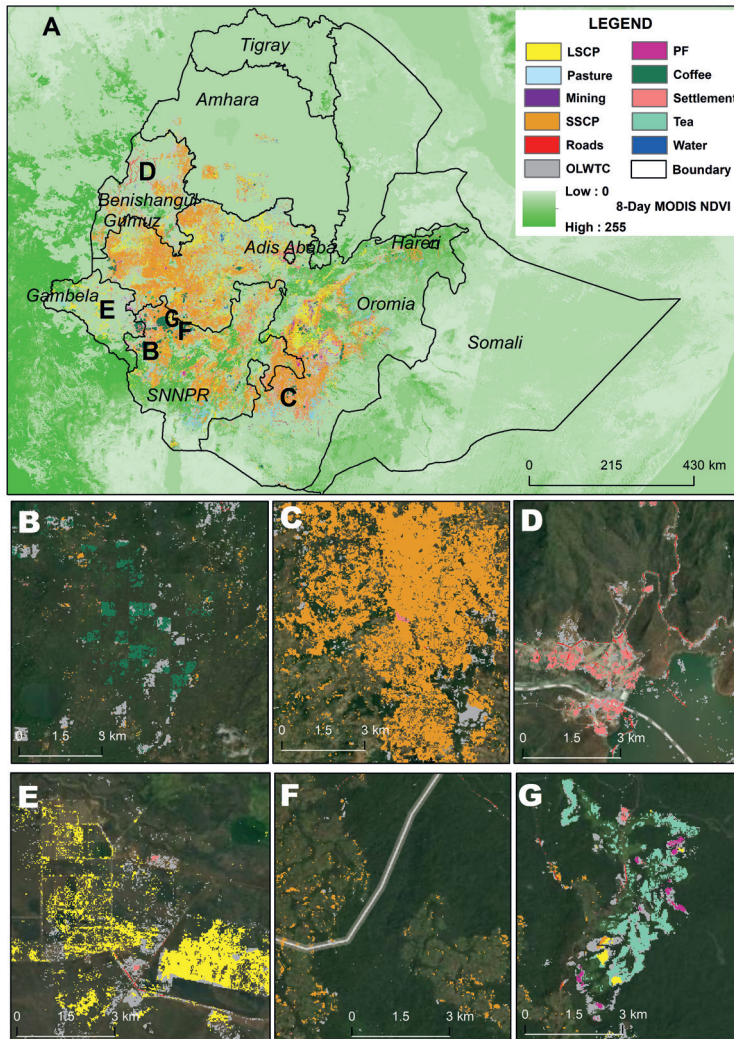


Figure 3.7: Classified land-use post-deforestation for the Ethiopia tropical forest for the period 2010 through to 2014. The green in A is NDVI basemap showing areas with forest cover as retrieved from USDA, 2017. Areas indicated by B, C, D, E, F and G are shown in zoomed in maps. Zoomed in maps show local patterns of the follow-up land-use with planet-NICFI as a base map. (B) Coffee crops (teal), (C) Small-scale cropland (orange) and settlement (pink), (D) Roads (red), settlement and dam construction (pink) in the woodlands of Benishangul Gumuz, (E) Large-scale croplands (yellow), (F) small-scale croplands (orange), and (G) Tea plantations (cyan). New roads (red) as detected in (D), (E), (F), and (G) provides accessibility to patches of land-use. SSCP, LSCP, PF correspond to small-scale cropland, large-scale cropland, and tree plantation while OLVTC correspond to other land with tree cover.

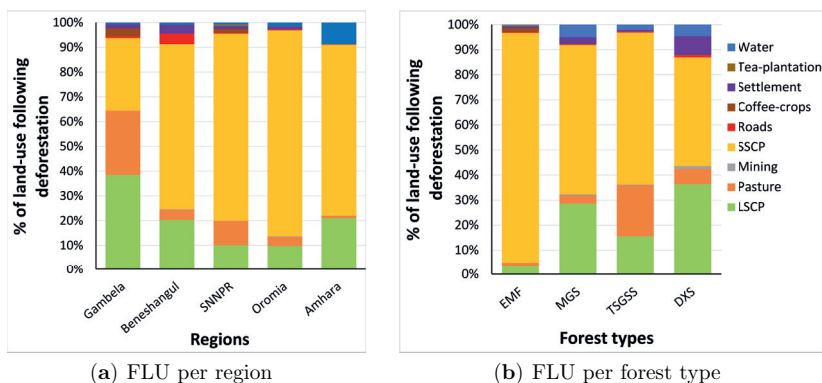


Figure 3.8: Proportions of post-deforestation land-use, (a) per region, and, (b) per forest type, for the Ethiopia tropical forest for the period 2010 through to 2014. SSCP correspond to small-scale cropland, LSCP to large-scale cropland, EMF to Ethiopia montane forests, MGS to montane grasslands and shrublands, TSGSS to tropical subtropical grasslands-savanna and shrublands, and DXS to Deserts and Xeric shrublands.

The performance of all models using the three datasets in identifying pasture versus other FLU classes is relatively low, indicating that pasture is indeed often mixed with other FLU i.e., small-scale croplands, settlement, and other land with tree cover. This is due to the fact that small holder farmers in Ethiopia keep their livestock close to home and bring them food and water to preserve the newly acquired deforested areas for farming and housing (Dow Goldman et al., 2020). On the other hand, pasture is a rare class, indicating that even greater amount of training data or even temporal data across the same seasons for pasture would be required to cover the spatial heterogeneity of pasture in Ethiopia.

In Section. 3.3.6 we observed that the class other land with tree cover, which includes forest regrowth, is over-predicted in most regions (Figure 3.13). This is because, although forest loss was detected, the transition to land-use classes such as agriculture, coffee, tea is a slow process and takes time. Looking at the satellite imagery (Figure 3.14), we see that the forest is cut down in several steps, where parts of the forest are deforested at different points in space and time. Since we use a single deforestation map for the whole period, this can lead to ambiguities in which the model may confuse forest regrowth with yet-to-be cut down forest. A potential solution for next research would be to start looking at what would be the best lag time to detect land-use after deforestation. Our assumption is that the model would perform better in an older deforested area as the land-use are more distinct after few years of human activities (Figure 3.14). It is also important to note that not all detected forest changes (i.e., in Hansen et al., 2013) were due to land-use conversion, as some of it may also be detected as a result of fire, landslides, and floods, which were not considered in this study.

Small-scale croplands is the dominant cause of forest loss in all regions and forest types of Ethiopia, Figure 3.8a, Figure 3.8b and Figure 3.13. Most of the small-scale clearing occurs at the edge of the forest, as seen in Figure 3.15. This is the common practice, as deforestation is done by small-scale farmers, often families, who farms a mixture of food, fruit crops, and livestock herds for some years, and when the soil loses its fertility they let the farms go fallow (Dow Goldman et al., 2020). Forest conversion into large-scale cropland is the second main driver of forest loss. The LSCP typically involves large-scale clear-cutting and are grown on an industrial scale (Figure 3.13, Figure 3.7). Most LSCP hotspots can be seen in Gambela, Benishangul Gumuz and SNNPR regions, and in all forest types with the exception of Flooded Grasslands & Savannas, indicating that LSCP is not limited to a single forest type or region (FAO, 2010).

In addition to small and large-scale cropland, the third and fourth dominant drivers of forest loss are pasture and settlement, respectively (Figure 3.8a and Figure 3.8b). This observation is in line with the results of recent similar studies (Betru et al., 2019; Hishe et al., 2021; Mengist et al., 2021; Sisay et al., 2021; Yahya et al., 2020) which used Landsat satellite imagery and focus group discussion to assess proximate drivers of forest loss in different parts of Ethiopia. However, these studies were conducted on few isolated study areas (local scale) and do not provide detailed identification of drivers of forest loss (fewer classes). Our research goes beyond small-scale, pixel-based methods, coarse spatial resolution benchmarking tasks to national scale, deep learning method and higher spatial resolution images. The increased spatial resolution of the satellite dataset (Planet-NICFI) to 5m, allows for more accurate and detailed identification of small features and those with fine spatial textures such as roads, mining, coffee crops and village settlement which would otherwise not be included (NICFI, 2021).

Our study contributes to reducing methodological, data, and knowledge gaps in more direct measures of proximate drivers of deforestation in Ethiopia based on satellite image assessments by using a robust semantic segmentation deep learning method. For small-scale and large-scale cropland, pasture, settlements, coffee-crops, roads, and mining, all of which are identified in dramatic forest declines in Ethiopia (Betru et al., 2019; FAO, 2010), our method provides a way of mapping the extent of these drivers on forest resources at a national scale. Even for drivers for which satellite imagery maps of land-use conversion exist (for example, agriculture and forest loss), our results provide additional information by offering higher thematic detail. Regional and global analyses (Curtis et al., 2018) have also incorporated information about spatial distributions of land-use to account for where drivers are likely to affect most forest. However, while important, such analyses still assume that drivers of deforestation are uniformly likely across the national scale. Our results show that patterns of deforestation drivers often differ at national scale based on region and forest type. This disparity in part relates to traditional representations of mainly dominant land-use leaving-out some types of land-uses (for instance, 'roads' providing accessibility to forests or dams, i.e., in Benishangul Gumuz (Figure 3.13), 'Mining' established deep

within forests, 'new settlements' and/or lack of distinction between small and large-scale cropland) (Curtis et al., 2018; FAO, 2010; Mengist et al., 2021). In addition, the effect of these drivers varies with the specific spatial context, so the same intensity of forest loss can have different impacts in different regions or on different forest type (Betru et al., 2019; FAO, 2010; Hishe et al., 2021; Mengist et al., 2021; Sisay et al., 2021; Yahya et al., 2020). For example, small-scale croplands affect a larger proportion of forests in Amhara and Benishangul Gumuz, where a bit of primary forest is left, than in the Gambela, SNNPR and Oromia where considerable forest remains inspite high rates of forest loss in both regions (Hansen et al., 2013). The opposite is true for large-scale croplands. This in turn may also affect the choice of policy process (reforestation or more conservation) to be implemented in either regions.

In summary, although Planet-NICFI or multi-temporal Sentinel-2 data obtained a substantially higher F1-score in identifying most of the FLU classes compared to single-time Sentinel-2 and Landsat-8, the latter can still be seen as an alternative when focusing on certain land-use classes. This is especially true in identifying large scale land-uses such as large-scale cropland where Planet-NICFI images had relatively similar accuracy as Sentinel-2 and Landsat-8 imagery (Figure 3.5). Thus the latter are suitable in regions where large scale land uses are a dominant cause of deforestation as it does not require intensive computational resource for analysis (Table 3.3). However, in regions where small scale land-uses (i.e., Mining, small-scale cropland, settlements) are a threat for deforestation Planet-NICFI would be the best choice for achieving higher classification accuracies (Figure 3.5). However, it is important to keep in mind that the use of Planet-NICFI for this type of analysis requires more computational resources (Table 3.3). Here, the use of open-source cloud-based computational platform like SEPAL (FAO, 2021) offers an opportunity to overcome this problem. Ethiopia is piloting the use of Planet-NICFI using SEPAL, which shows that such computational resources is accessible for developing countries like Ethiopia given the right mix of training and tools, opening new paths for the monitoring of the proximate drivers of deforestation at country and, eventually, continental scale.

3.5 Conclusion

This paper presents the use of high and medium resolution open-access satellite imagery for identifying post-deforestation land-use on a country-level using an Attention U-Net deep learning segmentation method. The land-use classification strategy was applied to a single-date, multi-date and an ensemble of Planet-NICFI, Sentinel-2 and Landsat-8 satellite data. This process relies on the use of a forest loss dataset to select forest loss areas, followed by the creation of a reference dataset through the visual interpretation of land-use following deforestation using Planet-NICFI imagery. Experimental results show that the performance of identifying and mapping land-use following deforestation

requires either (1) the use of high resolution satellite imagery or (2) use of temporal data for medium resolution satellite imagery. We also observed that the addition of an attention mechanism to the standard U-Net segmentation model increases model performance.

Our approach can support a more detailed spatial and temporal analysis of forest loss locations and its proximate drivers. The main contribution of our method is that it presents a new opportunity and possibility to identify land-use. The model can help identify and inform how forest in Ethiopia is currently being affected by a wider range of land-use activities than is currently thought. They can also help report previous and future proximate drivers assessments by providing a more systematic and updated understanding of potential drivers hotspots over the local and national scale.

Thus the value of this paper is in illuminating spatial patterns of deforestation drivers and elucidating an approach to identifying causes as well as aid in decision making within the context of national policy processes, recognizing that understanding the location of different proximate drivers of forest loss is vital for setting up effective forest conservation policy and responses.

In future research, we intend (1) to start looking at what would be the best time to detect land-use after deforestation, (2) to quantify the trend of pre-dominant drivers of forest loss over national and/or continental scale applied for previous and more recent time periods while leveraging seasonality, the availability of dense time series of HRSI and the free and open-source global forest loss data Hansen et al., 2013; Reiche et al., 2021 through attention U-Net deep learning method.

3.6 Appendix

3.6.1 Diagrams of individual deep learning model architectures

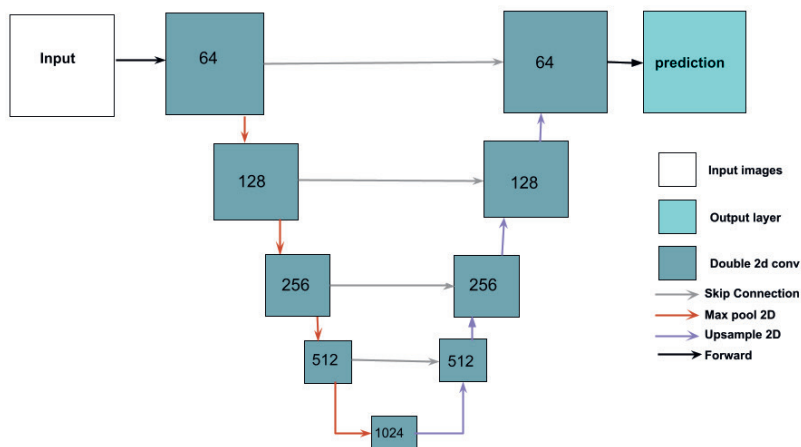


Figure 3.9: Schematic view of our U-net network for single-date images input. Inputs are tensors of size i width \times j height \times n bands. The colors represent, white = Input array, teal = Double 2D convolution operations, and cyan = output layer.

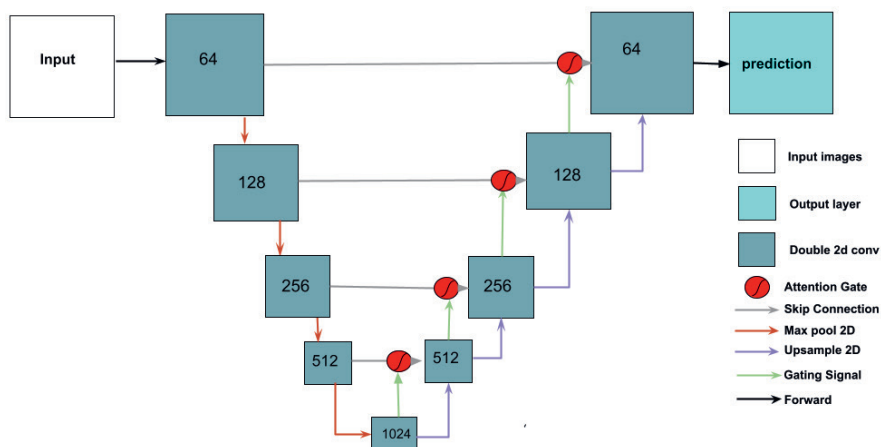


Figure 3.10: Schematic view of our attention U-net network for single-date images input. Inputs are tensors of size i width \times j height \times n bands. The colors represent, white = Input array, teal = Double 2D convolution operations, red = Attention gate, and cyan = output layer.

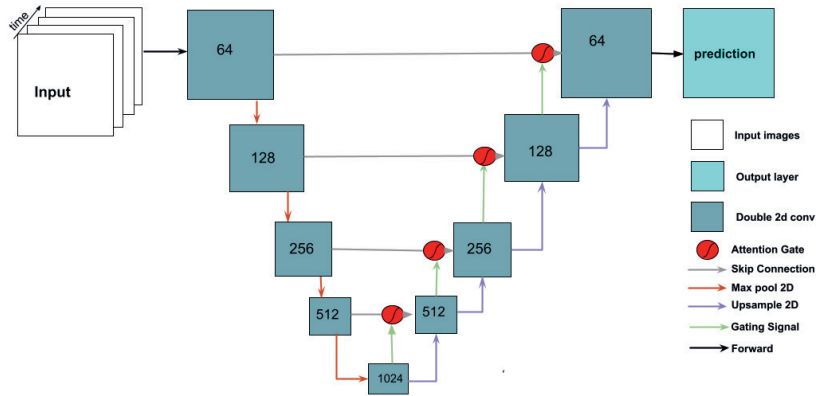


Figure 3.11: Schematic view of our Attention U-net network for multi-date images input. Inputs are tensors from four time steps (time 1 to time 4), each of size t time steps \times i width \times j height \times n bands. The model operates on a sequence of four input tensors, each composed of n bands. The network architecture automatically detect the useful features of the multiple input bands and combines this information for the following layers to predict the Land-use following deforestation. Note that this model setting is also useful to handle scenarios where either one of the input images are affected by clouds.

3.6.2 Model parameters

Table 3.2: Architecture of a standard U-Net, attention U-Net, temporal attention U-Net, and Ensemble of multi-sensor attention U-Net models

Parameters	Model Type and Dimensions			
	standard U-Net	attention U-Net	temporal attention U-Net	Ensemble
Input shape Planet-NICFI	128 x 128 x 7	128 x 128 x 7	128 x 128 x 28	128 x 128 x 28
Input shape Sentinel-2	64 x 64 x 12	64 x 64 x 12	64 x 64 x 48	64 x 64 x 48
Input shape Landsat-8	32 x 32 x 12	32 x 32 x 12	32 x 32 x 48	32 x 32 x 48
No. Conv layers	20	20	20	20
No. filter encoder	32, 64, 128, 256, 512, 1024	32, 64, 128, 256, 512, 1024	32, 64, 128, 256, 512, 1024	32, 64, 128, 256, 512, 1024
No. filter Decoder	32, 64, 128, 256, 512, 1024	32, 64, 128, 256, 512, 1024	32, 64, 128, 256, 512, 1024	32, 64, 128, 256, 512, 1024
Filter size	3 x 3	3 x 3	3 x 3	3 x 3
Padding	same	same	same	same
Pool size	2 x 2	2 x 2	2 x 2	2 x 2
Strides	1 x 1	1 x 1	1 x 1	1 x 1
Attention gate	-	yes	yes	yes
Learning rate	0.0001	0.0001	0.0001	0.0001
No. Classes	11	11	11	11

3.6.3 Workflow of this study

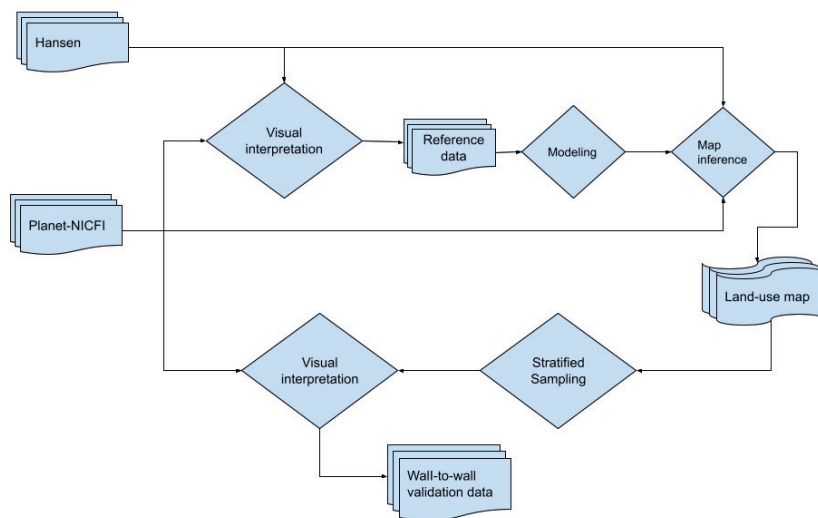


Figure 3.12: The flowchart showing the steps in data generation, modeling, map validation in our study

3.6.4 Spatial patterns of land-use following deforestation

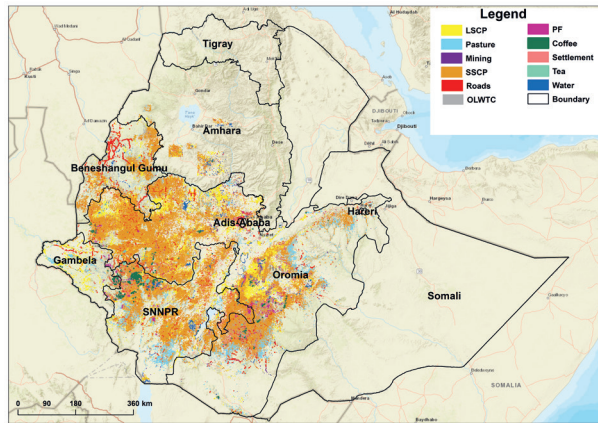


Figure 3.13: Spatial pattern of classified land-use following deforestation for the Ethiopia tropical forest for the period 2010 through to 2014. The map shows the follow-up land-use predicted using planet-NICFI image. Street map is used as a base map for display. SSCP and LSCP correspond to small-scale cropland and large-scale cropland, PF to tree plantation, and OLWTC to other land with tree cover.



Figure 3.14: Represents the planet-NICFI images, showing how FLU evolves over time from deforestation. This is one of the patches of land-use following deforestation (large-scale cropland) in Ethiopia where changes happened over n-years, (a) Planet-NICFI image 2016, (b) Planet-NICFI image 2017, (c) Planet-NICFI image 2018 and, (d) the Planet-NICFI image 2020, respectively.

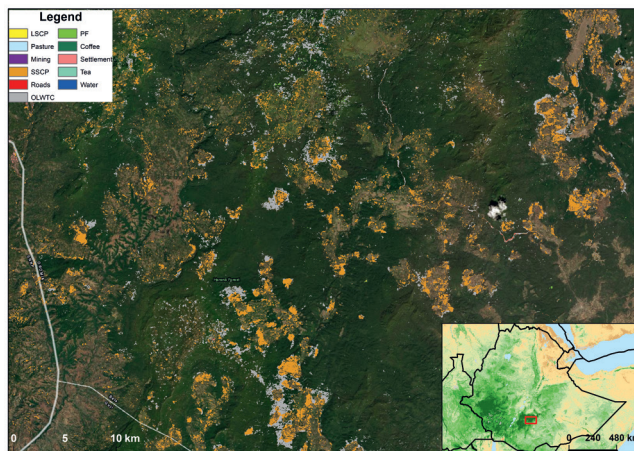


Figure 3.15: Classified land-use following deforestation for the Ethiopian tropical forest for the period 2010 through to 2014. Areas in orange color are the predicted small-scale clearing occurring at the edges of the forest. Roads in red color provides accessibility on new established patches of land-use following deforestation. SSCP and LSCP correspond to small-scale cropland and large-scale cropland, PF to tree plantation, and OLWTC to other land with tree cover.

3.6.5 Wall-to-wall validation samples

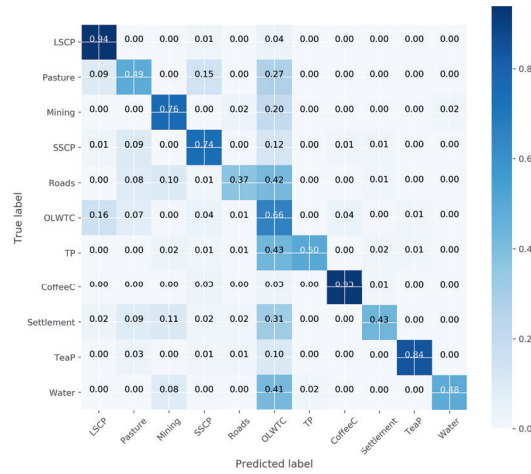


Figure 3.16: The percentage of true- and false predicted FLU's using attention U-Net deep learning method and Planet-NICFI images. SSCP and LSCP correspond to small-scale cropland and large-scale cropland, TP to tree plantation, TeaP to tea plantation, and OLWTC to other land with tree cover.

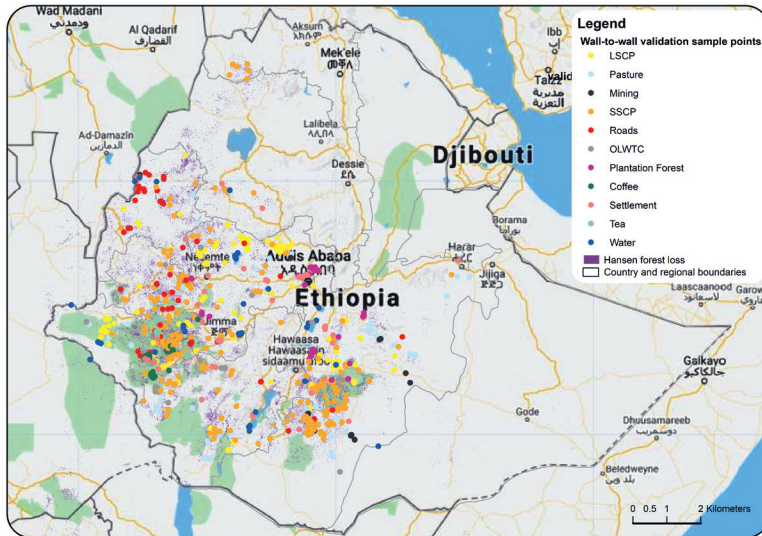


Figure 3.17: Visually interpreted data used for wall-to-wall validation of the land-use following deforestation product. SSCP and LSCP correspond to small-scale cropland and large-scale cropland, and OLWTC to other land with tree cover.

3.6.6 Computational Considerations

The use of high resolution Planet-NICFI and ensemble of multi-sensor data was more computationally expensive during training versus using the Sentinel-2 and Landsat-8 data (Table 3.3). This is due to the high number of pixels per unit in planet-NICFI data compared to Sentinel-2 and Landsat-8 data resulting in increasing computational resource and time demand. Likewise ensemble model requires training multiple models to retrieve predictions, hence requiring more time on data preparations for training, testing and when making predictions. Likewise in testing time we also observed slight differences between the datasets. This is useful information in relation to resource availability. The choice of whether to use high-resolution images or ensemble or high temporal medium resolution images will depend on available computational resources and time.

All data preprocessing, analysis and model development were done in (SEPAL 2.0). A cloud-based computing environment of FAO with instance type g8, NVIDIA Tesla M60 GPU 32GB RAM.

Table 3.3: The time for training and testing in minutes (m) of attention deep learning models using Planet-NICFI, Sentinel-2, and Landsat-8 datasets over a single-date, Multi-date and ensemble approach.

Model	Planet-NICFI		Sentinel-2		Landsat-8		Ensemble (Planet-NICFI,Sentinel-2,Landsat-8)	
	Training(m)	Testing(m)	Training(m)	Testing(m)	Training(m)	Testing(m)	Training(m)	Testing(m)
Single-date	1880.47	3.96	212.58	2.45	115.39	1.55	2208.4	6.96
Multi-date	4300.02	5.52	621.55	3.56	219.14	2.212	5140.71	8.63

CHAPTER 4



Deforestation, follow up land use and regrowth dynamics in Cote D'ivoire 2000-2019

This chapter is based on:

R. N. Masolele, Mathieu Decuyper, D. Marcos, V. D. Sy, Nandika Tsendbazar, Tor Vagen, and M. Herold (2022). Deforestation, follow up land use and regrowth dynamics in Cote D'ivoire 2000-2019.

Abstract

Primary forests in Cote D'ivoire are increasingly impacted by human land-use activities causing forest loss. Yet, efforts to mitigate the impact of these human-induced land-use changes are hampered by the limited availability of spatial and temporal information and thematic details of the land-use causing forest loss. In this study, we use an Attention deep learning model, high-resolution planet-NICFI images (5m), and expert-based visual interpreted reference land-use data on nine classes to classify and map land-use following deforestation in Ivory Coast. Our results show that the developed Attention U-Net model has the capability of identifying and mapping land-use following deforestation with an overall accuracy of 84%. Additionally, we provide estimates that protected forests in Ivory Coast are under pressure mainly due to expansion for cacao, cashew, oilpalm, and rubber. Importantly we show distinct patterns of commodity crops, with cashew dominating in the northern regions(dry forests) and cacao in the southern regions (humid forests), respectively. This result provides a new perspective to re-thinking the mitigation efforts for climate change that focuses not only on cacao and humid forests but also includes cashew as a potential direct driver of forest loss in the dry forests of the Ivory Coast. More importantly, the proposed method provides a system for which land-use change and commodity crops can be monitored more frequently, wall-to-wall, and reproducible for operational monitoring by governments or companies. Specifically useful for companies who want to monitor that their source of commodity crops is free from deforestation.

4.1 Introduction

Primary forests in Cote D'ivoire are increasingly impacted by human land-use activities causing forest loss (FAO, 2017). Yet, efforts to mitigate the impact of these human-induced land-use changes are hampered by the limited availability of spatial and temporal information and thematic details of the land-use causing forest loss. Historically forest loss in Ivory Coast or Côte d'Ivoire, was caused by human migration since its independence from France in 1960. Especially from the seventies to the nineties, there was a large migration from the neighboring country Burkina Faso (Blion, 1996). The country has experienced various political and military crises in the last decades. The political unrest and civil war in 1999 and 2002 caused the transfers of people, lower income, farming losses, loss of cattle, and numerous victims. The conflicts after the failed coup in 2002 went on for decades and left the country split in two (Annan, 2014). These various political and military crises have direct or indirect negative impacts on the environment, such as forest cover loss (Nackoney et al., 2014). This was also the case in the Ivory Coast, where the migration of people and general population increase is seen as the major cause for the deforestation (Chatelain et al., 2010) and is also perceived as such by local farmers (Kouassi et al., 2021). Ivory Coast has one of the highest deforestation rates in Africa. The forest area in the country has declined from 16 million hectares in 1960 to 3.4 million hectares in 2015 (FAO, 2017).

Where the deforested land was mainly used for small-scale shifting agriculture there was a shift towards more permanent cash crops since the migration (Chatelain et al., 2010). One of the most known cash crops is cacao. Ivory Coast is the world's leading producer of cacao and the demand puts even more pressure on the already fragmented forest. The protected government forest of Haut-Sassandra is one example where forest fragmentation intensified during and after the period of conflicts, replacing most of the endemic species for cacao production (Barima et al., 2016). Cacao is one of the country's leading foreign exchange earners, accounting for 40% of the export income and 10-15% of the GDP (Group, 2008; Tano, 2012) (Tano, 2012; World Bank Group, 2019). The pressure on the production due to a rising demand for cocoa, together with decreasing production capacity due to disease prevalence and cocoa trees getting older only increases the pressure on the remaining forest. Despite numerous pledges and claims regarding zero-deforestation cocoa by governments, NGOs, and private companies, deforestation continues (Ruf and Varlet, 2017). While there are several certification schemes for sustainable cocoa in place, most certified farms are in areas where (most) forest has already been cleared, and farmers that are deforesting are not allowed to be certified in the first place, and thus not prevent deforestation (Kroeger et al., 2017). While cocoa replaced much of the rainforest in the south to south-west of the country, more recently, a vast amount of cashew monocultures are replacing savannas and dry forests in the north (Erik Hoffner, 2021). However, there are currently no clear estimates of forest loss related to the rise of cashew and other cash crops.

This study addresses the problem of identifying direct drivers of deforestation or drivers of forest loss in the Ivory Coast. We aim to quantify forest loss and characterize the land use that follows, with a specific focus on prevalent and emerging commodity crops (cacao, cashew, oilpalm, rubber). Assessing the direct drivers contributing to Ivory Coast deforestation is critical to effectively support and enforce targeted conservation efforts and protect its remaining intact forest as well as support restoration efforts. More importantly, this study is more valuable in the current trend where government organizations in developed countries are imposing legislation promoting imports of deforestation-free products, in this case, commodity crops (Bager and Lambin, 2022; EUROPEAN COMMISSION, 2022). Thus companies sourcing from Ivory Coast would be required to show that their products are free from deforestation.

To achieve this, we quantify forest loss and the land use that follows by combining two relatively new tools: the forest change detection method, AVOCADO, by Decuyper et al., 2022, and the Attention U-Net model to predict follow-up land use (LU) by Masolele et al., 2022. We use the freely available high spatial resolution images (Planet-NICFI) 4.77m (NICFI, 2021) to train an Attention U-Net model and later predict the follow-up land use on the remaining forest in Ivory Coast. Furthermore, we assess temporal changes in deforestation and commodity cash crops in these areas. It is important to note that the algorithm used in this study (AVOCADO) has been used successfully to detect forest loss and regrowth in both humid and dry forests in Africa, while the Attention U-Net model achieved higher performances in classifying land-uses following deforestation in Ethiopia (Masolele et al., 2022). The advantage of using the Attention U-Net model derives from its ability to integrate attention gates into the standard U-Net architecture (Ronneberger et al., n.d.) to highlight vital information that is shared via skip connections (Oktay et al., 2018; Schlemper et al., 2019).

4.2 Methods and Data

4.2.1 Study area

In this study, we focus on the ‘Forêts Classées’ (FCs), national parks and reserves in Ivory Coast (Figure 4.1). The FCs are designated areas in which the forest is managed via the Forest Development Corporation (SODEFOR), which gives exploitation rights to private companies (UNEP-WCMC, 2020). In the national parks and reserves, no exploitation is allowed. Despite the more controlled status of these areas, there are still many reports of illegal trade (WCF, 2015), and therefore we focus on these areas.

4.2.2 Forest change detection

The forest loss and regrowth detection were based on all available Landsat data (level-1 terrain-corrected) between 1990 and 2019. The change detection of the FC’s was done by

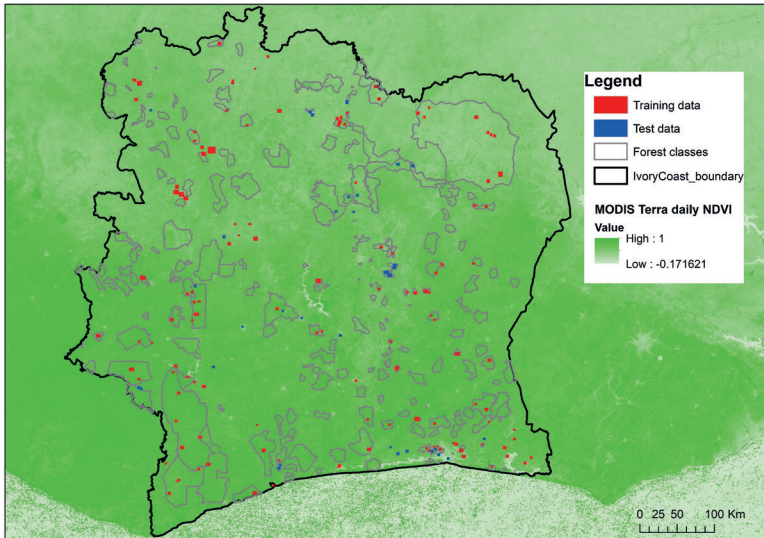


Figure 4.1: Map showing the location of ‘Forêts Classées’ (FCs), national parks, and reserves in Ivory Coast (polygons in grey color). The blue and red rectangular polygons show the spatial distribution of the training and test data across the Ivory Coast.

using the AVOCADO algorithm (Decuyper et al., 2022). Therefore we selected for each of the FC’s a nearby forest area as a reference forest and created wall-to-wall anomaly and change detection maps (see the detailed steps in Decuyper et al., 2022). This provides us with the information when a change (loss or regrowth) has occurred but does not give any information on the follow-up LU (Land-use).

4.2.3 Reference land-use data

A total of 200 images of size $\geq (2048 \times 2048)$ pixels containing forest loss locations were randomly sampled (Figure 4.1) using forest loss and regrowth products from Decuyper et al., 2022. The sampled locations were used as priors to annotate training and evaluation labels of post-deforestation land-use visually. We used high-resolution satellite imagery (HRSI), from Planet-NICFI, and Google Earth to visually interpret and collect reference sample data specifically for classifying drivers of forest loss in the Ivory Coast. In addition, other data sources from Econometric and the Center for International Forestry Research-World Agroforestry (CIFOR-ICRAF) were also helpful in interpreting and extracting land-use information. The collected labels consist of nine main classes of drivers of forest loss, namely: cacao, cashew, water, oil palm, rubber, natural forest, agriculture, built-up, and savanna.

Satellite Data We used mosaics of Planet-NICFI satellite imagery (NICFI, 2021) to automatically classify drivers of forest loss in Ivory Coast. The mosaics have a spatial resolution of 4.77m and temporal resolution of one month. Planet-NICFI image was used for this task due to its high spatio-temporal resolution, which provides more visual detail and less cloud cover, making it more useful than alternative satellite products for detailed assessment of drivers of forest loss (Masolele et al., 2022). The images come with four spectral bands, specifically - Blue, Green, Red, and Near-Infrared (NICFI, 2021). For our study we collected a median composite of Planet-NICFI images (December 2019 - December 2020) plus 3-vegetation indices (NDWI - the normalized difference water index, SAVI - the soil-adjusted vegetation index, and NDVI - the normalized difference vegetation index), resulting in a total of 7 bands.

4.2.4 Data Preprocessing

In total we used 200 Planet-NICFI image tiles of dimensions $\mathbf{x}_i \in \mathbb{R}^{w \times h \times d}$ and the corresponding FLU labels $\mathbf{y}_i \in \{0, 1\}^{w \times h \times c}$, where w , h and d specify the width, height and number of bands of an image and c specifies the number of classes. From 200 images we extracted a total of 525795 patches each having an overlap of three-quarters with others. This was essential to reduce the loss of data due to the border effects. The dimensions for each image patch were 256×256 pixels. We normalised each band $j \in \{1, \dots, d\}$ of each image patch x_i using a min-max such that all pixels are in the range of 0 and 1. The processed patches were later split into training, validation, and test data in a ratio of 80%, 10%, and 10%, respectively, (Figure 4.2).

4.2.5 Attention U-Net for classifying drivers of forest loss

Our work builds on the application of the Attention U-Net model developed by Masolele et al., 2022 for the classification of drivers of forest loss in Ethiopia. The architecture was chosen due to its proven ability to identify drivers of forest loss from satellite data. We used a pre-trained model on the Ethiopian dataset and fine-tuned it on the data collected for Ivory Coast. We assessed the performance of the model and the resulting maps of drivers of forest loss in the Ivory Coast. The advantage of using the Attention U-Net model derives from its ability to integrate attention gates into the standard U-Net architecture (Ronneberger et al., n.d.) to highlight vital information that is shared via skip connections (Schlemper et al., 2019).

4.2.6 Implementation Details

As discussed in the previous subsection, the model used for this study was adapted from Masolele et al., 2022. The model was developed using the Keras library and TensorFlow as the backend. Since the number and type of land-uses are different, we simply finetuned or modified the last layer to match the number of classes in Ivory Coast.

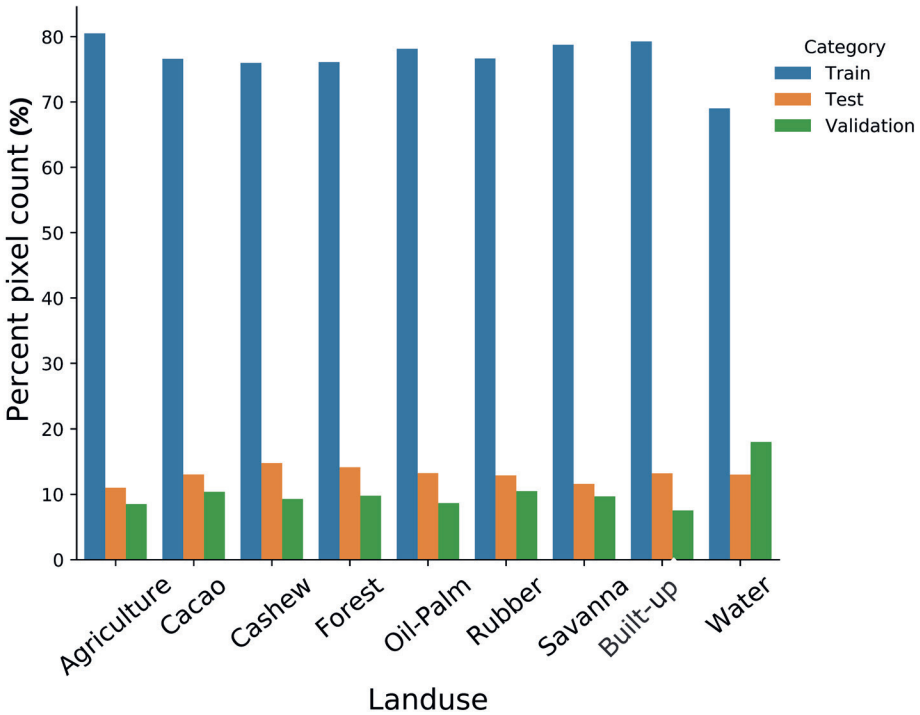


Figure 4.2: Shows the number of pixels in (%) for the training, validation, and test data over one of the random splits.

Other parameters remained unchanged. We trained the Attention U-Net model for 500 epochs using a batch size of 64. The multi-class categorical Focal Loss was used as an optimizer between the post-softmax probability and one-hot label corresponding to the type of driver in the image patch. The task of classifying drivers of forest loss was implemented and run in the Sepal geospatial analysis platform (SEPAL 2.0) FAO (2021). This is a cloud-based computing environment of FAO with instance type g8, NVIDIA Tesla M60 GPU 32GB RAM.

4.2.7 Model validation

We used Precision, Recall, F1-scores, micro-and macro average of F1-scores to evaluate the performance of the Attention U-Net model in classifying drivers of forest loss Masolele et al., 2022. The model performance in classifying the drivers of forest loss was validated using a held-out test data for 2020 (the same year as training data) and applying a three-fold approach.

4.2.8 Wall to Wall Prediction

After the model training and performance assessment was finalized, we then used the planet-NICFI mosaic imagery and the model to predict the drivers of forest loss in Ivory Coast that occurred between 2000 and 2019 using planet-NICFI imagery for 2020. Specifically, the driver prediction was based on areas considered to have the remaining forest in Ivory Coast and considering deforestation by Decuyper et al., 2022 (from 2000 – 2019). After the drivers were classified, we estimated the proportions of each driver per loss area Decuyper et al., 2022 based on a 5-year interval (2000-2004, 2005-2009, 2010-2014, and 2015-2019). This was done to show the temporal patterns and dominance of different deforestation drivers, thus its impact on forest conservation efforts.

4.2.9 Map accuracy assessment

We used stratified estimation of area and accuracy by Olofsson et al., 2014 to estimate the number of samples required to assess the output map of drivers of forest loss. The number of samples and accuracy were calculated based on four time periods of 5-year intervals (2000-2004, 2005-2009, 2010-2014, and 2015-2019) important for the assessment of change in the proportion of each driver of forest loss over the years. For each stratum (class), sample estimation weights were calculated based on the mapped area of each driver of forest loss for each time period. The resulting weights were used to calculate the number of samples required to assess the accuracy of the map for each driver over a five-year interval. A total of 545, 528,526, and 529 samples were used to assess the accuracy of the land-use following deforestation for the year 2000-2004, 2005-2009, 2010-2014, and 2015-2019. Following these, the accuracy of the map was calculated using the user's and producer's accuracies.

4.3 Results

4.3.1 Model Performance

The Attention U-Net model achieved an overall classification performance (F1-score) of 80%. The model performance results for each of the nine land-use types were; cacao (90%), cashew (68%), water (80%), oilpalm (79%), rubber (52%), Nature forest (92%), agriculture (89%), urban (92%), and savanna (72%) (Figure 4.3). From the result, we also observe that the class built-up and natural forest achieved the highest F1-scores compared to other land-use classes, which indicates the homogeneous nature of these land-uses.

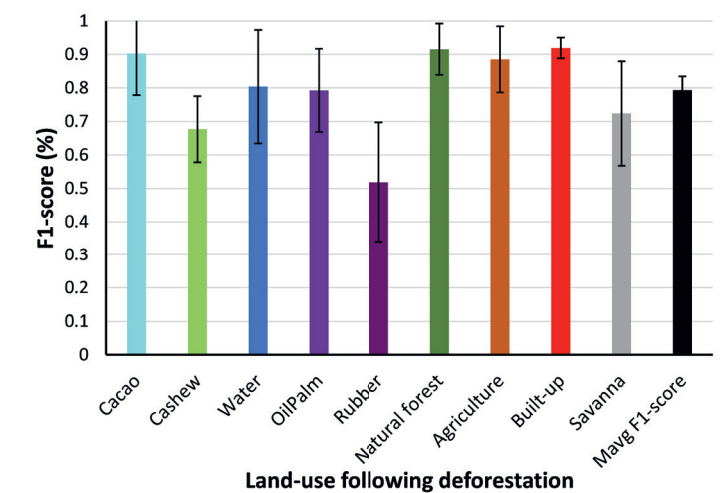


Figure 4.3: Model accuracies (F1-score) of land-use following deforestation. The error bar indicates the standard deviations of the F1-scores over three training cycles.

4.3.2 Change detection results

Using the Attention U-net model from (subsection 4.3.1), high-resolution planet-NICFI images for 2021, and forest regrowth data (Decuyper et al., 2022), we generated a wall-to-wall map of land-use following deforestation in Ivory Coast from 2000 to 2019 (Figure 5.5). The predicted map Figure 5.5 (right) shows that cashew is the dominant follow up land-use in the Northern regions, while forest-to-cacao conversion is more dominant in the southern regions of Ivory Coast. Likewise, the forest change detection results in Figure 5.5 indicates the spatial variation in time of deforestation from north to south, with earlier deforestation detected in the north (dark color) and recent deforestation detected in the southern regions, shown in light color, Figure 5.5 (left figure). In Figure 5.5, we also zoomed in to the FC's "Haut Sassandra which is an area with known forest conversion to cacao, and "Kobo" with recent cashew development.

4.3.3 Accuracies of the land-use map

After generating the map of land-use following deforestation for all forest classes in Ivory Coast (subsection 4.2.8), the next step was to validate the produced land-use map based on four periods (subsection 4.2.9). Our results of the comparison of the classified land-use map and reference land-use data indicated the reliability of our final predicted product of land-use following deforestation using the attention U-Net model. For the periods 2000-2004, 2005-2009, and 2010-2014, all validated land-use locations had users, producers, and F1-score higher than 73% with the exception of the user's accuracy for cacao in the period 2000-2004. Notably, the validation results for the period 2015-2019 showed a

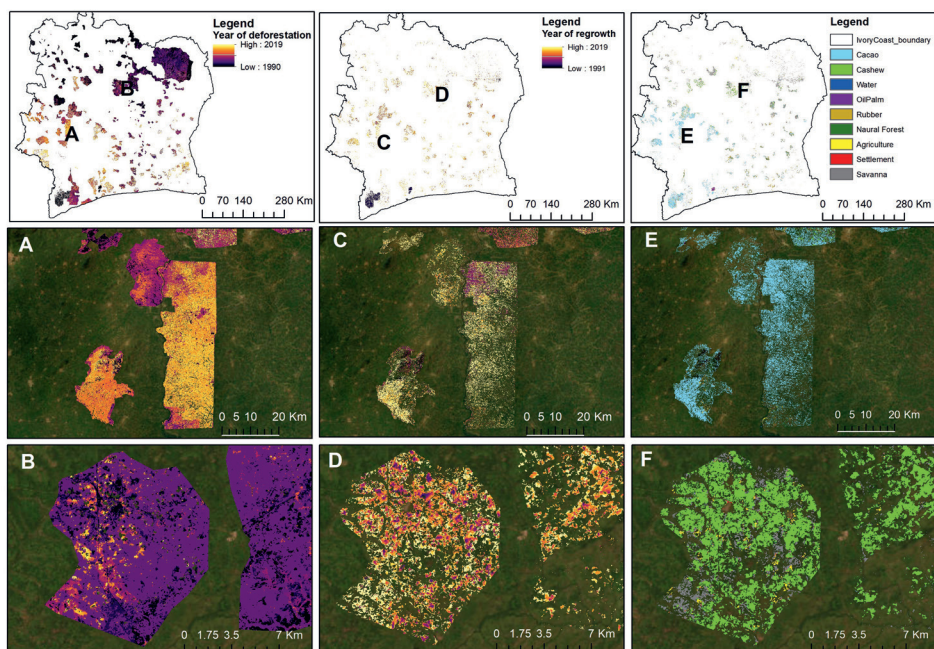


Figure 4.4: Map showing deforestation, regrowth, and follow-up land-use in Ivory Coast for the year 1990 to 2019. The land-use was predicted using planet-NICFI images on the ‘Forêts Classées’ (FCs), national parks, and reserves in Ivory Coast. The zoomed-in maps show deforestation in protected area of (A) Haut Sassandra, (B) Kobo, and corresponding regrowth and land-use in C, D, E, and F, respectively.

decrease in accuracy and F1-score compared to previous periods. This might be related to the confusion in similarities between land-uses at a young age, and thus making it challenging for the model to distinguish between them, for example, oil palm vs rubber, cashew vs cacao. This confusion can visibly be seen in Figure 4.5d.

4.3.4 Trend of forest loss and its drivers

After having generated and validated the map of land-use following deforestation in Ivory Coast (subsection 4.3.3). The next step was to assess the trend of change of forest loss and land-use following deforestation in Ivory Coast over 4 periods. Our results in (Figure 4.6) show that a small proportion of protected forest remains in Ivory Coast from as of 2019. Likewise, we also found a relatively constant trend for water, oilpalm, rubber, natural forest, and agriculture. Cacao had a positive trend increasing from 2000-2004 to 2015-2019. Cashew is observed to increase but at a slower rate compared to cacao, while agriculture, built-up and savanna showed a decreasing trend (Figure 4.6).

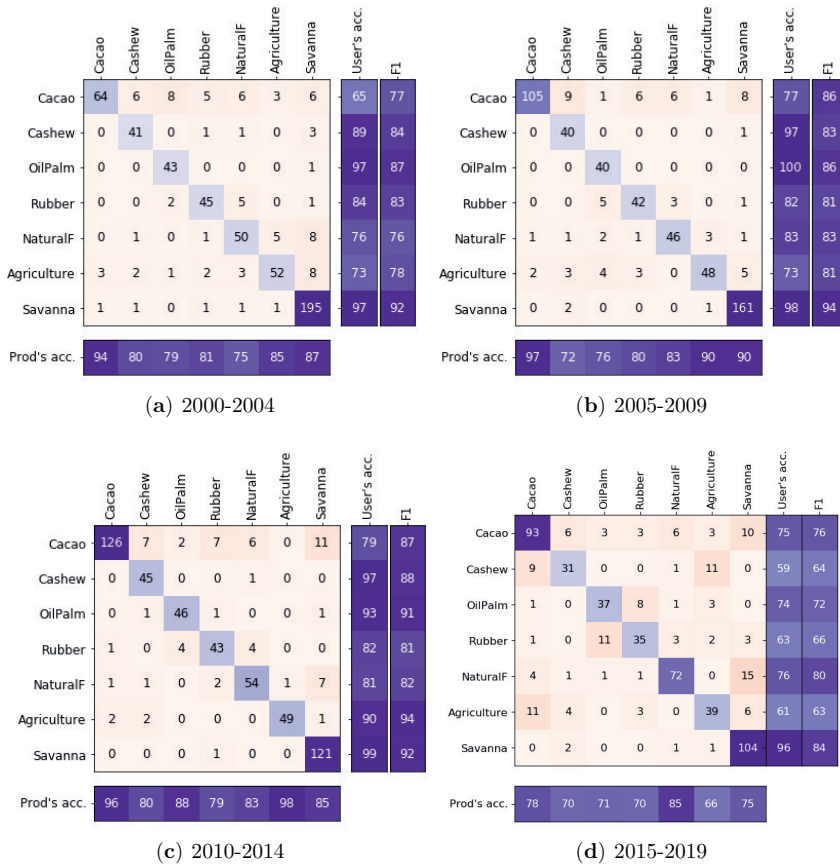


Figure 4.5: The confusion matrix showing the correct predicted and false predicted land-use following deforestation, users accuracy, producers accuracy and F1-score on the output map for the year (a) 200-2004, (b) 2005-2009, (c) 2010-2014, and (d) 2015-2019, respectively.

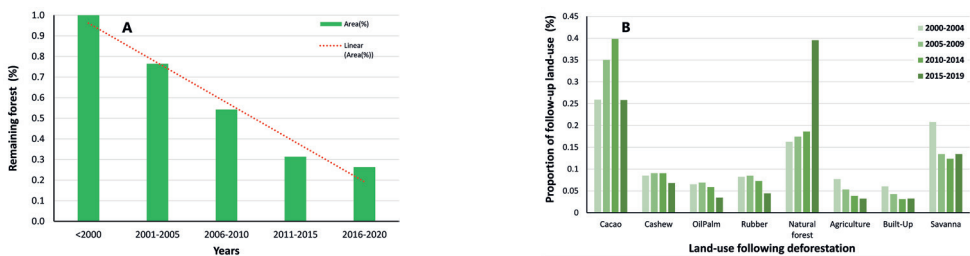


Figure 4.6: **A** shows the proportions of remaining forest in protected forest areas, and **B** proportion of land-use following deforestation in Ivory Coast for the four-time period of a five-year interval between 2000-2019.

4.4 Discussion

This study's aim was to classify land-use following deforestation in Ivory Coast with a specific focus on prevalent and emerging commodity crops such as cacao, cashew, oilpalm, and rubber. We used the AVOCADO algorithm for detecting forest loss and regrowth, followed by an Attention U-Net model for the classification task. In addition, we aimed at producing a high-resolution map of land-use following deforestation that would be useful for monitoring forest changes related to commodity crops at both local and national scale (NICFI, 2021). The generated land-use following deforestation map is especially valuable in the current trend where government organizations in developed countries are imposing legislation promoting imports of deforestation-free products, in this case, commodity crops (Bager and Lambin, 2022; EUROPEAN COMMISSION, 2022). Thus companies sourcing from Ivory Coast would be required to show that their products are free from deforestation. The method and results presented in this study provide a system for which land-use change and commodity crops can be monitored more frequently, wall-to-wall, and reproducible for operational monitoring by companies or governments.

4.4.1 Deforestation patterns in Ivory Coast

Our results in Figure 5.5 suggest that between the years 1990 to 2020, deforestation increased from the northern to the southern regions of the Ivory Coast. This trend is linked to the influx of people from neighboring Burkina Faso in the 70-80ties that were then relocated during the civil war in '99-'02 (Sabas et al., 2020). During the civil war and due to the relocation, lots of forests were lost (Nackoney et al., 2014). Thus today, only a small fraction of forests remain intact in Ivory Coast (Sabas et al., 2020). Efforts have been put forward to conserve and protect the remaining forest from further deforestation and degradation. Despite the existing effort, the remaining forests are threatened by increasing global demand for commodity crops such as cacao, cashew, oilpalm, and rubber (Barima et al., 2016; Ruf and Varlet, 2017). Ivory Coast is said to be one of the countries with favorable conditions for growing these crops (Sassen et al., 2022). Thus, without further action not so long all the remaining forest will be gone in the coming few years (Erik Hoffner, 2021).

4.4.2 Patterns of land-use following deforestation in Ivory Coast.

From our predicted wall-to-wall map of land use following deforestation, we identified a clear pattern for the dominance of forest conversion to cashew in the north and to cacao in the south. This difference between cash crops is most likely attributed to the difference in environmental conditions essential for growing each crop (Sassen et al., 2022). The north of the country is characterized as a dry forest, while the south is a tropical moist deciduous forest (Sabas et al., 2020). This also provides a new perspective to re-thinking

the mitigation efforts that focus only on cacao but also to include cashew as an important driver of forest loss in Ivory Coast (Erik Hoffner, 2021).

Recently, several studies have indicated the increase in cashew growing and export in Ivory Coast, thus creating a concern for forest conservation efforts (Erik Hoffner, 2021). From our results in (appendix 5.5), we observed a substantial increase in cashew farming in protected primary forests of the Ivory Coast. Similar trends of increase in cashew in Ivory Coast have been reported by Erik Hoffner, 2021; Monteiro et al., 2017. This is especially true in the northern regions, where its climate favors the establishment of cashew farms. According to Erik Hoffner, 2021, cashew was initially introduced in the northern regions for the purposes of reforestation; however, due to an increase in global demand, it is now being planted in cleared forests. This trend poses a challenge to existing forest conservation and climate change mitigation efforts (FAO, 2020).

Conversely, our results of wall-to-wall prediction in (appendix 4.7) show that the majority of cashew farming are established in areas outside the existing government forest classes, specifically in surrounding village forests, and agricultural areas. Thus, despite observing a substantial positive trend for cashew as the driver of forest loss in protected forest classes in the northern Ivory Coast. Care must be taken when interpreting the trend of cashew in (Figure 4.6) as it is only based on cashew established in protected forest classes (appendix 5.5). The fact that we detect little cashew yet could be due to several reasons : (i) Since most of the deforestation happen in dry forest and savanna, the deforestation algorithm used in this study (Decuyper et al., 2022) might be missing detecting some of the forest regrowth, (ii) it is also highly likely after deforestation there was first agriculture and/or degraded land that was later converted to cashew. So cashew was not the initial driver of deforestation in the north. (iii) since this is a more recent booming cash crop, some cashew plant-ages are still too young to be correctly classified by our model and thus get confused with agriculture or cacao. We recommend further experiments be conducted to improve the forest loss detection in dry forests and the classification performance of the deep learning model for young cashew crops. Importantly research determining the best lag time required to identify commodity crops would be important (Masolele et al., 2021).

In spite of the success of our approach in identifying land-use following deforestation in the Ivory Coast, our experiment was limited to the temporal availability of planet-NICFI data, which is from 2016 on-wards (NICFI, 2021). There is simply not enough high-resolution and freely available satellite data to predict land-use types accurately earlier in time (e.g., 1990-2015). This makes it also challenging to validate the land use by going back in time; hence we only relied on the current land-use as a proxy for deforestation drivers. Despite the shortcomings mentioned above, this method provides accurate estimates of deforestation and the commodity crops emerging over time (so far, numbers have been missing), and the results provide a tool to see where actions need to be taken.

4.4.3 Potential of deep learning for mapping land-use following deforestation.

We evaluated the performance of the Attention U-Net model on planet-NICFI images to map land-use following deforestation and regrowth in Ivory Coast. Specifically, the model was adapted from previous work (Masolele et al., 2022) and used a transfer learning approach to fit the model for Ivory Coast. Our results showed that without the need to train from scratch, we can re-use the existing model with a small finetuning to achieve higher model performance and wall-to-wall classification accuracies (Figure 4.5d, 4.3). More importantly, our model can be finetuned to predict a land-use with limited data, provided it has previous knowledge of the land-use type. This is an important aspect, especially for model transferability, since not always training data are available for identifying land-uses in new regions at all times. The re-use of the model not only makes the model training faster but also reduces efforts invested in data collection when applied to new area (Tasar et al., 2019). Further, this work was implemented in a free and openly available cloud computing environment for land monitoring (SEPAL); thus, can easily be reproduced and transferred to other areas with little adaptation (FAO, 2021).

4.5 Conclusion

In this study, we aimed to quantify forest loss and the land use that follows, with a specific focus on prevalent and emerging commodity crops on a national scale. Using the Attention U-Net method, we produced a map of land-use following deforestation in Ivory Coast for forest loss that occurred between 2000-2019. With this result, we were able to provide the spatial and temporal estimates of forest loss due to a certain number of essential commodity crops in the Ivory Coast, specifically cacao, cashew, oilpalm, and rubber. We found a substantial increase in cacao and cashew crops in protected forests of the Ivory Coast. Most importantly, we identified a clear pattern for the dominance of forest conversion to cashew in the northern regions and cacao in the southern regions. This difference between commodity crops is most likely attributed to the difference in environmental conditions essential for growing each crop. This study provides a new perspective to re-thinking the mitigation efforts that focus only on cacao but also include cashew as an important driver of forest loss in the Ivory Coast.

Currently, there are no clear estimates on forest loss related to the rise of commodity crops in the Ivory Coast. This study gives a clear demonstration of the capability of the deep learning model in identifying direct drivers of deforestation or drivers of forest loss in the Ivory Coast. Assessing the direct drivers contributing to Ivory Coast deforestation is critical to effectively support and enforce targeted conservation efforts and protect its remaining intact forest as well as support restoration efforts. This study also shows that the spatial-temporal detailed land-use maps are highly valuable for monitoring the impact of climate change mitigation actions and the consequences of adopting certain

land-use policies on forests. More importantly, they are more valuable in the current trend where government organizations in developed countries are imposing legislation promoting imports of deforestation-free products, in this case, commodity crops. Thus companies sourcing from Ivory Coast would be required to show that their products are free from deforestation. The method and results presented in this study provide a system for which national scale land-use change and commodity crops can be monitored more frequently, wall-to-wall, and reproducible for operational monitoring by companies or governments.

4.6 Appendix

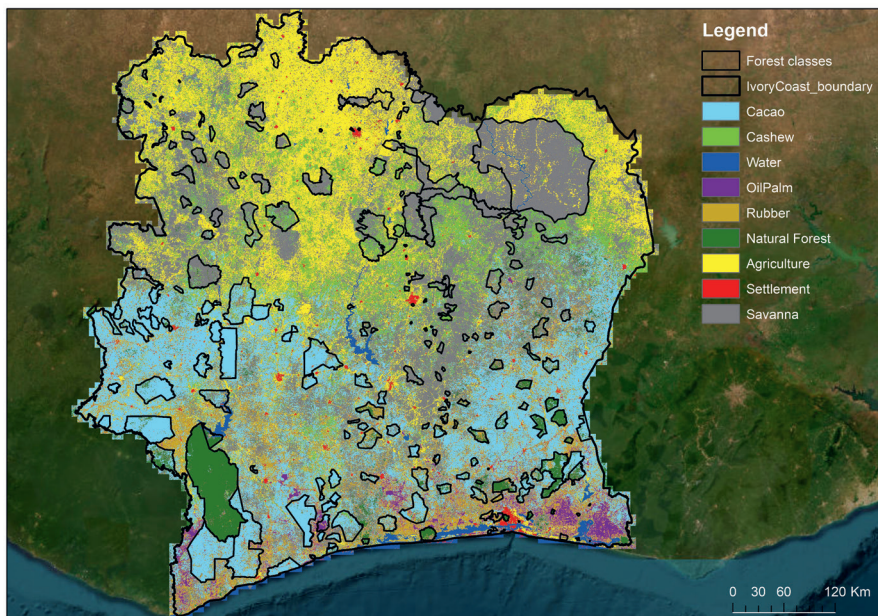


Figure 4.7: Wall-to-wall predicted land-use for the whole of Ivory Coast.

CHAPTER 5

5

Mapping the diversity of land uses following deforestation across Africa

This chapter is based on:

R. N. Masolele, V. D. Sy, D. Marcos, J. Verbesselt, F. Gieseke, Itohan-Osa Abu, C. Martius, and M. Herold (2022). Mapping the diversity of land uses following deforestation across Africa.

Abstract

African forest is increasingly declining as a result of human land-use change activities. However, consistently characterized maps of human land-use activities causing forest loss are not available at the spatial-temporal resolution and thematic detail suitable for decision-making at local and regional scales. So far, land-use activities causing forest loss in Africa have been mapped only on a coarser scale and focused largely on humid forests. Here we present the first high-resolution (5 m) and continental-scale mapping of land use following deforestation in Africa, which covers 13.85% of the estimated world's forest area, including humid and dry forests. We use reference data of 15 land use classes from 30 countries to train a deep learning model for predicting land use following deforestation (F1-score 84 ± 0.7) for Africa. Our results show that drivers of forest loss vary by region. In general, small-scale cropland is the dominant driver of forest loss in Africa, with a large hotspot seen in Madagascar and DRC. Further, commodity crops such as cacao, oil palm, and rubber are the dominant drivers of forest loss in the humid forests of western and central Africa, forming an "*arc of commodity crops*". At the same time, the hotspots for cashew are mostly found to increasingly dominate in the dry forests of both western and southern-eastern Africa, while larger hotspots for large-scale croplands were found in Nigeria and Zambia. The increased expansion of cacao, cashew, oil palm, rubber, and large-scale croplands observed in humid and dry forests of western and south-eastern Africa suggests they are vulnerable to future land-use changes by commodity crops, thus creating challenges for achieving the net-zero pledges, Redd+ initiatives, and sustainable development goals.

5.1 Introduction

Understanding the dynamics of land-use following deforestation is an important step in climate change mitigation, having a significant effect on forest biomass, biodiversity, and the water cycle (Spracklen et al., 2015). Over the past two decades, Africa has been experiencing a rapid decline in its forest cover (Hansen et al., 2013). The implications of which is the decline in species richness, changes in the water cycle, and loss of forest carbon stock (Zeng et al., 2018). The complexion of these changes can vary depending on the location, intensity, and spatial extent of forest loss. Thus understanding the spatial-temporal extent and patterns of the drivers of forest loss in Africa is crucial to comprehending its negative impacts on the forest ecosystem and its contribution to greenhouse gas emissions.

Previous studies suggest agriculture-related land-use change as Africa's main cause of deforestation (Curtis et al., 2018). However, such information is derived from coarser thematic maps or sample-based land-use statistics (Fritz et al., 2022). There is a lack of thematically detailed data both at small and large-scale to link deforestation to its respective drivers (Pendrill et al., 2022). Specifically, the much-needed and highly detailed thematic information on the types of direct drivers causing deforestation in Africa is rarely observed in the literature, except for a few countries (mainly in the tropical humid forests) (Fritz et al., 2022; Tyukavina et al., 2018). The availability of large-scale, thematically detailed, and high-resolution maps of land use following deforestation in Africa is essential for strategic planning and implementation of deforestation mitigation actions by governments and forest protection agencies (IPCC, 2021).

In addition, most studies focus their driver assessment on the knowledge of localizing specific drivers in specific regions or countries. For example, recent studies projected an expansion of oil-palm plantations, cacao in west Africa (Abu et al., 2021; Descals et al., 2021b), and small-scale agriculture in the Democratic Republic of Congo (Tyukavina et al., 2018). The generally accepted view of forest conversion in Africa aligns with the historical expectation of persistence of various states of subsistence agriculture activities, but little conversion to newly introduced or other types of land uses not previously found in the current location (Fisher, 2010). Aligning with the general view that certain land uses are restricted in certain geographical locations, thus overlooking the diverse actual causes of forest loss critical for deforestation monitoring and mitigation efforts at both local and regional scales.

Despite the availability of national or regional statistics to document the trends of forest loss, consistent, detailed, spatially explicit estimates of the continent's drivers of forest loss area are lacking (De Sy et al., 2015; FAO, 2010; FAO, 2016; Hansen et al., 2013). Many efforts to map drivers of forest loss rely on expert-based visual interpretation from samples of high-resolution satellite images (De Sy et al., 2019; Tyukavina et al., 2018). However,

the limitation of expert/sample-based visual interpretation is that it lacks detail and consistency in identifying and mapping the drivers over large regions and across time. This, in turn, causes a broad generalization of the drivers of forest loss and, thus, misses most areas and limits the level of detail in pinpointing the exact causes of forest loss useful for government agencies (local, national) responsible for forest monitoring (Curtis et al., 2018). For example, although a recent study of tropical humid forest change ostensibly tracked agriculture expansion over time, its delineation of land uses largely relied on sample-based single-date expert interpretation, and the wall-to-wall-map was not reported (Fritz et al., 2022).

The absence of detailed systematic monitoring of forest loss drivers complicates assessments of Redd+ efforts and net zero commitments on reducing the impacts of land-use change on forest ecosystems (Curtis et al., 2018; De Sy et al., 2019; FAO, 2010; IPCC, 2021). Generalization and confusion between land-use and landcover change maps produced at a global scale lead to ‘cryptic forest loss’ and/or overestimates certain land-use and land cover (Curtis et al., 2018). This is especially true in Africa, with its rapid deforestation rates and diverse land uses (FAO, 2020; Hansen et al., 2013). National reporting indicates a substantial net increase in forest loss (FAO, 2020), but tracking net changes in the area of frequently disturbed land covers like forest regrowth can underestimate the occurrence of tree crop expansion as, with time, they become confused or resemble forest trees (FAO, 2020; Masolele et al., 2022). This is especially true in dry forests where tree crops (i.e., cashew) resemble forest trees (i.e., Miombo) (Hansen et al., 2013). Thus, it remains unclear whether natural forest recovery or tree crops are driving expansions in forest cover in Africa. Specifically in countries such as the Ivory Coast, Ghana, and Eastern regions of Tanzania and Mozambique, where commodity crops are dominant.

Mapping drivers of forest loss consistently across space and time using satellite data is challenging, especially using the moderate spatial resolution imagery(10–30 m) needed for comprehensive regional coverage (Finer et al., 2018). This challenge arises in part from spectral and structural similarities and differences between land-use practices (Curtis et al., 2018; Pandey et al., 2018; Pelletier et al., 2019). Land uses over large scale are spectrally heterogeneous, with substantial variation in spectral signatures across space, time, elevation, soil types, forest types, and disturbance intensities. These land-use similarities and differences, coupled with geographic variation in spectral reflectance, neighborhood features, phenology, and persistent tropical cloudiness, make it difficult to distinguish land uses using satellite imagery consistently . Although variability of land-uses has constrained its classification at larger scales(Masolele et al., 2021), maps based on automated classification of remotely sensed imagery have successfully monitored drivers of forest loss at regional scales (for example, (Curtis et al., 2018)). However, the spatial, temporal, and thematic detail of the regional maps of land-use after deforestation is limited, and varies widely across different geographies and land-use types. .

To address these uncertainties, we undertook a continental assessment of the direct drivers of forest loss here, defined as a human-related land-use conversion or land-use following deforestation. We focused on the tropics (30° N to 30° S) due to the prevalence of natural forest conversion to agriculture, mining, settlements, and commodity tree crops across tropical latitudes and high rates of potential carbon sequestration from tropical tree regrowth. We aimed to use high-resolution remote sensing data (NICFI, 2021), deep learning (Masolele et al., 2022), and active learning (AL) (Joshi et al., 2010; Rawat et al., 2022) to accurately identify and map land use following deforestation and assess the trend and hotspots of land-use conversion across countries, and regions in Africa (UNEP-WCMC and IUCN, 2022).

5.2 Methods

5.2.1 Study area

This study was carried out within the African continent along 30° south and 30° north, which covers countries in western, central, eastern, and southern Africa (Figure 5.1). The region is characterized by humid forests as well as dry forests. The study area was defined based on the coverage of high-resolution Planet-NICFI data (NICFI, 2021).

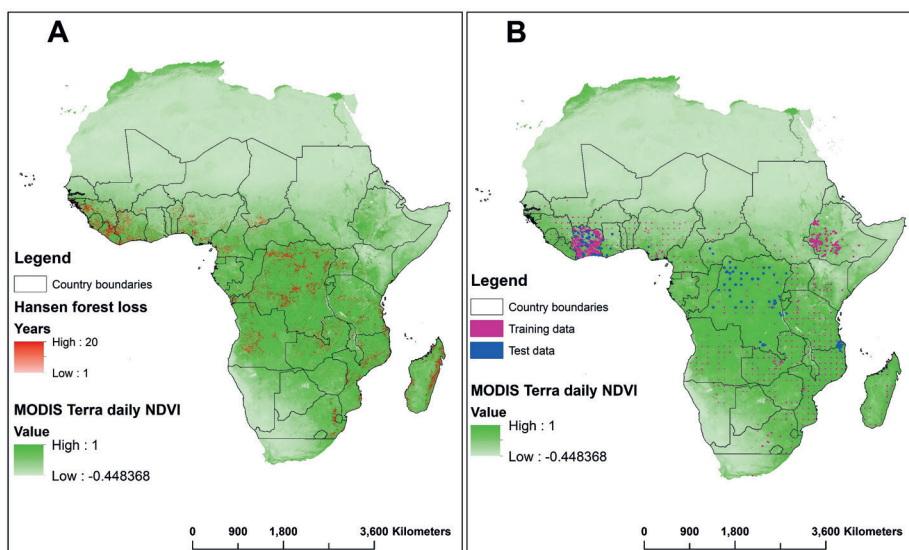


Figure 5.1: Map showing study location in the African continent along 30° south and 30° north. **A**, is the study area map with forest loss locations between 2001 and 2020, and **B**, shows the locations of the training and testing data. The basemap is the MODIS Terra daily normalised vegetation index retrieved from Google earth engine.

5.2.2 Data

Reference land-use data We identified 15 land-use following deforestation classes as the main direct drivers of deforestation in Africa using information from De Sy et al., 2019; Descals et al., 2021b; FAO & JRC, 2012a; Fritz et al., 2022; Masolele et al., 2021; Masolele et al., 2022. The land-use data from Fritz et al., 2022 was obtained via crowdsourcing using citizen science while Masolele et al., 2021; Masolele et al., 2022 annotated the land-use data using high-resolution images in collaboration with stakeholders on the respective country. The data from De Sy et al., 2019; FAO & JRC, 2012a is based on the FAO global Remote Sensing Survey for 2010, where they used a systematic sampling along latitude and longitude with grids spaced 10km by 10km. Other reference data was retrieved from open source data available via online searching GRID, 2022; IPIS, 2022; Sirko et al., 2021; WRI, 2017. The land-use classes identified and annotated for this study are small-scale cropland, large-scale cropland, pasture, mining, roads, other-land with tree cover, plantation forest, coffee, settlement, tea plantation, water, oil-palm, rubber, cashew, and cacao. However, it is important to highlight that the majority of reference labels are available as point vectors, or their polygon contains a mix of land-use classes and does not accurately delineate the land-use borders, making it challenging for direct use in the semantic segmentation task. Thus, extra annotation was implemented using an AL process described in subsection 5.2.5.

Satellite imagery We used yearly mosaics of high-resolution planet-NICFI images with 5m resolution to train a deep learning model and map drivers of deforestation in continental Africa (30 °south and 30 ° north) (NICFI, 2021). The images consist of four spectral bands, namely blue, green, red, and near-infrared. Since image mosaics are created from a combination of many sensors and cover various regions in Africa, they have variability in spectral and visual appearance. To correct for this, all the images were normalized such that the range of pixel values is between 0 to 1. Additional vegetation indices such as the normalized difference vegetation index-(NDVI), soil-adjusted vegetation index - (SAVI), and the normalized difference moisture index - (NDMI) were created to enhance models' capability to segregate land-use following deforestation (Masolele et al., 2021; Masolele et al., 2022).

5.2.3 Data preprocessing

For this study, we created three data pools: (1) a pool of annotated training data, (2) a pool of unannotated training data, and (3) independent test data Figure 5.3. In total, we had 2357 images acquired from all across Africa (refer subsection 5.2.2, of which only 895 images were having annotations. 80% of the 895 images were placed in a pool of training data, while 20% was left out as independent test data. The remaining 1462 images were placed in a pool of unannotated training data. The unannotated data was later used in subsection 5.2.5 in an active learning cycle where model uncertainty was used to

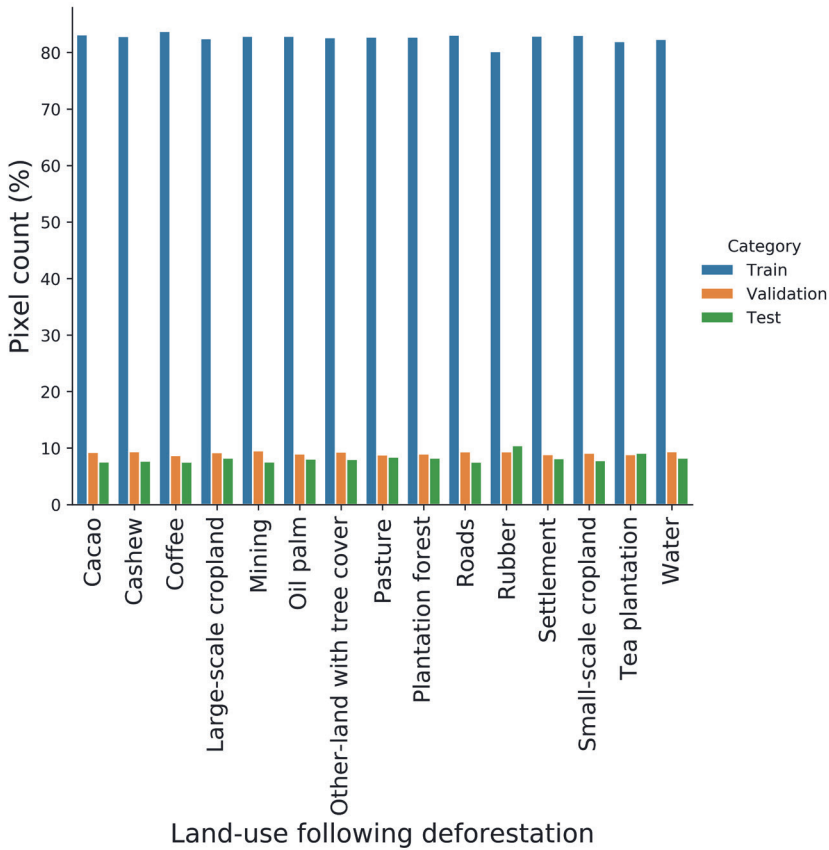


Figure 5.2: Shows the number of pixels in (%) used for the model training, validation, and testing.

decide which images are useful for improving the model performance. The land-use class distribution for initial model training, validation and testing is shown in Figure 5.2.

5.2.4 Research design

In this study, we used high-resolution satellite images from Planet-NICFI (4.77 m), to better characterize the spectral, and spatial patterns of land-use following deforestation. We used Hansen forest loss dataset between 2001 and 2020 as a proxy for forest loss to estimate land-use following deforestation (Hansen et al., 2013). From this dataset, we selected mapped loss images ≥ 3.8 ha in size that persisted from 2001 to at least through the end of 2020 ($n = 1821$). Over each resulting patch of loss pixels, we extracted Planet-NICFI imagery and reference labels. We then used labeled training data and deep learning to predict patch-level land use for 2022 as a proxy for the driver of deforestation

from 2001 to 2020. The output was a 5 m resolution classified map of land-use following deforestation.

Then, to assess the spatial hotspots and temporal extent of land-use expansion across Africa, the classified land-use map was intersected with available spatial data on yearly Hansen forest loss, biomes, national borders, and protected areas.

5.2.5 Models and implementation details

In this study, we adopted the Attention U-Net model developed by Masolele et al., 2022 for the classification of land-use following deforestation in Ethiopia, since this architecture had provided high performance in identifying drivers of forest loss from satellite data. The model was used to upscale the characterization of land-use after forest loss in Africa in high thematic detail (fifteen classes) and spatial coverage (continental Africa and Madagascar (30 °south and 30 ° north), as opposed to nine land-use classes and the national scale for which the base model was developed. Although the model had shown to perform well in classifying land-use following deforestation at a country scale, the limited availability of training data and heterogeneity of land-uses across Africa would prevent it from being usable at the continental scale. To counteract this, we incorporated AL in the training process to inform data selection and optimize the labeling process required for the model to learn new and informative features from diverse data sets across regions in Africa. We tested the ability of the attention U-Net model to effectively learn from multiple new data-set across different regions in the continent and be applied to different classes from another set of regions. In addition, we performed an independent assessment of the resulting maps of drivers of forest loss in the whole of tropical Africa.

Model details The model was created using the Keras library (Chollet et al., 2015) and TensorFlow (Abadi et al., 2015) as the backend. We trained the attention U-Net model for 200 epochs using a batch size of 64. For every convolutional block, we added a padding operation to ensure that the size of the last layer stays comparable to the input layer and followed by a non-linearity function-ReLU. The features in the convolution layers were normalized using Batch normalization followed by a regularization dropout rate of 0.1 and Adam optimizer with a learning rate (lr) of 10^{-4} . The multi-class categorical Focal Loss was used as an optimizer between the post-softmax probability and one-hot label corresponding to the type of driver in the image patch. The task of classifying drivers of forest loss was implemented and run in the Sepal geospatial analysis platform (SEPAL 2.0) FAO, 2021. This is a cloud-based computing environment of FAO with instance type g8, NVIDIA Tesla M60 GPU 32GB RAM.

Active learning One challenge of employing a deep learning methodology is that it tends to require a large amount of data for training (Reichstein et al., 2019; Zhu et al., 2017). In reality, there exists a limited amount of training labels to cover the variability

of all land-use classes (Reichstein et al., 2019), and the task of labeling all the required land-use data using satellite imagery on a continental scale can be expensive (Tasar et al., 2019). Indeed, during initial model training using the annotated data described in subsection 5.2.2, we achieved an unsatisfactory model classification performance on some of the land-uses on independent datasets, with F1-score of 0.05, 0.1, 0.41, 0.25, and 0.14 for mining, roads, settlement rubber, and cashew, respectively. To be able to improve the classification performance of the model for these land-uses we had to adopt AL (Joshi et al., 2010; Rawat et al., 2022) to identify images where the model provides highly uncertain predictions to identify the most informative images and annotate more labels from these images as an addition in the training pool.

Iterative pool-based learning We first train our model using a set of annotated data and assess its accuracy using the independent test data. The first training is done on what is called a pool of annotated data. We then use the trained algorithm to select a set of images from a pool of unannotated data to be annotated by a human annotator. For image selection, we employ entropy

$$H(Y) = - \sum_{i=1}^k p_i \log(p_i).$$

as an uncertainty measure for unlabeled images, not in the training set. $\sum_{i=1}^k$ stands for the sum of images' possible values, given a discrete class membership Y and probability i . Only images with entropy (> 0.6) were assigned for manual annotation and then later added to the training pool. The process was repeated two times until the best accuracy was obtained for all the classes. In total, 716 labeled images from the training pool were used in the initial training. In the second cycle using AL, we annotated 372 images which were then added to the training pool for second round of model training, followed by 554 images for the third AL training cycle, Figure 5.3. The final model performance assessment for each cycle was done on 179 separate independent test data, not in either training pool.

5.2.6 Wall-to-wall mapping

We used FAO and SURFSARA cloud computing platforms (FAO, 2021; SURFsara, 2022) to run inference of the fifteen land-use following deforestation classes across the entire African continent, 30 ° south, 30 ° north (NICFI, 2021). The inference was run on 5m resolution freely available planet-NICFI imagery using the attention U-Net model trained in subsection 5.2.5. We used planet-NICFI imagery for the year 2022 as a proxy for predicting land-use following deforestation from the year 2000 to 2020. The inference was only applied to forest loss areas identified in (Hansen et al., 2013).

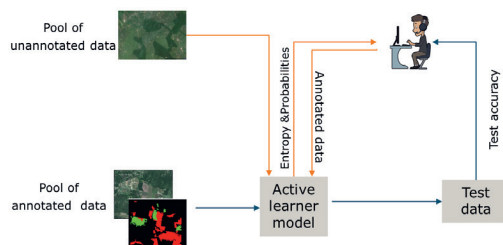


Figure 5.3: The process of active learning with a pool of annotated data for initial model training, a pool of unannotated data for iterative labeling, and test data for independent testing.

5.2.7 Assessment of the accuracy of wall-to-wall map

We used stratified estimation of area and accuracy by (Olofsson et al., 2014) to estimate the number of samples required to assess the output map of drivers of forest loss. The number of samples and accuracy were calculated based on four lustra (20001-2005, 2006-2010, 2011-2015, and 2016-2020) important for the assessment of change in the proportion of each driver of forest loss over the years. For each strata(class), sample estimation weights were calculated based on the area estimation of each driver of forest loss for each time period. The resulting weights were used to calculate the number of samples required to assess the accuracy of the map for each driver over a five-year interval. Following these, the accuracy of the map was calculated using the user's and producer's accuracies.

5.2.8 Hotspot analysis of the wall-to-wall map

Hotspot analysis is an interesting visualization technique to get insight into the data that can inform targeted actions, resource allocation and decision-making for forest conservation (Huggins et al., 2022). We used the kernel density estimation technique (KDE) to estimate the hotspot of the fifteen land-use following deforestation classes predicted in our wall-to-wall map. KDE uses a bandwidth of a specified size to estimate the density of pixels of a land-use within a location to create heatmaps for each land-use. By using the KDE package in python (PyPI, 2022), we run a kernel of size $0.1^\circ \times 0.1^\circ$ to predict the hotspot of each of the fifteen land-use following deforestation classes presented in this study. The output is a smoothed-continuous map of pixel size $0.1^\circ \times 0.1^\circ$, with each pixel representing the density of a given land-use.

5.3 Results

5.3.1 Importance of active learning for land-use classification

It has been largely proposed that AL could be leveraged to combine heterogeneous data sources with limited labels for the task of semantic segmentation (Rawat et al., 2022; Tasar et al., 2019). Here we present the results of using AL to map land-use following deforestation at a continental scale for which reference labels are limited, geographically scattered, and heterogeneous. Using independent test samples, on three attempts, we improved the classification performance on all land-use classes. Specifically, the micro and macro average F1-score improved from 43% and 50% to 84%, respectively (Figure 5.4). Note that the diverse spatial location and limited labels are partially responsible for the low accuracy of the initial model.

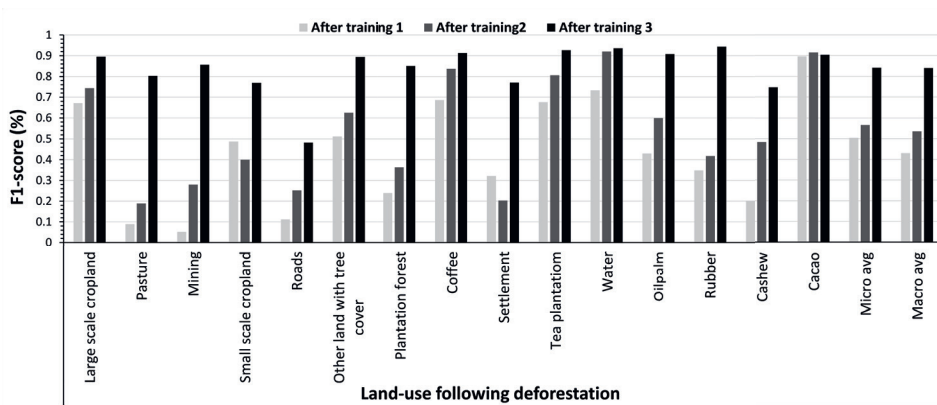


Figure 5.4: The bar chart shows the performance of the attention U-Net model in classifying land-use following deforestation over three active learning cycles in Africa.

5.3.2 Generating land-use map prediction at scale

Using our final attention U-Net model developed in subsection 5.2.6, we created the first wall-to-wall map of the land-use following deforestation across Africa covering forest loss from the year 2001 to 2020 (Figure 5.5). The output predicted map is available at a spatial resolution of 5m, with fifteen land-use classes. Explicitly the predicted land-use map has four properties: continental coverage, high spatial resolution, more thematic detail, and yearly temporal coverage. The output map was validated using stratified estimation of area and accuracy (Olofsson et al., 2014) with users accuracy of 85%, producers accuracy of 84%, and F1-score of 85% (Figure 5.6).

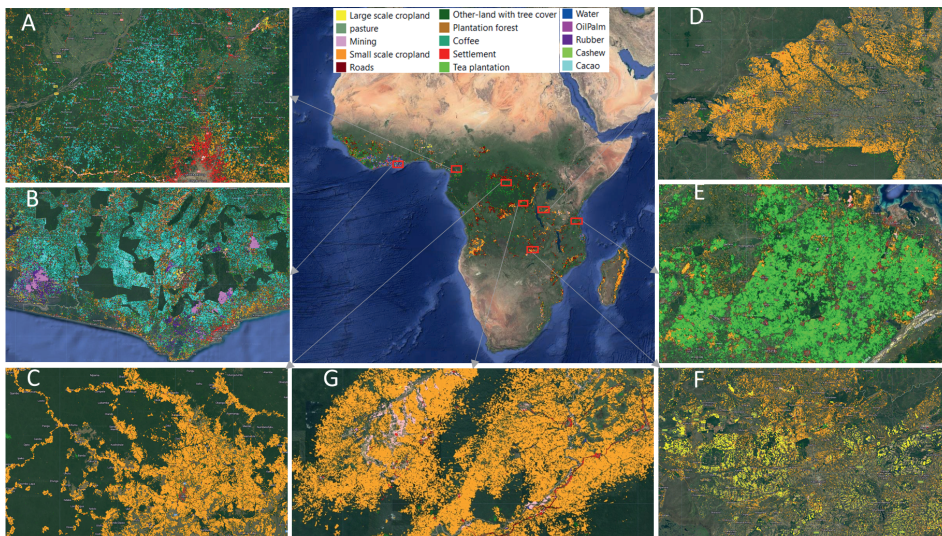


Figure 5.5: A 5m resolution classified map of land-use following deforestation in Africa (30 °south and 30 ° north) for the year 2001 to 2020 using planet-NICFI images and Hansen data as proxy for forest loss. The zoomed-in maps show (A) cacao expansion in Cameroon and (B) in Ghana, (C) small-scale cropland expansion in the DRC, and (D) in Tanzania, a mix of small-scale and large-scale cropland expansion in Zambia, while (E) shows a mix of mining along rivers, roads, small-scale cropland in DRC for the same period.

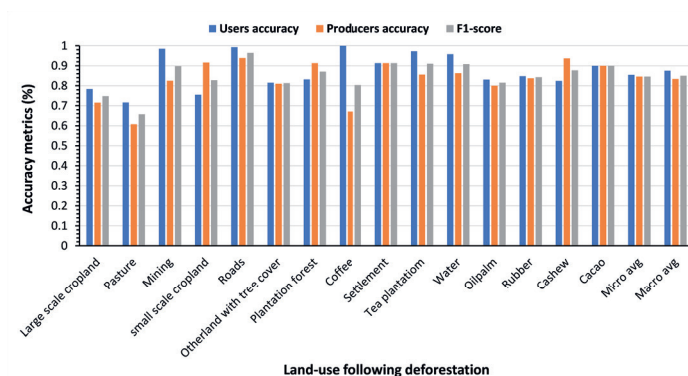


Figure 5.6: The users, producer’s accuracy and F1-score of the wall-to-wall map generated in (Figure 5.5).

5.3.3 Proportion of land-use following deforestation by country

Small-scale cropland was the dominant driver of forest loss in Africa, resulting in 64% of total forest loss from the year 2001 to 2020 (Figure 5.7). This was also the case for most countries, regardless of their contribution to total forest loss, a notably high proportion of small-scale cropland was observed in Madagascar (88%), followed by (85%) in the Democratic Republic of Congo (DRC), Burundi (81%), Comoros (79%), Malawi (76%), Angola (75%) and Mozambique (74%). Other-land with tree cover (OLWTC) was the second highest driver of forest loss in Africa and contributed to 10% of all forest loss in Africa. The highest proportion was observed in Gabon (34%) and Equatorial Guinea (34%). OLWTC constitutes all forest conversion related to fire, windthrow, lightning, speculative clearings, abandoned croplands, and regrowth (Pendrill et al., 2022). Large-scale cropland was the third highest driver of forest loss in Africa (9%), with the highest proportions by country found in Cape Verde (67%), Gambia (53%), Niger (50%), Sudan (47%), and Nigeria (44%). Likewise, the highest proportion of tea plantation establishments was observed in Kenya (4%) and Rwanda (3%).

The proportion of forest conversion for commodity crops such as cacao, cashew, oil palm, rubber, and coffee accounted for 7% of all forest loss in Africa. By country, the highest proportion of cacao was found in Ghana (25%), Ivory Coast (21%), and Liberia (15%); While cashew in Ivory Coast constituted (7%), Ghana, Guinea, and Tanzania each constituted (6%), and Mozambique (5%); On the other hand a high proportion of oil palm was found in Gabon (6%), with Liberia, Ghana, and Ivory Coast each having (2%); A high proportion of rubber was mostly found in Gabon (7%), Ivory Coast and Cameroon were having each (3%), and Liberia (2%); While the contribution of coffee was mostly found in in Kenya (1%). Additionally, the highest proportion of pasture was observed in Niger (27%), Somalia (22%), and Kenya (18%).

106 Mapping the diversity of land uses following deforestation across Africa

The conversion of forest settlement was mostly observed in Gambia (10%), Rwanda (8%), and Equatorial Guinea (6%); similarly, roads constituted a majority of forest loss in Equatorial Guinea (14%), Gabon (6%), Congo (5%), and Cameroon (3%), while mining had a higher proportion in Cape Verde (12%), Botswana (7%), and Equatorial Guinea (5%). Water was mostly observed in Niger (14%), with most changes associated with meandering rivers. Not surprisingly, the highest proportion of plantation forests was found in southern African countries such as Eswatini (46%) and South Africa (37%).

5.3.4 Trend of land-use following deforestation in Africa

Having predicted the land-use following deforestation across Africa for the year 2001 to 2020, we attempted to estimate the trend of the land-use for the entire study area and across four regions in Africa (Figure 5.8) **A** based on area and proportion per lustrum. These regions are western, central, eastern, and southern Africa. Our results suggest an increasing trend in the area of all land-use following deforestation, with the exception of pasture and plantation forest (Figure 5.8) **B**. However, when the trend was calculated based on the proportion of each land-use per lustrum, only small-scale cropland showed a positive increasing trend in three regions of western, central, and east Africa with the exception of southern Africa region (Figure 5.8) **C**. This show that although the area of almost every land-use is increasing per lustrum, the change is not proportionate.

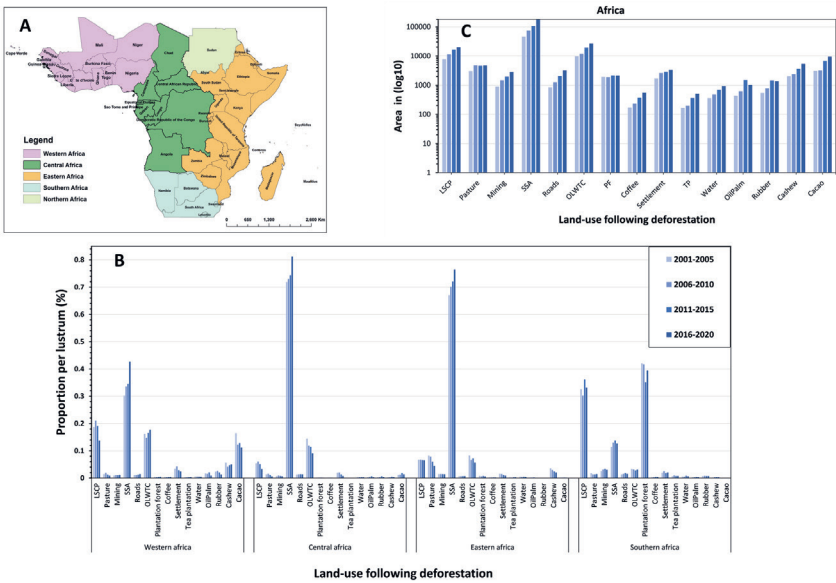


Figure 5.8: Trend of land-use following deforestation in lustrum from 2001-2020 across four regions of Africa, shown in **A** are corresponding regions, in **B** we show the trend based on the area (\log_{10} – *scale*) for the entire continent and in **C** based on the proportion of land-use following deforestation per region per lustrum. SSCP and LSCP stands for small-scale cropland and large-scale cropland, while OLWTC stands for other-land with tree cover.

5.3.5 Hotspots of land-use following deforestation in Africa

We observed a considerable spatial variation of hotspots of land-use following deforestation across continental Africa (Figure 5.9). The major hotspot locations are small-scale cropland in the Democratic Republic of Congo (DRC), Angola, and Madagascar; large-scale cropland in Nigeria and Zambia; Pasture across east Africa but mainly in Tanzania; Major hotspot

for cacao is largely along the southern regions of west Africa but also in central Africa and form what we call an *arc of cacao*, (see Figure 5.9); We also observe hotspots for cashew in northern and central regions of Ivory Coast, Ghana, east-southern Tanzania, and northern Mozambique; Hotspots for oil palm were highly observed in Ivory Coast, Ghana, Liberia, Cameroon, and Uganda; coffee in Kenya, Ethiopia; Tea plantation in Kenya, Rwanda, and Malawi; Rubber in Ivory Coast, Ghana, Liberia, Cameroon, and Gabon; Plantation forest in South Africa, and Eswatini; Roads in Ghana, Cameroon, Liberia, and Equatorial Guinea; Settlements in Ivory Coast, Liberia, Nigeria, and Cameroon; Mining in Ghana, Angola and parts of Eastern DRC; Hotspot for water was mostly observed along meandering rivers of the coast of Ivory Coast, Ghana, DRC, and along the coast (islands) of Uganda. Of most importance, we observe commodity crops hotspots dominating in western and central African regions and partially forming an arc along the coast of the Atlantic ocean (Figure 5.9). In general these hotspot maps conveys an eye catching message to forest conservation agencies, decision and policy makers by showing the exact causes and locations of forest loss, for which more effort need to be directed and prepare best strategies for mitigation actions for future forest conservation.

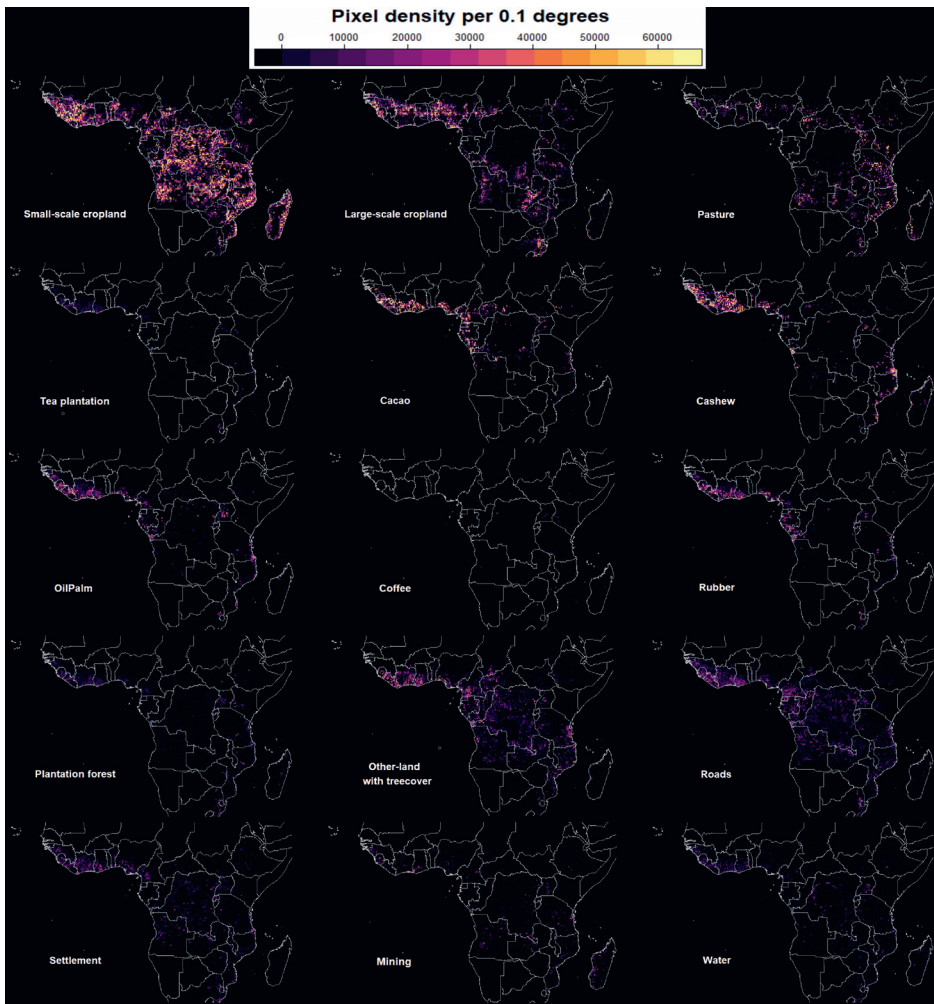


Figure 5.9: Hotspots of different land-use following deforestation in Africa along 30° south and 30° north, for the year 2001 to 2020. The color bar shows the estimated pixel density of each land-use in a given location.

5.4 Discussion

Access to large-scale, high-resolution, and thematically detailed information on land-use following deforestation is important for effective forest conservation, Redd+ initiatives, net-zero goals, and climate change mitigation action (Austin et al., 2019). In this study, we take advantage of recently available high-resolution satellite image (5 m), heterogeneous

reference land-use data (multi-source data), deep learning techniques and AL to assess land use following deforestation in continental Africa between 30 ° south, 30 ° north.

New approach for large-scale mapping of land-use following deforestation Our results in subsection 5.3.1 achieve generalizability at a continental scale and show that it is possible to map land-use following deforestation at a large-scale with high spatial resolution images (5 m) and high thematic detail. In order to bridge across multiple regional reference datasets we applied AL for iterative training, data selection, and labeling Rawat et al., 2022. The use of AL substantially improved the performance of the deep learning model to classify land-use following deforestation for continental Africa over the traditional model training approaches. Particularly in cases where the training data is limited, heterogeneous and the model is not able to generalize across regions, thus a need to intelligently add labels that the model needs to achieved higher accuracy in the prediction process. We hope these model performance gains, coupled with an iterative process of AL, will complement existing visual interpretation methods, thus accelerating tracking land-use following deforestation at a global scale on a wall-to-wall and more frequently. Similar improvements using AL has been reported in (Bengar et al., 2021; Kim et al., 2015; Ma et al., 2011; Tuntiwachiratrakun and Vateekul, 2017; Wang et al., 2017; Wu et al., 2014).

Land-use following deforestation and its implications for forest monitoring

Our finding on wall-to-wall land-use prediction (subsection 5.3.2, 5.3.3) indicates that small-scale cropland is the dominant driver of forest loss in continental Africa. This is similar to findings reported in (Curtis et al., 2018). A notably high proportion of small-scale cropland was found in Madagascar and DRC. According to (Tyukavina et al., 2018) an increase in population and political conflicts are the indirect cause of increasing forest loss due to small-scale cropland in DRC, while in Madagascar, is solely associated with population growth along the western coast Moser, 2008. Interestingly, small-scale cropland was the only land-use class that showed an increasing trend of change in relation to other land uses per stratum from the year 2001 to 2020. This increase was observed in western, central, and eastern Africa. Conversely, however, when we analyze the trend based on area change, the area of every land-use increased per stratum with the exception of plantation forest and pasture. This is due to the fact that plantation forests are cleared and re-planted on rotational bases, mostly in exact same locations, which may result in false positive detections of forest loss by the algorithms used in Hansen et al., 2013. While for pasture, this might be related to confusion with other-land with tree cover during the classification process.

Forest conversion to commodity crops was another important direct driver of forest loss in Africa (Figure 5.9). Using the kernel density estimation method, we identified distinct hotspot patterns of commodity crops in areas of western and central Africa, specifically cacao, cashew, oilpalm, and rubber, with other hotspots for cashew in Tanzania

and Mozambique. According to Jalloh et al., 2013; Roessler et al., 2022, the favorable climate condition is the reason for the increasing expansion of commodity crops in these locations. Conversely, land-uses such as tea plantation, coffee, and pasture dominates in east Africa (Abdalla Juma and Administration, 2019; Hylander et al., 2013; Karuri, 2021). Its proximity to the equator creates favorable conditions for these land-uses (Patay et al., 2016). For example, the increase in the establishment of tea and coffee plantations in Rwanda, Kenya, Ethiopia, and Uganda ensures an all-year-round supply of fresh tea to the global markets, which would be challenging in other regions (Abdalla Juma and Administration, 2019; Hylander et al., 2013; Karuri, 2021; Patay et al., 2016). Previously these commodities were for export; however, the current increase in domestic consumption has created demand within the region, thus the need for more plantations (Dufrière, 2019). On the other hand, east Africa is known to host nomadic communities with animal grazing/pasture as their main land-use activity (Fratkin, 2001; Homewood et al., 2004; Wynants et al., 2019). Specifically, Ethiopia, Tanzania, and Kenya are known to have a large number of cattle per household (Fratkin, 2001). However, the lack of grazing areas and water due to drought and global warming has forced the pastoral communities to move to forested areas where they can get forage for their cattle as well as an opportunity to diversify their practices by farming (silvopastoral) (Homewood et al., 2004). This is commonly observed in Ethiopia, Kenya, and Tanzania.

Another highlight is the number of access roads and settlements detected largely in west Africa and central Africa (Figure 5.9). Growth in the number of roads and settlements in west Africa is closely linked to the complexity of agricultural activities (Herrmann et al., 2020; Moriconi-Ebrard et al., 2016; Roessler et al., 2022). The increase in commodity crops has also caused an increase in settlement and the number of roads which are essential to provide accommodation and accessibility for farming communities (Roessler et al., 2022). Conversely, in central African countries, a majority of newly developed roads are associated with an increase in logging activities around the congo basin (Kleinschroth et al., 2019). However, our analyses also indicate that logging roads disappear with time as a result of abandonment and regrowth. Similar studies by Kleinschroth et al., 2019 report a higher number of roads in central Africa linked to logging activities. Additionally, mining is most prominent in Ghana, eastern DRC, and Angola, with artisanal mining as the main driver of forest loss along river lines of Ghana and eastern DRC (Figure 5.9). The presence of mining along rivers has caused not only the loss of forests and wildlife habitat but also a decrease in the quality of water (Edwards et al., 2014). This poses a health problem to surrounding communities as they become exposed to a toxic chemical used for extracting minerals. Thus a successful forest conservation action would not only save forests but also save communities from health hazards posed by being exposed to mining activities.

Institutional involvement in the expansion of commodity crops As indicated above, in our analysis, western African countries, specifically Ghana, Ivory Coast, and

Liberia, have the greatest rate of forest conversion for commodity crop production. In Western Africa, the growth in the production of commodity crops such as cocoa, cashew, oil palm, and rubber is attributable to unique climatic conditions (Jalloh et al., 2013; Roessler et al., 2022). During colonial authority, cashew, cocoa, and rubber were introduced, and seedlings were brought from Latin America (Roessler et al., 2022). Forest zones were the primary producers of cocoa, rubber, and palm oil, whereas savannas were suitable for groundnut. During and after the fall of the Atlantic slave trade, slave labor played a crucial role in the rise of commodity crop production in many regions of Western Africa (Austin, 2009).

These commodity crops fared remarkably well in West Africa because millions of smallholder farmers were able to manage their fields using short-term intercropping and intercropping depending on space and soil fertility to respond to the growing demand for commodity crops and poor soils (Bekunda et al., 2010). Several African research and extension institutions, such as the West Africa Agricultural Productivity Program (WAAPP), the Cocoa Research Institute of Nigeria (CRIN), the Rubber Research Institute of Nigeria (RRIN), the Nigerian Institute of Oil Palm Research (NIFOR), and the Ghanaian Ministry of Food and Agriculture (MOFA), have been established in order to address constraints in the production and supply of cash crop seeds and seedlings and to provide credit facilities (Babu et al., 2017; Bekunda et al., 2010). The primary objective of genetic modification initiatives in Africa has been to raise the agricultural yields required by African consumers and producers of commodity crops. The increased cultivation of these crops, however, has come at the loss of tropical forests.

The "commodity crop revolution" brought up new geographical disparities and increased existing ones, which resulted in bigger migratory flows than ever before (Austin, 2009; Haas and Travieso, 2022). Population migrations have a long pre-colonial history related to slave raids as well as free cyclical migration (Adepoju, 2011). Even though many people moved from Nigeria to Ghana, the vast majority of them worked as farmhands in colonial Nigeria. At the time, Nigeria was experiencing a rise in exports of cocoa beans from the southwest, palm oil from the southeast, and groundnuts from parts of the central north. Ghana was one of the primary destinations for these migrants (Haas and Travieso, 2022). During the dry season of 1952–53 in Nigeria, some 190,000 migrants were recorded moving southward from the northern part of the country. In addition, research has demonstrated that the cultivation of commodity crops has a significant positive effect on household income by alleviating poverty in many African communities, and this has an effect on household migration decisions in many west African countries, including Burkina Faso, Ghana, the Ivory Coast, and Nigeria (Bryceson, 2007; Haas and Travieso, 2022). Due to infrastructure development, rising cash crop output (coffee, cocoa, groundnut), mining sector growth, and the exploration of crude oil, the area has seen an increase in labor migration (Adepoju, 2011; Quartey et al., 2020). Many people from the Sahel, including some with their families, moved to commodity crop farms in Ghana, Senegal, Côte d'Ivoire,

and Nigeria. Ghana and Côte d'Ivoire largely drew Malians, Chadians, Burkinabes, and Nigeriens to their cocoa plantations, while Senegal and the Gambia supplied labour on their cotton and groundnut farms (Haas and Travieso, 2022; Quartey et al., 2020).

Limitation and future opportunities In this study, we used high-resolution planet-NICFI images available for the year 2022 as a proxy for mapping land-use following deforestation from the year 2001 to 2020. The planet-NICFI image was used because of its high-resolution and high performance when used in detecting subtle changes in land-uses. However, we acknowledge that the output land-uses classified with 2022 images might not indicate the primary cause of deforestation in earlier deforestation years. In fact, we might be identifying a secondary land-use or regrowth. Thus care must be taken when using these data to compute statistics of land-uses for forest loss for the previous years 2001 to 2015. For example, areas where logging roads existed in earlier years, say 2001 to 2015, will now have regrowth or be covered by trees by 2022 and hence be classified as other-land with tree cover.

Additionally, despite the success of planet-NICFI data in classifying land-use following deforestation in continental Africa. Persistence cloud cover provided challenges in mapping some parts of the congo basin and west Africa. We acknowledge the existence of misclassification in parts where planet-NICFI images are covered with cloud cover and haze (Bae et al., 2019; Reiche et al., 2018). The inclusion of synthetic aperture radar data (SAR) offers a complementary advantage in detecting land-use in these areas. SAR has the characteristics of imaging through clouds, haze, day and night. It is expected that future missions of SAR data, such as the National Aeronautics and Space Administration (NASA) and the Indian Space Research Organization (ISRO) SAR (NISAR) expected to be launched in 2023 (Rosen et al., 2017) will bridge this gap by providing SAR data continuously in all weather conditions useful for forest monitoring. The NISAR data will be acquired at L-band with a 12-day revisit time, range, and azimuth resolution of 3-10m and 7m, respectively. One advantage of L-band SAR is that it can penetrate through a forest canopy, thus useful even in detecting subtle land-uses such as logging roads and artisanal mining in areas where optical data fail to do so due to canopy coverage (Reiche et al., 2021).

CHAPTER 6



Synthesis

6.1 Main results

This thesis has explored the use of deep learning methods to gain an understanding of the proximate drivers of deforestation in the tropics with a focus on identifying land-use following deforestation through freely available satellite imagery. The use of satellite imagery and deep learning to identify land-use offers promising improvements over traditional methods like field surveys and sample-based visual interpretation, enabling the generation of continental scale, up-to-date, maps. In addition, the identification of land-use instead of land-cover allows for more detailed insights into the economic drivers of deforestation.

This thesis provides strategies to facilitate automated land-use mapping and shows through case studies how to achieve that goal. Specifically, we developed a deep learning method to classify land-use following deforestation and test the application of the method for wall-to-wall mapping over national and continental scales. The end result consists of the code produced during this thesis, the weights of the trained deep-learning model, and the generated land-use maps. In this section, we provide the key findings of each research question formulated in chapter 1 and discuss the challenges and opportunities for future research.

6.1.1 How can we use deep learning for assessing land-use following deforestation using remote sensing data?

Satellite imagery has so far been most often used in mapping land-cover as opposed to land-use. Land-use is much harder to assess with only spectral information from medium resolution multi-spectral satellite images, such as Landsat, which does not have the necessary spatial resolution allowing to discriminate between fine-grained land-use classes. The current state-of-art identification of land-use following deforestation largely depends on visual interpretation of high-resolution satellite images. However, even with high-resolution images, it is expensive and time-consuming to identify land use following deforestation with visual interpretation alone. Thus developing a deep learning model capable of accurately identifying land-use following deforestation, can complement human visual interpretation using satellite images in the light of climate change. Accurate models in this setting refer to models that simultaneously attain high-harmonic mean (F1-score) of recall and precision (i.e. high percentage of land-use following deforestation successfully classified (recall) and being true positives(precision)).

To have a full understanding of the design of the deep learning model architecture employed for the classification of land-use following deforestation, we firstly identified the models based on the ability to retrieve spatial, temporal, and a combination of spatio-temporal characteristics of land-use following deforestation in satellite images. The models include the spatial model (convolution neural network - 2D-CNN), temporal model (Long short-term memory recurrent neural network - LSTM), and spatio-temporal models (3D

convolutional neural network - 3D-CNN, Hybrid of CNN and LSTM, ConvLSTM, and CNN Multi-Head Self-Attention - CNN-MHSA). In Chapter 2 we assess the performance of each of these model designs in both continental and pan-tropical settings.

Our results showed that deep learning models making explicit use of spatio-temporal patterns achieved the highest overall F1-score compared to models designed to focus only on spatial or temporal features. This suggests that spatio-temporal models, in particular those using attention-based mechanisms such as CNN-MHSA, are able to cope with high levels of heterogeneity in the data, thus boosting the generalization performance of the model in identifying land-use following deforestation.

We also observed that the 2D-CNN (spatial model) achieved higher classification performance on the continental scale compared to the LSTM. This indicates that spatial patterns of land-use are more useful for land-use characterization than temporal ones when considering the problem at the regional level. This may indicate a higher level of heterogeneity in terms of the temporal patterns that characterize each land-use, possibly due to regional differences in seasonality and land-use practices.

We also found that models focusing on spatial patterns (2D-CNN) only performed competitively in the continental setting but not in the pan-tropical one, suggesting that land-use types within a region are more readily characterized by their spatial patterns than their temporal signature. This effect disappears at the pan-tropical level, pointing to different spatial patterns across the tropics. Indeed, this is the setting where it was most advantageous to use spatio-temporal models and, particularly, the attention-based CNN-MHSA. We hypothesize that the arbitrary temporal interactions allowed by attention-based models provide an edge against the noise derived from the high cloud cover characteristic of the tropics.

In terms of computation time, the optimal architectures for temporal and spatial-temporal models resulted in more computationally intensive models at training time compared to the spatial model (2D-CNN), indicating a trade-off between time, resources, and accuracy, for large-scale application.

6.1.2 How can these methods be applied to analyses land-use following deforestation in different national/regional context?

This research question was linked to the studies in chapters 3 and 4. In Chapter 3, a fully convolutional deep learning model (U-Net) with an attention block was trained to classify land-use following deforestation in Ethiopia. The developed attention U-Net model has an advantage over the traditional U-Net model in that it weighs different parts of the image by giving large weights on important parts and small weights on less important parts. The model was trained on three data modalities with different spatial resolutions in this case planet-NICFI (5m), sentinel-2 (10m) and Landsat-8 (30m). The planet-NICFI

images (or high-resolution images) achieved higher classification accuracy (F1-score) than baseline models of Sentinel-2 and Landsat-8 in classifying land-use following deforestation in Ethiopia. The higher accuracy by the Planet-NICFI model is particularly observed on independent test data for the FLU type, large-scale cropland (90%), mining (53%), small-scale cropland (72%), roads (54%), coffee crops (86%), settlement (52%), and tea plantation (85%). Similar accuracy (higher than 80%) was attained when validating wall-to-wall maps produced using high-resolution Planet-NICFI satellite imagery in Ethiopia. The accuracy assessment of the wall-to-wall map using stratified estimation of area and accuracy showed the reliability of the final land-use following deforestation product produced by the Attention U-Net model.

The findings in Chapter 3 also show the confusion in identifying pasture versus other FLU classes, indicating that pasture is indeed often mixed with other FLU, i.e., small-scale croplands, settlements, and other land with tree cover. This is because smallholder farmers in Ethiopia keep their livestock close to home and bring them food and water to preserve the newly acquired deforested areas for farming and housing. On the other hand, pasture is a rare class in our training data, indicating a large amount of training data across spatial and temporal scales would be required to cover the spatial heterogeneity of pasture in Ethiopia.

As stated above, the attention U-Net model performed well in classifying land-use following deforestation in Ethiopia. However, this leads to the question of how useful the model is when applied in classifying land-use following deforestation in another country with different land-use types, class definitions, patterns, geographies, seasonality, and forest types. In Chapter 4, we dive into applying the model from Chapter 3 (Ethiopia) to classify land-use in Ivory Coast, where forest loss is mainly caused by increased demand for commodity crops (i.e., cacao, cashew, oil palm, and rubber). We adopted transfer learning by finetuning the last layer of the attention U-Net model to adapt to the type and number of classes represented in the Ivory Coast. In Ethiopia, we had eleven classes, while in Ivory Coast we had nine land-use classes. This resulted in a deep-learning model that was able to classify land-use following deforestation in the Ivory Coast with a micro-average F1-score of more than 79%. This means that with fine-tuning, the deep learning model can now be adapted and applied to classify land-use following deforestation in another country. However, care needs to be taken that the satellite image data type are the same and are pre-processed in a similar manner. Overall, Chapter 4 shows the importance of using the existing model to adapt to solving another problem in another country with different land-use types, environmental and geographical settings.

6.1.3 How can we leverage heterogeneous reference data to increase the thematic detail of land-use following deforestation mapping?

Developing a deep learning model for regional or continental scale mapping involves the use of a large number of data sets. However, land-use data sets suitable for deep learning are scarce, especially in the Global South. A few available datasets are not readily usable for deep learning applications due to differences in acquisition characteristics and geography. However, the use of deep learning models to track land-use following deforestation across regions over a large scale requires models that are able to generalize across regions. Of central interest in this thesis is the active learning proposed in Chapter 5. Active learning aims to reduce the amount of work of the human annotator by only selecting images during model training that are useful for improving the model's capability to distinguish land-uses across domains. Experiments in Chapter 5 showed that employing deep learning with the assistance of active learning in the annotation of heterogeneous data during model training resulted in an increase in accuracy in identifying land-use following deforestation on independent test datasets. By using active learning (Chapter 5), the classification F1-score of land-use classes such as mining, roads, settlement, rubber, and cashew improved from initially 5%, 10%, 41%, 25%, 14% to 89%, 53%, 92%, 56%, and 92% respectively (more than five-fold improvement). In other words, this means that attention U-Net model together with active learning are now able to identify more than 80% of the land-use in Planet-NICFI imagery and that only pasture achieved an F1-score of less than 50%. This shows the importance of a human working together with the deep learning model during the training, data selection, and annotation process, rather than just adding more data to train a complex model with the hope it will perform well.

6.2 Reflection and outlook

6.2.1 Increasing need for monitoring land-use following deforestation.

Forests are increasingly threatened by human activities, a result of an increase in human population and thus demand for agricultural products; the projections indicate a likely acceleration of this trend in the coming years (UNFCCC, 2021). Therefore, measures to counteract this trend are in high demand. In this context, it is important that these measures are applied systematically, which requires an assessment of the spatio-temporal extent of the land-use changes related to forest loss. A few years back, several companies sourcing commodity crops (e.g., cacao, cashew, oil palm, rubber, and coffee) from forested regions pledged to end deforestation in their supply chain by sourcing agricultural commodity products only from sustainable sources by 2020. However, that goal has not been reached (Bager and Lambin, 2022). This is because there is a lack of a system in place to track and continually monitor the origin of forest-risk commodities (John et al., 2022). Most companies do not know what percentage of commodity crops they sell are

produced with zero net deforestation (Bager and Lambin, 2022). Thus, to help companies avoid sourcing products from unsustainable sources, this thesis proposes the use of freely available high-resolution satellite images (with high visual and spatial detail) and deep learning technologies for efficient land-use identification at scale. This technology will help companies track the source and type of the commodity crop to ensure that the purchased product does not come from unsustainable sources (EUROPEAN COMMISSION, 2022). This will also help improve transparency in the traceability of commodity crops as well as support bodies responsible for certification on responsible forest management to avoid letting companies greenwash their practices.

Similarly, just recently, the European parliament passed a bill to stop import of all commodities linked to deforestation including cacao, cashew, coffee, oil palm, wood, soy, and cattle (EUROPEAN COMMISSION, 2022). This is an important pathway for the European Union (EU) as it plans to achieve its carbon neutrality ambitions by 2050, as set out in its European Green Deal Investment Plan (EUROPEAN COMMISSION, 2020). It is important to note that the consumption of commodity crops in the EU contributes to about 10% of the Earth's deforestation (NGIS, 2022). Thus, the new legislation aims to ensure that consumers in Europe only purchase commodity crop products that are free from deforestation. This new legislation will apply to all commodity crops produced on deforested land after December 2019 (EUROPEAN COMMISSION, 2022). However, the key to compliance with the new legislation requires traceability and transparency across the whole chain, including the producers, traders and consumers. This calls for satellite-based methods capable of identifying deforestation as well as the follow-up land-use to understand the direct driver of deforestation (NGIS, 2022). The use of satellite data and citizen science, together with state-of-the-art technologies, such as the deep learning algorithm, would enable the tracing of the origin footprint of the commodity crop in an open, transparent, and accessible manner to the public.

Another societal aspect of growing interest is the utilization of land-use change data for assessing the effects of population growth, governments policy changes, war, and economic growth on forests. For example, a recent study by Chatelain et al., 2010; Kouassi et al., 2021; Nackoney et al., 2014 assessed the effects of immigration on forests in West Africa by linking it to the trend in deforestation. Another study by Brannstrom et al., 2008; Stickler et al., n.d. also assessed the impacts government policy changes on tropical forests. This data could also be useful to study the interaction and causal effects between land-use types. Study by Sonter et al., 2017 and by Edwards et al., 2014 assessed the impact of mining on increased deforestation related to other land-uses in the Amazon and African forests. This is important information for forest management planning and mitigation action in terms of prioritising the causal agents of deforestation instead of the effects. For example, mining can be the cause of increased deforestation for settlements and small-scale croplands Sonter et al., 2017. Thus, making efforts to protect forest against mining activities can have a profound effects on the later.

Other needs of land-use data emanating from this thesis include the need for countries to include the land-use change data in their nationally determined contributions reporting (NDC) on emissions to the UNFCCC (GOFC-GOLD, 2016). This can only be achieved if countries have access to state-of-art methodologies that serve as a basis for assessing land-use changes and consequently use this data for estimating emissions from these changes (De Sy et al., 2019). The value of this thesis comes from the fact that it uses freely available satellite data, methods, and computational resources that can easily be implemented by countries to track land-uses after deforestation and estimate its emission contributions at a national scale.

6.2.2 The potential of deep learning for mapping land-use following deforestation.

The deep learning methods proposed in this thesis have essentially been customised towards classifying land-use following deforestation using medium and high-resolution optical satellite images. While the presented model architecture and training definition depends on location and scale to some extent (i.e. number and type of land-use - Chapter 3), the methods have potential to be applied to different geographies as well. For example, Chapter 4 shows an application of attention U-Net model from Chapter 3 on the classification of land-use following deforestation in Ivory coast. Compared to the traditional land-use classes classified in chapter 3 with visible geometric properties (i.e., agricultural croplands, settlements, plantations); the commodity crops in Chapter 4 such as cacao, cashew pose the opposite problem, in that they resemble or grow mixed with naturally regenerated trees (agroforestry system). In both cases, the end effect for a human annotator in separating commodity crops from natural forests is prohibitively expensive, unless assisted by deep learning algorithms (computer vision). In Chapter 4, this is made possible through an extension of attention U-Net model to work with large patches of size 256 x 256 pixels and having reference data and images for multiple years, instead of patch size of 128 x 128 pixels and single date image (Chapter 3). The result is that despite the fundamental differences in land-use type and geographical variation, it is possible to identify land-use following deforestation with a high degree of recall and precision by adapting the methods in response to the geographical variation and heterogeneity of land-uses.

Similarly rather than training individual deep learning models per country, in Chapter 5 we presented a single model that can be applied to classify land-use following deforestation regardless of the spatial location of deforestation (in this case Africa). The deep learning model was adapted to work beyond the national context (Chapter 3 and 4). Having models that are able to generalize across regions could potentially enhance tracking land-use following deforestation in a flexible manner (Reichstein et al., 2019; Zhu et al., 2017). For example, an active learning approach presented in Chapter 5 provides a collaborative approach between human and deep learning models, with human acting as a helper to the model by providing additional insight (annotations) useful for better separability between

land-use classes. The result is a high-quality deep learning classifier that can be applied to identify land-use following deforestation with low adaptation efforts to a variety of biomes in the African continent along 30 degrees north to 30 degrees south. However, it is unclear if this approach can be applied to classify land-use following deforestation at a global scale, but if possible, it could open new opportunities for repeated wall-to-wall mapping of land-use following deforestation at a global scale in a more spatial and thematic detail useful for global stockpile, net-zero, and REDD+ processes.

Besides land-use classification in multi-class settings, deep learning also offers the potential for more hybrid and advanced tracking that could be applied with benefits to forest monitoring. The first example is the hybrid model for forest loss and land-use detection, where the model first identifies whether the pixel has been disturbed or deforested before assigning a land-use class. Unlike land-use classification, forest loss detection involves the use of multi-temporal images to extract features before and after deforestation that highlight the subtle changes between images rather than just a single image. However, the challenge would be the computational cost (time and resources) to implement such a model for large-scale applications. The success of this approach will largely depend on access to increasingly high computing cloud platforms (FAO, 2021; Google Earth Engine, 2020). Likewise, forest loss detection has been extensively studied in humid forests and, to a lesser extent, in dry forests (Hansen et al., 2013; Reiche et al., 2021). This poses a challenge on the use of the existing forest loss product as a reference for large-scale land-use prediction, specifically in the dry forests where most forest losses are missed out (Hansen et al., 2013). A hybrid model capable of accurately detecting forest loss in both forest types and eventually predicting deforestation would help reduce the double amount of work involved in producing and accessing these products.

Another example of the potential application of deep learning for forest monitoring efforts could be in forecasting areas of future expansion of commodity crops. This involves the inclusion of data outside of the remote sensing domain such as market demands, population increase, and policy changes. However, the challenge would be how to best integrate data from different domains for deep learning land-use forecasting. The availability of a deep learning model capable of timely forecasting of future areas of commodity crop expansion could enable effective planning and provide insight on potential areas where forest conservation efforts should be strengthened. Similar efforts using deep learning have been realized in forecasting forest areas at risk of future deforestation (Ball et al., 2022).

A further potential application would be the inclusion of citizen science and deep learning in tracking direct drivers of deforestation. Unlike classification in satellite images, citizen science involves collaborating with the public in data collection, analyzing results, and giving feedback (Austin et al., 2019; Fritz et al., 2022). For forest conservation efforts to be effective, their monitoring must also incorporate public input and engagement in

crafting solutions (McKinley et al., 2017). This involves a completely new challenge not addressed in a traditional classification task. For example, a platform or an app where citizen scientists would report information (i.e., coordinates, causes of deforestation, current land-use) and add pictures related to deforestation globally (Austin et al., 2019). These data, satellite images, together with deep learning models can be combined to improve the monitoring of forest resources. The context of citizen science and deep learning offers a number of application opportunities for monitoring direct and maybe even indirect drivers of deforestation, essential for achieving net-zero, NDC, Redd+ efforts, and sustainable development goals.

6.2.3 Potential future space data to enhance the accuracy of land-use mapping.

Monitoring forests and the associated land-use changes require continual and frequent availability of up-to-date remote sensing data. The recent advances and availability of free and open-source remote sensing satellite imagery like Landsat 1–5, 7, 8–9 and Sentinel-1, 2A, 2B have extensively enabled the assessment of changes in land-use (Curtis et al., 2018; De Sy et al., 2019; Masolele et al., 2021), changes in land-cover (Brown et al., 2022; Tsendbazar et al., 2021), forest characteristics (Lu et al., 2004; Mutanga et al., 2012; Potapov et al., 2021), and in forest disturbances monitoring (Decuyper et al., 2022; Reiche et al., 2021; Ye et al., 2021). The policy of free and open data with respect to the Landsat and Sentinel satellites means increased accessibility of moderate resolution images to commercial and noncommercial players, which is essentially relevant to the assessment of land-use changes over the pan-tropics in a medium spatial and high temporal detail (Curtis et al., 2018; Hansen et al., 2013; Schepaschenko et al., 2019). Nevertheless, the moderate spatial resolution limits its use in identifying the land-use following deforestation in much subtle and fine detail (Irvin et al., 2020; Masolele et al., 2021). Additionally, the heterogeneous nature of land-use after deforestation, in spatial and temporal dimension (i.e., a mix of land-use with remaining tree cover, changes of land-use signature with seasonality and growth), creates a higher requirement on the spatial-temporal resolutions of the remote sensing data. The considerable increase in the capacity of the new generation sensors to detect subtle change has opened and will continue to open new opportunities for forest monitoring with higher accuracy (Finer et al., 2018; Gallwey et al., 2020; Masolele et al., 2021; Meng et al., 2017; Zhang et al., 2019). The studies conducted in chapters 3, 4 and 5 of this thesis further demonstrated that the higher-resolution data in this case planet-NICFI achieves higher accuracies in identifying land-use following deforestation on a national and regional scale. Using planet-NICFI images at 5m resolution enabled even the detection of finer details of land-uses such as the complexity of small-scale cropland and its access roads which otherwise would not be detected with medium-resolution images.

Although in Chapter 3, we demonstrated that a single-date medium resolution Landsat and sentinel-2 data are not able to achieve the higher classification accuracy as planet-NICFI

data. However, the data are able to achieve higher accuracies using a time-series of data as opposed to using single date images. In chapter 3 of this thesis, we further demonstrated that given the availability of temporal reference data, the classification of land-use following deforestation using time-series Landsat or Sentinel-2 data is possible.

In spite of the success of planet-NICFI data in classifying land-use following deforestation at a national and regional scale, some challenges remain. For example, the persistent cloud cover and haze make it challenging to track land-use following deforestation in some parts of tropical regions (i.e., Gabon, Congo, Ivory coast) (Reiche et al., 2021). The inclusion of synthetic aperture radar data (SAR) offers a complementary advantage in detecting land-use in these areas. SAR data is characterized by its ability to penetrate through clouds, thus offering consistent, global cloud-free images which can be combined with optical images to increase the classification performance of the deep learning model in cloud areas. Currently, there exist SAR satellite missions such as sentinel-1 and ALOS/PALSAR annual mosaics, which provide images at C and L-band with a spatial and temporal resolution of 10m, 25m, 6-day, and 1-year, respectively (Ballère et al., 2021; Reiche et al., 2018). One advantage of L-band SAR is that it can penetrate through a forest canopy, thus useful in detecting logging roads and artisanal mining in areas where optical data fail to do so due to canopy coverage. However, its lower resolution makes it challenging to detect these subtle detail. Future availability of high-resolution SAR data (i.e. $\geq 5m$) with longer wavelength will increase the model's capacity in detecting land-use activities under the canopy, i.e., logging roads. According to Rosen et al., 2017, NASA is expecting to launch a SAR satellite by 2023 which will provide full polarimetric L-band SAR data with a 12-day revisit cycle and a range, azimuth resolution of 3 10 m and 7m respectively. The delivered L-band SAR images would improve the classification of land-use following deforestation in more spatial and temporal detail by complementing existing optical data. A similar launch mission in 2023 is planned by European Space Agency - ESA (BIOMASS mission); the satellite will provide SAR data at the P-band wavelength, which has more canopy penetration capability than C and L-band. In addition, ESA is also planning to launch an L-band synthetic aperture radar (ROSE-L mission) by 2028 (ESA, n.d.). The mission will provide continuous monitoring of the earth's surface and will be a great addition to the existing satellite missions.

Besides the freely available and open SAR data, recently, there has also been an increase in the constellation of small commercial SAR satellite missions such as CAPELLA SPACE (Capella space, 2022) and ICEYE (Iceye, 2022). These constellations of small SAR satellites provide repeated imaging of the earth and provide SAR data which comes with much higher resolution and temporal coverage. For example, CAPELLA SPACE provides daily all-weather high-resolution SAR data at a 0.5m to 1.3m resolution, while ICEYE provides daily SAR data at a 2m spatial resolution. The value of these missions is that they provide data that enables the persistent monitoring of forest conditions and land-use change day and night and in all weather conditions with high spatial detail, which

is essential for features and pattern detection by the deep learning model in land-use assessment. With more spatial detail of SAR data means more detection of more thematic detail; thus the output product becomes useful for application and decision-making at both local and regional scales. However, the only downside is the high monetary resources required to purchase and use these data over large areas. An extension of the NICFI program to include SAR data in its program will complement an already existing and operational usage of high-resolution satellite data for tropical forest monitoring, (ie., the planet-NICFI program).

Another interesting earth observation mission useful for forests and land-use change monitoring is the German space-borne imaging spectrometer mission known as the Environmental Mapping and Analysis Program (EnMAP), which was launched in April 2022. The EnMap provides hyperspectral imaging capabilities of the earth's surface from the visible (420nm) to shortwave infra-red region (2450nm) of the spectrum. The satellite provides global imaging of the earth at a spatial resolution of 30m, a temporal resolution of 4 days, and a spectral resolution of 230 bands (Guanter et al., 2015). The rich spectral resolution of these data is especially useful for tracking changes in forests and monitoring more thematic detail land-uses on any place on earth and adds values to already existing spatial-temporal information obtained from high-resolution images.

Previously there was a cry that in spite of having a large amount of satellite data, the computational infrastructure to process the data was limited (Alshari and Gawali, 2021). Specifically the use of a large amount of data for large-scale applications. The recent development of cloud computing platforms enhanced with graphical processing unit (GPU) for parallel processing and data storage has improved use and application. In spite of many of the cloud computing platforms being a commercial services such as Amazon Web Services (AWS) and Google Cloud, open service infrastructures are also coming up. For example, the analysis of this whole thesis was implemented largely in SEPAL geospatial analysis platform hosted at (FAO, 2021) and partly in the Dutch national Supercomputer service (SURFsara) (SURFsara, 2022). These platforms provide ease of access, storage, processing, and analysis of a large amount of earth observation data for forest and land-use change monitoring at the global scale and even at high-resolution. The availability of GPU means much faster processing, 10 to 20 time the speed of the CPU, which effectively improve the repeated implementation and employment of the deep learning models for continual monitoring of forests and land-use change, thus supporting the Redd+, NDC, and net-zero efforts (e.g. reducing emissions from deforestation and forest degradation (REDD), carbon sequestration in forests) (GOFC-GOLD, 2016).

References

- Abadi, M., P. Barham, J. Chen, Z. Chen, A. Davis, J. Dean, M. Devin, S. Ghemawat, G. Irving, M. Isard, M. Kudlur, J. Levenberg, R. Monga, S. Moore, D. G. Murray, B. Steiner, P. Tucker, V. Vasudevan, P. Warden, M. Wicke, Y. Yu, and X. Zheng (2015). “TensorFlow: A system for large-scale machine learning”. In: *Proceedings of the 12th USENIX Symposium on Operating Systems Design and Implementation, OSDI 2016*. USENIX Association, 265–283. DOI: 10.5555/3026877.3026899.
- Abdalla Juma, S. and P. Administration (2019). “The Black Tea Industry in East Africa: History, Culture, Trends, and Opportunities”. *Journal of Economics and Sustainable Development* 10.6, 160–170. DOI: 10.7176/JESD/10-6-19.
- Abebe, S. T., A. B. Dagneu, V. G. Zeleke, G. Z. Eshetu, and G. T. Cirella (2019). “Willingness to Pay for Watershed Management”. *Resources 2019, Vol. 8, Page 77* 8.2, 77. DOI: 10.3390/RESOURCES8020077.
- Abu, I. O., Z. Szantoi, A. Brink, M. Robuchon, and M. Thiel (2021). “Detecting cocoa plantations in Côte d’Ivoire and Ghana and their implications on protected areas”. *Ecological Indicators* 129, 107863. DOI: 10.1016/J.ECOLIND.2021.107863.
- Adepoju, A. (2011). “Reflections on international migration and development in sub-Saharan Africa”. *African Population Studies* 25.2, 298–319. DOI: 10.11564/25-2-233.
- Alshari, E. A. and B. W. Gawali (2021). “Evaluation of the potentials and challenges of land observation satellites”. *Global Transitions Proceedings* 2.1, 73–79. DOI: 10.1016/J.GLTP.2021.01.010.
- Annan, N. (2014). “Violent conflicts and civil strife in West Africa: Causes, challenges and prospects”. *Stability* 3.1. DOI: 10.5334/sta.da.
- Arévalo, P., P. Olofsson, and C. E. Woodcock (2019). “Continuous monitoring of land change activities and post-disturbance dynamics from Landsat time series : A test methodology for REDD + reporting”. *Remote Sensing of Environment* January 2018, 1–14. DOI: 10.1016/j.rse.2019.01.013.
- Asselen, S. van and P. H. Verburg (2012). “A Land System representation for global assessments and land-use modeling”. *Global Change Biology* 18.10, 3125–3148. DOI: 10.1111/j.1365-2486.2012.02759.x.

- Austin, G. (2009). “Cash Crops and Freedom: Export Agriculture and the Decline of Slavery in Colonial West Africa*”. *International Review of Social History* 54.1, 1–37. DOI: 10.1017/S0020859009000017.
- Austin, K. G., A. Schwantes, Y. Gu, and P. S. Kasibhatla (2019). “What causes deforestation in Indonesia?” *Environmental Research Letters* 14.2, 024007. DOI: 10.1088/1748-9326/AAF6DB.
- Babu, S. C., E. Oyedipe, O. Ajakaiye, and K. Ajoni (2017). “Strategies for restructuring the Agricultural Research Council of Nigeria: Process, opportunities, and lessons - IFPRI Publications Repository - IFPRI Knowledge Collections”. Washington, D.C.
- Bae, S., S. R. Levick, L. Heidrich, P. Magdon, B. F. Leutner, S. Wöllauer, A. Serebryanyk, T. Nauss, P. Krzystek, M. M. Gossner, P. Schall, C. Heibl, C. Bässler, I. Doerfler, E. D. Schulze, F. S. Krah, H. Culmsee, K. Jung, M. Heurich, M. Fischer, S. Seibold, S. Thorn, T. Gerlach, T. Hothorn, W. W. Weisser, and J. Müller (2019). “Radar vision in the mapping of forest biodiversity from space”. *Nature Communications* 2019 10:1 10.1, 1–10. DOI: 10.1038/s41467-019-12737-x.
- Bager, S. L. and E. F. Lambin (2022). “How do companies implement their zero-deforestation commitments?”. *Journal of Cleaner Production* 375, 134056. DOI: 10.1016/J.JCLEPRO.2022.134056.
- Ball, J. G., K. Petrova, D. A. Coomes, and S. Flaxman (2022). “Using deep convolutional neural networks to forecast spatial patterns of Amazonian deforestation”. *Methods in Ecology and Evolution* 13.11, 2622–2634. DOI: 10.1111/2041-210X.13953.
- Ballère, M., A. Bouvet, S. Mermoz, T. Le Toan, T. Koleck, C. Bedeau, M. André, E. Forestier, P. L. Frison, and C. Lardeux (2021). “SAR data for tropical forest disturbance alerts in French Guiana: Benefit over optical imagery”. *Remote Sensing of Environment* 252, 112159. DOI: 10.1016/J.RSE.2020.112159.
- Balzter, H., B. Cole, C. Thiel, and C. Schmullius (2015). “Mapping CORINE land cover from Sentinel-1A SAR and SRTM digital elevation model data using random forests”. *Remote Sensing* 7.11, 14876–14898. DOI: 10.3390/rs71114876.
- Barima, Y. S. S., A. T. M. Kouakou, I. Bamba, Y. C. Sangne, M. Godron, J. Andrieu, and J. Bogaert (2016). “Cocoa crops are destroying the forest reserves of the classified forest of Haut-Sassandra (Ivory Coast)”. *Global Ecology and Conservation* 8, 85–98. DOI: <https://doi.org/10.1016/j.gecco.2016.08.009>.
- Bazi, Y., L. Bashmal, M. M. A. Rahhal, R. A. Dayil, and N. A. Ajlan (2021). “Vision Transformers for Remote Sensing Image Classification”. *Remote Sensing* 13.3, 516. DOI: 10.3390/rs13030516.
- BBC (2019). *Did Ethiopia plant four billion trees this year? - BBC News*.

- Bekunda, M., N. Sanginga, and P. L. Woomer (2010). “Restoring Soil Fertility in Sub-Sahara Africa”. *Advances in Agronomy* 108.C, 183–236. DOI: 10.1016/S0065-2113(10)08004-1.
- Bengar, J. Z., J. Van De Weijer, L. L. Fuentes, and B. Raducanu (2021). “Class-Balanced Active Learning for Image Classification”. *Proceedings - 2022 IEEE/CVF Winter Conference on Applications of Computer Vision, WACV 2022*, 3707–3716. DOI: 10.48550/arxiv.2110.04543.
- Berhan, T. and G. Egziabher (1991). “Diversity of the Ethiopian flora”. *Plant Genetic Resources of Ethiopia*, 75–81. DOI: 10.1017/CB09780511551543.005.
- Betru, T., M. Tolera, K. Sahle, and H. Kassa (2019). “Trends and drivers of land use/land cover change in Western Ethiopia”. *Applied Geography* 104, 83–93. DOI: 10.1016/J.APGEOG.2019.02.007.
- BioCarbon Fund (2020). *BioCarbon Fund Initiative for Sustainable Forest Landscapes*. Tech. rep.
- Bishaw, B. (2001). “Deforestation and Land Degredation in the Ethiopian Highlands: A Strategy for Physical Recovery”. *Northeast African Studies* 8.1, 7–25. DOI: 10.1353/NAS.2005.0014.
- Boriah, S. (2010). “Time Series Change Detection: Algorithms for Land Cover Change”. PhD thesis. University of Minnesota, 1–160.
- Bp, G., A. Raju, and G. S. Dwarakish (2015). “Different Approaches for Land Use Land Cover Change Detection : A Review Different Approaches for Land Use Land Cover Change Detection : A Review”. October.
- Brannstrom, C., W. Jepson, A. M. Filippi, D. Redo, Z. Xu, and S. Ganesh (2008). “Land change in the Brazilian Savanna (Cerrado), 1986-2002: Comparative analysis and implications for land-use policy”. *Land Use Policy* 25.4, 579–595. DOI: 10.1016/j.landusepol.2007.11.008.
- Brown, C. F., S. P. Brumby, B. Guzder-Williams, T. Birch, S. B. Hyde, J. Mazzariello, W. Czerwinski, V. J. Pasquarella, R. Haertel, S. Ilyushchenko, K. Schwehr, M. Weisse, F. Stolle, C. Hanson, O. Guinan, R. Moore, and A. M. Tait (2022). “Dynamic World, Near real-time global 10m land use land cover mapping”. *Scientific Data* 2022 9:1 9.1, 1–17. DOI: 10.1038/s41597-022-01307-4.
- Bryceson, D. F. (2007). “African rural labour, income diversification & livelihood approaches: a long-term development perspective”. <https://doi.org/10.1080/03056249908704377> 26.80, 171–189. DOI: 10.1080/03056249908704377.
- Campbell, D. J., D. P. Lusch, T. A. Smucker, and E. E. Wangui (2005). “Multiple Methods in the Study of Driving Forces of Land Use and Land Cover Change : A Case Study of SE Kajiado District , Kenya”. 33.6, 763–794. DOI: 10.1007/s10745-005-8210-y.

- Capella space (2022). *SAR Imagery Products - Capella Space*.
- Carter, S., M. Herold, V. Avitabile, S. de Bruin, V. De Sy, L. Kooistra, and M. C. Rufino (2017). “Agriculture-driven deforestation in the tropics from 1990–2015: emissions, trends and uncertainties”. *Environmental Research Letters* 13.1, 014002. DOI: 10.1088/1748-9326/AA9EA4.
- Castelluccio, M., G. Poggi, C. Sansone, and L. Verdoliva (2015). “Land Use Classification in Remote Sensing Images by Convolutional Neural Networks”. *Computer Vision And Pattern Recognition*, 1–11. DOI: 10.1021/cr8002505.
- Castilla, G. and G. J. Hay (2007). “Uncertainties in land use data”. *Hydrology and Earth System Sciences Discussions* 11.6, 1857–1868.
- Chatelain, C., A. Bakayoko, P. Martin, and L. Gautier (2010). “Monitoring tropical forest fragmentation in the Zagné-Taï area (west of Taï National Park, Côte d’Ivoire)”. *Biodiversity and Conservation* 19.8, 2405–2420. DOI: 10.1007/s10531-010-9847-4.
- Chollet, F. et al. (2015). *Keras*.
- CIFOR (2021). *Reducing deforestation and forest degradation, and conservation of Forests at the Green Climate Fund Too much, too little, or just enough? - CIFOR Forests News*.
- Cole, B., G. Smith, and H. Balzter (2018). “Acceleration and fragmentation of CORINE land cover changes in the United Kingdom from 2006–2012 detected by Copernicus IMAGE2012 satellite data”. *International Journal of Applied Earth Observation and Geoinformation* 73. June, 107–122. DOI: 10.1016/j.jag.2018.06.003.
- Comber, A., H. Balzter, B. Cole, P. Fisher, S. C. Johnson, and B. Ogotu (2016). “Methods to quantify regional differences in land cover change”. *Remote Sensing* 8.3, 1–19. DOI: 10.3390/rs8030176.
- Cook, M., J. R. Schott, J. Mandel, and N. Raqueno (2014). “Development of an Operational Calibration Methodology for the Landsat Thermal Data Archive and Initial Testing of the Atmospheric Compensation Component of a Land Surface Temperature (LST) Product from the Archive”. *Remote Sensing 2014, Vol. 6, Pages 11244-11266* 6.11, 11244–11266. DOI: 10.3390/RS61111244.
- Curtis, P. G., C. M. Slay, N. L. Harris, A. Tyukavina, and M. C. Hansen (2018). “Classifying drivers of global forest loss”. *Forest Ecology* 1111. September, 1108–1111.
- De Sy, V. (2016). *Remote sensing of land use and carbon losses following tropical deforestation*. DOI: 10.18174/380263.
- De Sy, V., M. Herold, F. Achard, V. Avitabile, A. Baccini, S. Carter, J. G. Clevers, E. Lindquist, M. Pereira, and L. Verchot (2019). “Tropical deforestation drivers and associated carbon emission factors derived from remote sensing data”. *Environmental Research Letters* 14.9, 094022. DOI: 10.1088/1748-9326/ab3dc6.
- De Sy, V., M. Herold, F. Achard, R. Beuchle, J. G. Clevers, E. Lindquist, and L. Verchot (2015). “Land use patterns and related carbon losses following deforestation in South

- America". *Environmental Research Letters* 10.12, 124004. DOI: 10.1088/1748-9326/10/12/124004.
- Decuyper, M., R. O. Chávez, M. Lohbeck, J. A. Lastra, N. Tsendbazar, J. Hackländer, M. Herold, and T. G. Vågen (2022). "Continuous monitoring of forest change dynamics with satellite time series". *Remote Sensing of Environment* 269, 112829. DOI: 10.1016/J.RSE.2021.112829.
- Descals, A., S. Wich, E. Meijaard, D. L. A. Gaveau, S. Peedell, and Z. Szantoi (2021a). "High-resolution global map of smallholder and industrial closed-canopy oil palm plantations". *Earth System Science Data* 3, 1211–1231. DOI: 10.5194/essd-13-1211-2021.
- (2021b). "High-resolution global map of smallholder and industrial closed-canopy oil palm plantations". *Earth Syst. Sci. Data* 13, 1211–1231. DOI: 10.5194/essd-13-1211-2021.
- Dinerstein, E., D. Olson, A. Joshi, C. Vynne, N. D. Burgess, E. Wikramanayake, N. Hahn, S. Palminteri, P. Hedao, R. Noss, M. Hansen, H. Locke, E. C. Ellis, B. Jones, C. V. Barber, R. Hayes, C. Kormos, V. Martin, E. Crist, W. Sechrest, L. Price, J. E. Baillie, D. Weeden, K. Suckling, C. Davis, N. Sizer, R. Moore, D. Thau, T. Birch, P. Potapov, S. Turubanova, A. Tyukavina, N. De Souza, L. Pintea, J. C. Brito, O. A. Llewellyn, A. G. Miller, A. Patzelt, S. A. Ghazanfar, J. Timberlake, H. Klöser, Y. Shennan-Farpón, R. Kindt, J. P. B. Lillesø, P. Van Breugel, L. Graudal, M. Voge, K. F. Al-Shammari, and M. Saleem (2017). "An Ecoregion-Based Approach to Protecting Half the Terrestrial Realm". *BioScience* 67.6, 534–545. DOI: 10.1093/BIOSCI/BIX014.
- Doggart, N., T. Morgan-Brown, E. Lyimo, B. Mbilinyi, C. K. Meshack, S. M. Sallu, and D. V. Spracklen (2020). "Agriculture is the main driver of deforestation in Tanzania". *Environmental Research Letters* 15.3, 034028. DOI: 10.1088/1748-9326/ab6b35.
- Dow Goldman, E., M. Weisse, N. Harris, and M. Schneider (2020). "Estimating the Role of Seven Commodities in Agriculture-Linked Deforestation: Oil Palm, Soy, Cattle, Wood Fiber, Cocoa, Coffee, and Rubber". *World Resources Institute*. DOI: 10.46830/WRITN.NA.00001.
- Dufrène, B. (2019). *Africa Dominates World Tea Exports, While Still Evolving - Tea & Coffee Trade Journal*.
- Edwards, D. P., S. Sloan, L. Weng, P. Dirks, J. Sayer, and W. F. Laurance (2014). "Mining and the African Environment". *Conservation Letters* 7.3, 302–311. DOI: 10.1111/CONL.12076.
- Erik Hoffner (2021). *Forests falling for cashew monocultures: A 'repeated mistake' in Côte d'Ivoire (commentary)*.
- ESA (n.d.). *ESA - Contract signed for new Copernicus ROSE-L mission*.
- Ethiopian Forest Division (2022). *Monitoring RIP-DD intervention in the forests of south-western Ethiopia: Land use land cover change detection for the period 2018 - 2022*.

- EUROPEAN COMMISSION (2020). *COMMUNICATION FROM THE COMMISSION :The European Green Deal*.
- (2022). *Proposal for a REGULATION OF THE EUROPEAN PARLIAMENT AND OF THE COUNCIL on the making available on the Union market as well as export from the Union of certain commodities and products associated with deforestation and forest degradation and repealing Regulation (EU) No 995/2010*.
- FAO (2010). *GLOBAL FOREST RESOURCES ASSESSMENT 2010*. Tech. rep. Rome: Forestry Department Food and Agriculture Organization of the United Nations.
- (2014). “Agriculture, Forestry and Other Land Use Emissions by Sources and Removals by Sinks”.
- (2016). *State of the World’s Forests 2016. Forests and agriculture: land-use challenges and opportunities*. Tech. rep. Rome: Food and Agriculture Organization of the United Nation, 126.
- (2017). *Données forestières de base pour la redd+ en côte d’ivoire*, 1–32.
- (2020). *Global Forest Resources Assessment 2020 Main report*. Tech. rep. Rome, Italy: FAO, 184. DOI: 10.4060/ca9825en.
- (2021). “SEPAL, a big-data platform for forest and land monitoring”. Rome, Italy.
- FAO & JRC (2012a). “Global forest land-use change 1990-2005”. Rome.
- (2012b). “Global forest land-use change 1990-2005”. Rome.
- Finer, M., S. Novoa, M. J. Weisse, R. Petersen, J. Mascaro, T. Souto, F. Stearns, and R. García Martínez (2018). “Combating deforestation: From satellite to intervention”. *Science* 360.6395, 1303–1305. DOI: 10.1126/science.aat1203.
- Fisher, B. (2010). “African exception to drivers of deforestation”. *Nature Geosci.* 3.6, 375–376. DOI: 10.1038/ngeo873.
- Fratkin, E. (2001). “East African Pastoralism in Transition: Maasai, Boran, and Rendille Cases”. *African Studies Review* 44.3, 1–25. DOI: 10.2307/525591.
- Friis Ib, Demissew Sebsebe, and reugel Paulo van B (2010). *Atlas of the Potential Vegetation of Ethiopia*. Ed. by Selskab Det Kongelige Danske Videnskabernes. The Royal Danish Academy of Sciences and Letters.
- Fritz, S., J. C. Laso Bayas, L. See, D. Schepaschenko, F. Hofhansl, M. Jung, M. Dürauer, I. Georgieva, O. Danylo, M. Lesiv, and I. McCallum (2022). “A Continental Assessment of the Drivers of Tropical Deforestation With a Focus on Protected Areas”. *Frontiers in Conservation Science* 0, 13. DOI: 10.3389/FC0SC.2022.830248.
- Fritz, S., L. See, C. Perger, I. McCallum, C. Schill, D. Schepaschenko, M. Duerauer, M. Karner, C. Dresel, J. C. Laso-Bayas, M. Lesiv, I. Moorthy, C. F. Salk, O. Danylo, T. Sturn, F. Albrecht, L. You, F. Kraxner, and M. Obersteiner (2017). “A global dataset

- of crowdsourced land cover and land use reference data”. *Scientific Data* 4.1, 1–8. DOI: 10.1038/sdata.2017.75.
- Gallwey, J., C. Robiati, J. Coggan, D. Vogt, and M. Eyre (2020). “A Sentinel-2 based multispectral convolutional neural network for detecting artisanal small-scale mining in Ghana: Applying deep learning to shallow mining”. *Remote Sensing of Environment* 248, 111970. DOI: 10.1016/J.RSE.2020.111970.
- Geist, H. J. and E. F. Lambin (2001). *What drives tropical deforestation? A meta-analysis of proximate and underlying causes of deforestation based on subnational case study evidence*. Tech. rep. 4.
- Getahun, K., J. Poesen, and A. Van Rompaey (2017). “Impacts of Resettlement Programs on Deforestation of Moist Evergreen Afromontane Forests in Southwest Ethiopia”. *Mountain Research and Development* 37.4, 474–486. DOI: 10.1659/MRD-JOURNAL-D-15-00034.1.
- Gibbs, H. K., S. Brown, J. O. Niles, and J. A. Foley (2007). “Monitoring and estimating tropical forest carbon stocks: making REDD a reality”. *Environmental Research Letters* 2.2007, 045023. DOI: 10.1088/1748-9326/2/4/045023.
- Gilles, L. and K. Manoj (n.d.). *Bayesian optimization with skopt — scikit-optimize 0.8.1 documentation*.
- Global Forest Review (2022). *About the Global Forest Review — Global Forest Review*. Tech. rep. Washington, DC: World Resources Institute.
- GOFC-GOLD (2016). *A sourcebook of methods and procedures for monitoring and reporting anthropogenic greenhouse gas emissions and removals associated with deforestation, gains and losses of carbon stocks in forests remaining forests, and forestation. GOFC-GOLD Report version COP22-1*. (GOFC-GOLD Land Cover Project Office, Wageningen University, The Netherlands).
- Google Earth Engine (2020). *USGS Landsat 7 Surface Reflectance Tier 1 — Earth Engine Data Catalog*.
- GRID (2022). *Welcome - GRID3*.
- Group, F. (2008). “Introduction to the Polarimetric Target Decomposition Concept 6.1”.
- Guanter, L., H. Kaufmann, K. Segl, S. Foerster, C. Rogass, S. Chabrillat, T. Kuester, A. Hollstein, G. Rossner, C. Chlebek, C. Straif, S. Fischer, S. Schrader, T. Storch, U. Heiden, A. Mueller, M. Bachmann, H. Mühle, R. Müller, M. Habermeyer, A. Ohndorf, J. Hill, H. Buddenbaum, P. Hostert, S. Van Der Linden, P. J. Leitão, A. Rabe, R. Doerffer, H. Krasemann, H. Xi, W. Mauser, T. Hank, M. Locherer, M. Rast, K. Staenz, and B. Sang (2015). “The EnMAP Spaceborne Imaging Spectroscopy Mission for Earth Observation”. *Remote Sensing 2015, Vol. 7, Pages 8830-8857* 7.7, 8830–8857. DOI: 10.3390/RS70708830.

- Haas, M. d. and E. Travieso (2022). “Cash-Crop Migration Systems in East and West Africa : Rise, Endurance, Decline”. *Migration in Africa*, 231–255. DOI: 10.4324/9781003225027-16.
- Habte, D. G., S. Belliethathan, and T. Ayenew (2021). “Evaluation of the status of land use/land cover change using remote sensing and GIS in Jewha Watershed, Northeastern Ethiopia”. *SN Applied Sciences* 3.4, 1–10. DOI: 10.1007/S42452-021-04498-4/TABLES/6.
- Hansen, M., P. Potapov, B. Margono, S. Stehman, S. Turubanova, and A. Tyukavina (2014). *Response to comment on "High-resolution global maps of 21st-century forest cover change"*. DOI: 10.1126/science.1248817.
- Hansen, M. C., S. V. Stehman, and P. V. Potapov (2010a). “Quantification of global gross forest cover loss”. *Proceedings of the National Academy of Sciences* 107.19, 8650–8655. DOI: 10.1073/pnas.0912668107.
- (2010b). “Quantification of global gross forest cover loss”. *Proceedings of the National Academy of Sciences* 107.19, 8650–8655. DOI: 10.1073/pnas.0912668107.
- Hansen, M., P. V. Potapov, R. Moore, M. Hancher, S. A. Turubanova, A. Tyukavina, D. Thau, S. V. Stehman, S. J. Goetz, T. R. Loveland, A. Kommareddy, A. Egorov, L. Chini, C. O. Justice, and J. R. Townshend (2013). “High-resolution global maps of 21st-century forest cover change”. *Science* 342.6160, 850–853. DOI: 10.1126/science.1244693.
- Harfoot, M. B. J., A. Johnston, A. Balmford, N. D. Burgess, S. H. M. Butchart, M. P. Dias, C. Hazin, C. Hilton-Taylor, M. Hoffmann, N. J. B. Isaac, L. L. Iversen, C. L. Outhwaite, P. Visconti, and J. Geldmann (2021). “Using the IUCN Red List to map threats to terrestrial vertebrates at global scale”. *Nature Ecology & Evolution* 2021, 1–10. DOI: 10.1038/s41559-021-01542-9.
- Helber, P., B. Bischke, A. Dengel, and D. Borth (2017). “EuroSAT : A Novel Dataset and Deep Learning Benchmark for Land Use and Land Cover Classification”. *EuroSAT*, 9.
- Herold, M., X. Liu, and K. C. Clarke (2003). “Spatial Metrics and Image Texture for Mapping Urban Land Use”. *American Society for Photogrammetry and Remote Sensing* 69.9, 1001.
- Herrmann, S. M., M. Brandt, K. Rasmussen, and R. Fensholt (2020). “Accelerating land cover change in West Africa over four decades as population pressure increased”. *Communications Earth & Environment* 2020 1:1 1.1, 1–10. DOI: 10.1038/s43247-020-00053-y.
- Hishe, H., K. Giday, J. Van Orshoven, B. Muys, F. Taheri, H. Azadi, L. Feng, O. Zamani, M. Mirzaei, and F. Witlox (2021). “Analysis of Land Use Land Cover Dynamics and Driving Factors in Desa’a Forest in Northern Ethiopia”. *Land Use Policy* 101, 105039. DOI: 10.1016/J.LANDUSEPOL.2020.105039.

- Homewood, K., E. Coast, and M. Thompson (2004). “In-Migrants and Exclusion in East African Rangelands: Access, Tenure and Conflict”. *Africa: Journal of the International African Institute* 74.4, 567. DOI: 10.2307/3556842.
- Hosonuma, N., M. Herold, V. De Sy, R. S. De Fries, M. Brockhaus, L. Verchot, A. Angelsen, and E. Romijn (2012). “An assessment of deforestation and forest degradation drivers in developing countries”. *Environmental Research Letters* 7.4, 044009. DOI: 10.1088/1748-9326/7/4/044009.
- Hu, Y., Y. Wong, W. Wei, Y. Du, M. Kankanhalli, and W. Geng (2018). “A novel attention-based hybrid CNN-RNN architecture for sEMG-based gesture recognition”. *PLOS ONE* 13.10. Ed. by H. He, e0206049. DOI: 10.1371/journal.pone.0206049.
- Huang, B., B. Zhao, and Y. Song (2018). “Urban land-use mapping using a deep convolutional neural network with high spatial resolution multispectral remote sensing imagery”. *Remote Sensing of Environment* 214. April, 73–86. DOI: 10.1016/j.rse.2018.04.050.
- Huggins, X., T. Gleeson, M. Kummu, S. C. Zipper, Y. Wada, T. J. Troy, and J. S. Famiglietti (2022). “Hotspots for social and ecological impacts from freshwater stress and storage loss”. *Nature Communications* 2022 13:1 13.1, 1–11. DOI: 10.1038/s41467-022-28029-w.
- Hughes, L. H., M. Schmitt, L. Mou, Y. Wang, and X. X. Zhu (2018). “Identifying Corresponding Patches in SAR and Optical Images With a Pseudo-Siamese CNN”. *IEEE Geoscience and Remote Sensing Letters*, 1–5. DOI: 10.1109/LGRS.2018.2799232.
- Hylander, K., S. Nemomissa, J. Delrue, and W. Enkosa (2013). “Effects of Coffee Management on Deforestation Rates and Forest Integrity”. *Conservation Biology* 27.5, 1031–1040. DOI: 10.1111/COBI.12079.
- Iceye (2022). *Satellite Missions — ICEYE*.
- Interdonato, R., D. Ienco, R. Gaetano, and K. Ose (2018). “DuPLO: A DUal view Point deep Learning architecture for time series classificatiOn”, 32.
- IPCC (2013). *Climate Change 2013*. Tech. rep. Cambridge University Press, Cambridge, United Kingdom and New York, NY, USA: Cambridge University Press, Cambridge, United Kingdom and New York, NY, USA, 1535 pp, 1535.
- (2021). *Summary for Policymakers*. In: *Climate Change 2021: The Physical Science Basis. Contribution of Working Group I to the Sixth Assessment Report of the Intergovernmental Panel on Climate Change [Masson-Delmotte, V., P. Zhai, A. Pirani, S. L. Connors, C. Péan*. Tech. rep.
- IPIS (2022). *Open Data - IPIS*.
- Irvin, J., H. Sheng, N. Ramachandran, S. Johnson-Yu, S. Zhou, K. Story, R. Rustowicz, C. Elsworth, K. Austin, and A. Y. Ng (2020). “ForestNet: Classifying Drivers of Deforestation in Indonesia using Deep Learning on Satellite Imagery”. In: *34th Conference on Neural Information Processing Systems*. Vancouver, 10.

- Jalloh, A., G. C. Nelson, T. S. Thomas, R. Zougmore, and H. Roy-Macauley (2013). “West African Agriculture and Climate Change”. *International Food policy Research Institute*. Ed. by A. Jalloh, Gerald C. Nelson, Timothy S. Thomas, Robert Zougmore, and Harold Roy-Macauley, 408. DOI: 10.2499/9780896292048.
- John, L., H. Camilla, Y. Zhi Yi, B. Richard, C. Peter, H. Thomas, H. Frederic, H. Nick, H. Niklas, H. Angel, K. Takeshi, and S. Steve (2022). *Net Zero Tracker*. Tech. rep. Energy and Climate Intelligence Unit, Data-Driven EnviroLab, NewClimate Institute, Oxford Net Zero.
- Johnson, J. M. and T. M. Khoshgoftaar (2019). “Survey on deep learning with class imbalance”. *Journal of Big Data* 6.1, 1–54. DOI: 10.1186/s40537-019-0192-5.
- Joshi, A. J., F. Porikli, and N. Papanikolopoulos (2010). “Multi-class active learning for image classification”, 2372–2379. DOI: 10.1109/CVPR.2009.5206627.
- Karuri, A. N. (2021). “Adaptation of Small-Scale Tea and Coffee Farmers in Kenya to Climate Change”. *African Handbook of Climate Change Adaptation*, 29–47. DOI: 10.1007/978-3-030-45106-6{_}70.
- Kellenberger, B., D. Marcos, and D. Tuia (2018). “Detecting Mammals in UAV Images : Best Practices to address a substantially Imbalanced Dataset with Deep Learning”. *Remote Sensing of Environment*.
- Kennedy, R. E., Z. Yang, and W. B. Cohen (2010). “Detecting trends in forest disturbance and recovery using yearly Landsat time series: 1. LandTrendr - Temporal segmentation algorithms”. *Remote Sensing of Environment* 114.12, 2897–2910. DOI: 10.1016/j.rse.2010.07.008.
- Kim, H. G., J. Roh, H. Lee, G. Kim, and S. Y. Lee (2015). “Active learning for large-scale object classification: From exploration to exploitation”. *HAI 2015 - Proceedings of the 3rd International Conference on Human-Agent Interaction*, 251–254. DOI: 10.1145/2814940.2814989.
- Kim, O. S. (2010). “An Assessment of Deforestation Models for Reducing Emissions from Deforestation and Forest Degradation (REDD)”. *Transactions in GIS* 14.5, 631–654. DOI: 10.1111/j.1467-9671.2010.01227.x.
- Kit, O. and M. Lüdeke (2013). “Automated detection of slum area change in Hyderabad , India using multitemporal satellite imagery”. *ISPRS Journal of Photogrammetry and Remote Sensing* 83, 130–137. DOI: 10.1016/j.isprsjprs.2013.06.009.
- Kleinschroth, F., N. Laporte, W. F. Laurance, S. J. Goetz, and J. Ghazoul (2019). “Road expansion and persistence in forests of the Congo Basin”. *Nature Sustainability* 2019 2:7 2.7, 628–634. DOI: 10.1038/s41893-019-0310-6.
- Koh, L. P., Y. Zeng, T. V. Sarira, and K. Siman (2021). “Carbon prospecting in tropical forests for climate change mitigation”. *Nature Communications* 2021 12:1 12.1, 1–9. DOI: 10.1038/s41467-021-21560-2.

- Kong, Y.-L., Q. Huang, C. Wang, J. Chen, J. Chen, and D. He (2018). “Long Short-Term Memory Neural Networks for Online Disturbance Detection in Satellite Image Time Series”. *Remote Sensing* 10, 13. DOI: 10.3390/rs10030452.
- Kouassi, J.-L., A. Gyau, L. Diby, Y. Bene, and C. Kouamé (2021). *Assessing Land Use and Land Cover Change and Farmers’ Perceptions of Deforestation and Land Degradation in South-West Côte d’Ivoire, West Africa*. DOI: 10.3390/land10040429.
- Kroeger, A., H. Bakhtary, F. Haupt, and C. Streck (2017). *Eliminating deforestation from the cocoa supply chain*.
- Kumar, S., R. Krishna, R. Shiv, and B. B. Dubey (2019). “HybridSN: Exploring 3D-2D CNN Feature Hierarchy for Hyperspectral Image Classification”. *IEEE Geoscience and Remote Sensing Letters*. DOI: 10.1109/LGRS.2019.2918719.
- Lambin, E. F., H. K. Gibbs, R. Heilmayr, K. M. Carlson, L. C. Fleck, R. D. Garrett, Y. Le Polain De Waroux, C. L. McDermott, D. McLaughlin, P. Newton, C. Nolte, P. Pacheco, L. L. Rausch, C. Streck, T. Thorlakson, and N. F. Walker (2018). “The role of supply-chain initiatives in reducing deforestation”. *Nature Climate Change* 2018 8:2 8.2, 109–116. DOI: 10.1038/s41558-017-0061-1.
- Latawiec, A. and D. Agol (2015). *Sustainability Indicators in Practice*. Ed. by M. Golachowska-Poleszczuk and A. Topolska. Warsaw/Berlin: De Gruyter Open Ltd, 1–271.
- Lecun, Y., Y. Bengio, and G. Hinton (2015). “Deep learning”. *Nature* 521.7553, 436–444. DOI: 10.1038/nature14539.
- Lemenih, M. and H. Kassa (2014). “Re-Greening Ethiopia: History, Challenges and Lessons”. *Forests* 2014, Vol. 5, Pages 1896-1909 5.8, 1896–1909. DOI: 10.3390/F5081896.
- Li, Y., H. Zhang, and Q. Shen (2017). “Spectral–Spatial Classification of Hyperspectral Imagery with 3D Convolutional Neural Network”. *Remote Sensing* 9.1, 67. DOI: 10.3390/rs9010067.
- Li, Z., H. Bagan, and Y. Yamagata (2018). “Analysis of spatiotemporal land cover changes in Inner Mongolia using self-organizing map neural network and grid cells method”. *Science of the Total Environment* 636, 1180–1191. DOI: 10.1016/j.scitotenv.2018.04.361.
- Liu, X., C. Kang, L. Gong, and Y. Liu (2016). “Incorporating spatial interaction patterns in classifying and understanding urban land use”. *International Journal of Geographical Information Science* 30.2, 334–350. DOI: 10.1080/13658816.2015.1086923.
- Lu, D. (2007). “The potential and challenge of remote sensing-based biomass estimation”. <http://dx.doi.org/10.1080/01431160500486732> 27.7, 1297–1328. DOI: 10.1080/01431160500486732.
- Lu, D., P. Mausel, E. Brondízio, and E. Moran (2004). “Relationships between forest stand parameters and Landsat TM spectral responses in the Brazilian Amazon Basin”. *Forest Ecology and Management* 198.1-3, 149–167. DOI: 10.1016/j.foreco.2004.03.048.

- Luus, F. P., B. P. Salmon, F. Van Den Bergh, and B. T. Maharaj (2015). "Multiview Deep Learning for Land-Use Classification". *IEEE Geoscience and Remote Sensing Letters* 12.12, 2448–2452. DOI: 10.1109/LGRS.2015.2483680.
- Ma, L., Y. Liu, X. Zhang, Y. Ye, G. Yin, and B. A. Johnson (2019). *Deep learning in remote sensing applications: A meta-analysis and review*. DOI: 10.1016/j.isprsjprs.2019.04.015.
- Ma, T., J. Ge, and J. Wang (2011). "Combining active learning and semi-supervised for improving learning performance". *ACM International Conference Proceeding Series*. DOI: 10.1145/2093698.2093871.
- Marmanis, D., M. Datcu, T. Esch, and U. Stilla (2016). "Deep learning earth observation classification using ImageNet pretrained networks". *IEEE Geoscience and Remote Sensing Letters* 13.1, 105–109. DOI: 10.1109/LGRS.2015.2499239.
- Mas, J.-f., R. Lemoine-rodríguez, R. González-lópez, A. Piña-garduño, and E. Herrera-flores (2017). "Land use / land cover change detection combining automatic processing and visual interpretation". *European Journal of Remote Sensing* 50.1, 626–635. DOI: 10.1080/22797254.2017.1387505.
- Masolele, R. N., V. De Sy, M. Herold, D. Marcos Gonzalez, J. Verbesselt, F. Gieseke, A. G. Mullissa, and C. Martius (2021). "Spatial and temporal deep learning methods for deriving land-use following deforestation: A pan-tropical case study using Landsat time series". *Remote Sensing of Environment* 264, 112600. DOI: 10.1016/J.RSE.2021.112600.
- Masolele, R. N., V. D. Sy, D. Marcos, J. Verbesselt, F. Gieseke, K. A. Mulatu, Y. Moges, H. Sebrala, C. Martius, and M. Herold (2022). "Using high-resolution imagery and deep learning to classify land-use following deforestation: a case study in Ethiopia". *GIScience & Remote Sensing* 59.1, 1446–1472. DOI: 10.1080/15481603.2022.2115619.
- McKinley, D. C., A. J. Miller-Rushing, H. L. Ballard, R. Bonney, H. Brown, S. C. Cook-Patton, D. M. Evans, R. A. French, J. K. Parrish, T. B. Phillips, S. F. Ryan, L. A. Shanley, J. L. Shirk, K. F. Stepenuck, J. F. Weltzin, A. Wiggins, O. D. Boyle, R. D. Briggs, S. F. Chapin, D. A. Hewitt, P. W. Preuss, and M. A. Soukup (2017). "Citizen science can improve conservation science, natural resource management, and environmental protection". *Biological Conservation* 208, 15–28. DOI: 10.1016/J.BIOCON.2016.05.015.
- Meng, R., J. Wu, K. L. Schwager, F. Zhao, P. E. Dennison, B. D. Cook, K. Brewster, T. M. Green, and S. P. Serbin (2017). "Using high spatial resolution satellite imagery to map forest burn severity across spatial scales in a Pine Barrens ecosystem". *Remote Sensing of Environment* 191, 95–109. DOI: 10.1016/J.RSE.2017.01.016.
- Mengist, W., T. Soromessa, and G. L. Feyisa (2021). "Monitoring Afromontane forest cover loss and the associated socio-ecological drivers in Kaffa biosphere reserve, Ethiopia". *Trees, Forests and People* 6, 100161. DOI: 10.1016/J.TFP.2021.100161.

- Minh, D. H. T., D. Ienco, R. Gaetano, N. Lalande, E. Ndikumana, F. Osman, and P. Maurel (2018). “Deep Recurrent Neural Networks for Winter Vegetation Quality Mapping via Multitemporal SAR Sentinel-1”. *IEEE Geoscience and Remote Sensing Letters* January, 6. DOI: 10.1109/LGRS.2018.2794581.
- Ministry of Mines and Petroleum (2021). *Ethiopia Mining Cadastre eGov Portal – Trimble Landfolio - Cadastre Map*.
- Monteiro, F., L. Catarino, D. Batista, B. Indjai, M. C. Duarte, and M. M. Romeiras (2017). “Cashew as a High Agricultural Commodity in West Africa: Insights towards Sustainable Production in Guinea-Bissau”. *Sustainability 2017, Vol. 9, Page 1666* 9.9, 1666. DOI: 10.3390/SU9091666.
- Moran, D., S. Giljum, K. Kanemoto, and J. Godar (2020). “From Satellite to Supply Chain: New Approaches Connect Earth Observation to Economic Decisions”. *One Earth* 3.1, 5–8. DOI: 10.1016/J.ONEEAR.2020.06.007.
- Moriconi-Ebrard, F., D. Harre, and P. Heinrigs (2016). “Urbanisation Dynamics in West Africa 1950–2010”. *OECD. West African Studies*. DOI: 10.1787/9789264252233-EN.
- Moser, C. (2008). “An economic analysis of deforestation in Madagascar in the 1990s”. *Environmental Sciences* 5.2, 91–108. DOI: 10.1080/15693430801912170.
- Müller, H., P. Rufin, P. Griffiths, A. J. Barros Siqueira, and P. Hostert (2015). “Mining dense Landsat time series for separating cropland and pasture in a heterogeneous Brazilian savanna landscape”. *Remote Sensing of Environment* 156, 490–499. DOI: 10.1016/j.rse.2014.10.014.
- Mutanga, O., E. Adam, and M. A. Cho (2012). “High density biomass estimation for wetland vegetation using worldview-2 imagery and random forest regression algorithm”. *International Journal of Applied Earth Observation and Geoinformation* 18.1, 399–406. DOI: 10.1016/j.jag.2012.03.012.
- Nackoney, J., G. Molinario, P. Potapov, S. Turubanova, M. C. Hansen, and T. Furuichi (2014). “Impacts of civil conflict on primary forest habitat in northern Democratic Republic of the Congo, 1990–2010”. *Biological Conservation* 170, 321–328. DOI: <https://doi.org/10.1016/j.biocon.2013.12.033>.
- Neagoe, V. E., M. Neghina, and M. Datcu (2012). “Neural network techniques for automated land-cover change detection in multispectral satellite time series imagery”. *International Journal of Mathematical Models and Methods in Applied Sciences* 6.1, 130–139.
- NGIS (2022). *European Parliament pass bill to ban imports of deforestation-linked commodities*.
- Nguyen, L. H., D. R. Joshi, D. E. Clay, and M. Henebry (2018). “Characterizing land cover / land use from multiple years of Landsat and MODIS time series : A novel approach

- using land surface phenology modeling and random forest classifier”. *Remote Sensing of Environment* December. DOI: 10.1016/j.rse.2018.12.016.
- NICFI (2021). *NICFI Program - Satellite Imagery and Monitoring — Planet*.
- Nomura, K., E. T. Mitchard, S. J. Bowers, and G. Patenaude (2019). “Missed carbon emissions from forests: Comparing countries’ estimates submitted to UNFCCC to biophysical estimates”. *Environmental Research Letters* 14.2. DOI: 10.1088/1748-9326/AAFC6B.
- Nowak, D. J., S. Hirabayashi, A. Bodine, and E. Greenfield (2014). “Tree and forest effects on air quality and human health in the United States”. *Environmental Pollution* 193, 119–129. DOI: 10.1016/J.ENVPOL.2014.05.028.
- Oehmcke, S., C. Thrysøe, A. Borgstad, M. Antonio, V. Salles, M. Brandt, and F. Gieseke (2019). “Detecting Hardly Visible Roads in Low-Resolution Satellite Time Series Data”. In: *2019 IEEE International Conference on Big Data*. Los Angeles: IEEE. DOI: 10.1109/BigData47090.2019.9006251.
- Oktay, O., J. Schlemper, L. L. Folgoc, M. Lee, M. Heinrich, K. Misawa, K. Mori, S. McDonagh, N. Y. Hammerla, B. Kainz, B. Glocker, and D. Rueckert (2018). “Attention U-Net: Learning Where to Look for the Pancreas”. In: *1st Conference on Medical Imaging with Deep Learning (MIDL 2018)*. Amsterdam.
- Olofsson, P., G. M. Foody, M. Herold, S. V. Stehman, C. E. Woodcock, and M. A. Wulder (2014). *Good practices for estimating area and assessing accuracy of land change*. DOI: 10.1016/j.rse.2014.02.015.
- Olofsson, P., S. V. Stehman, C. E. Woodcock, D. Sulla-Menashe, A. M. Sibley, J. D. Newell, M. A. Friedl, and M. Herold (2012). “A global land-cover validation data set, part I: fundamental design principles”. *International Journal of Remote Sensing* 33.18, 5768–5788. DOI: 10.1080/01431161.2012.674230.
- Pan, W., H. Narasimhan, P. Protopapas, P. Kar, and H. G. Ramaswamy (2017). “Optimizing the Multiclass F-measure via Biconcave Programming”. In: *2016 IEEE 16th International Conference on Data Mining (ICDM)*. Barcelona: IEEE. DOI: 10.1109/ICDM.2016.0143.
- Pandey, B., Q. Zhang, and K. C. Seto (2018). “Time series analysis of satellite data to characterize multiple land use transitions : a case study of urban growth and agricultural land loss in India”. *Journal of Land Use Science* 13.3, 221–237. DOI: 10.1080/1747423X.2018.1533042.
- Patay, É. B., T. Bencsik, and N. Papp (2016). “Phytochemical overview and medicinal importance of Coffea species from the past until now”. *Asian Pacific Journal of Tropical Medicine* 9.12, 1127–1135. DOI: 10.1016/J.APJTM.2016.11.008.
- Pelletier, C., G. I. Webb, and F. Petitjean (2019). “Temporal Convolutional Neural Network for the Classification of Satellite Image Time Series”. *Remote Sensing* March 2017, 1–22.

- Pendrill, F., T. A. Gardner, P. Meyfroidt, U. M. Persson, J. Adams, T. Azevedo, M. G. B. Lima, M. Baumann, P. G. Curtis, V. D. Sy, R. Garrett, J. Godar, E. D. Goldman, M. C. Hansen, R. Heilmayr, M. Herold, T. Kuemmerle, M. J. Lathuillière, V. Ribeiro, A. Tyukavina, M. J. Weisse, and C. West (2022). “Disentangling the numbers behind agriculture-driven tropical deforestation”. *Science* 377.6611. DOI: 10.1126/SCIENCE.ABM9267.
- Pengra, B., J. Long, D. Dahal, S. V. Stehman, and T. R. Loveland (2015). “A global reference database from very high resolution commercial satellite data and methodology for application to Landsat derived 30m continuous field tree cover data”. *Remote Sensing of Environment* 165, 234–248. DOI: 10.1016/j.rse.2015.01.018.
- Potapov, P., X. Li, A. Hernandez-Serna, A. Tyukavina, M. C. Hansen, A. Kommareddy, A. Pickens, S. Turubanova, H. Tang, C. E. Silva, J. Armston, R. Dubayah, J. B. Blair, and M. Hofton (2021). “Mapping global forest canopy height through integration of GEDI and Landsat data”. *Remote Sensing of Environment* 253, 112165. DOI: 10.1016/J.RSE.2020.112165.
- PyPI (2022). *spatial-kde · PyPI*.
- Quarrey, P., M. B. Setrana, and C. A. Tagoe (2020). *Migration in West and North Africa and across the Mediterranean - Chapter 21*.
- Rawat, S., A. L. Chandra, S. V. Desai, V. N. Balasubramanian, S. Ninomiya, and W. Guo (2022). “How Useful Is Image-Based Active Learning for Plant Organ Segmentation?” *Plant Phenomics* 2022. DOI: 10.34133/2022/9795275.
- RCMRD (2018). *Ethiopia Sentinel2 Land Use Land Cover 2016 — GeoNode*.
- UN-REDD (2017). *Annual Report 2017 — UNREDD*. Tech. rep. United Nations.
- Reiche, J., E. Hamunyela, J. Verbesselt, D. Hoekman, and M. Herold (2018). “Improving near-real time deforestation monitoring in tropical dry forests by combining dense Sentinel-1 time series with Landsat and ALOS-2 PALSAR-2”. *Remote Sensing of Environment* 204, 147–161. DOI: 10.1016/J.RSE.2017.10.034.
- Reiche, J., A. Mullissa, B. Slagter, Y. Gou, N.-E. Tsendbazar, C. Odongo-Braun, A. Vollrath, M. J. Weisse, F. Stolle, A. Pickens, G. Donchyts, N. Clinton, N. Gorelick, and M. Herold (2021). “Forest disturbance alerts for the Congo Basin using Sentinel-1”. *Environ. Res. Lett* 16, 24005. DOI: 10.1088/1748-9326/abd0a8.
- Reichstein, M., G. Camps-Valls, B. Stevens, M. Jung, J. Denzler, N. Carvalhais, and. Prabhat (2019). “Deep learning and process understanding for data-driven Earth system science”. *Nature* 566, 204. DOI: 10.1038/s41586-019-0912-1.
- Roessler, P., Y. I. Pengl, R. Marty, K. S. Titlow, and N. van de Walle (2022). “The cash crop revolution, colonialism and economic reorganization in Africa”. *World Development* 158. DOI: 10.1016/j.worlddev.2022.105934.

- Ronneberger, O., P. Fischer, and T. Brox (2015). “U-Net: Convolutional Networks for Biomedical Image Segmentation”. In: *Medical Image Computing and Computer-Assisted Intervention – MICCAI 2015. MICCAI 2015. Lecture Notes in Computer Science*. Ed. by N. Navab, J. Hornegger, W. Wells, and A. Frangi. Vol. 9351. Springer, Cham, 234–241. DOI: 10.1007/978-3-319-24574-4_{_}28.
- (n.d.). “U-Net: Convolutional Networks for Biomedical Image Segmentation” (), 1–8.
- Rosen, P. A., Y. Kim, R. Kumar, T. Misra, R. Bhan, and V. R. Sagi (2017). “Global persistent SAR sampling with the NASA-ISRO SAR (NISAR) mission”. *2017 IEEE Radar Conference, RadarConf 2017*, 0410–0414. DOI: 10.1109/RADAR.2017.7944237.
- Rousset, G., M. Despinoy, K. Schindler, and M. Mangeas (2021). “Assessment of Deep Learning Techniques for Land Use Land Cover Classification in Southern New Caledonia”. *Remote Sensing 2021, Vol. 13, Page 2257* 13.12, 2257. DOI: 10.3390/RS13122257.
- Ruf, F. and F. Varlet (2017). “The myth of zero deforestation cocoa in Côte d’Ivoire”. *ETFRN News* 58, 86–92.
- Rußwurm, M. and M. Körner (2017). “Multi-temporal land cover classification with long short-term memory neural networks”. *International Archives of the Photogrammetry, Remote Sensing and Spatial Information Sciences - ISPRS Archives* 42.1W1, 551–558. DOI: 10.5194/isprs-archives-XLII-1-W1-551-2017.
- Rußwurm, M. and M. Körner (2018). “Multi-Temporal Land Cover Classification with Sequential Recurrent Encoders”. *ISPRS International Journal of Geo-Information* 7.128, 1–19. DOI: 10.3390/ijgi7040129.
- (2020). “Self-attention for raw optical Satellite Time Series Classification”. *ISPRS Journal of Photogrammetry and Remote Sensing* 169, 421–435. DOI: 10.1016/j.isprsjprs.2020.06.006.
- Rußwurm, M., S. Wang, M. Körner, and D. Lobell (2020). “Meta-Learning for Few-Shot Land Cover Classification”. In: *In Proceedings of the IEEE/CVF Conference on Computer Vision and Pattern Recognition Workshops*, 200–201.
- Sabas, B. Y. S., K. G. Danmo, K. A. T. Madeleine, and B. Jan (2020). “Cocoa Production and Forest Dynamics in Ivory Coast from 1985 to 2019”. *Land 2020, Vol. 9, Page 524* 9.12, 524. DOI: 10.3390/LAND9120524.
- Sandker, M., O. Carrillo, C. Leng, D. Lee, R. d’Annunzio, and J. Fox (2021). “The Importance of High-Quality Data for REDD+ Monitoring and Reporting”. *Forests 2021, Vol. 12, Page 99* 12.1, 99. DOI: 10.3390/F12010099.
- Sassen, M., A. van Soesbergen, A. P. Arnell, and E. Scott (2022). “Patterns of (future) environmental risks from cocoa expansion and intensification in West Africa call for context specific responses”. *Land Use Policy* 119, 106142. DOI: 10.1016/J.LANDUSEPOL.2022.106142.

- Schepaschenko, D., L. See, M. Lesiv, J. F. Bastin, D. Mollicone, N. E. Tsendbazar, L. Bastin, I. McCallum, J. C. Laso Bayas, A. Baklanov, C. Perger, M. Dürauer, and S. Fritz (2019). “Recent Advances in Forest Observation with Visual Interpretation of Very High-Resolution Imagery”. *Surveys in Geophysics* 40.4, 839–862. DOI: 10.1007/S10712-019-09533-Z.
- Schlemper, J., O. Oktay, M. Schaap, M. Heinrich, B. Kainz, B. Glocker, and D. Rueckert (2019). “Attention gated networks: Learning to leverage salient regions in medical images”. *Medical Image Analysis* 53, 197–207. DOI: 10.1016/J.MEDIA.2019.01.012.
- Shi, X., Z. Chen, H. Wang, D.-Y. Yeung, W.-K. Wong, W.-C. Woo, and H. Kong Observatory (2015). “Convolutional LSTM Network: A Machine Learning Approach for Precipitation Nowcasting”. In: *Proceedings of the 28th International Conference on Neural Information Processing Systems*, 802–810.
- Silva, A. L., D. S. Alves, and M. P. Ferreira (2018). “Landsat-Based Land Use Change Assessment in the Brazilian Atlantic Forest : Forest Transition and Sugarcane Expansion”. *Remote Sensing*, 20. DOI: 10.3390/rs10070996.
- Sirko, W., S. Kashubin, M. Ritter, A. Annkah, Y. Salah, E. Bouchareb, Y. Dauphin, D. Keyzers, M. Neumann, M. Cisse, and J. Quinn (2021). *Continental-Scale Building Detection from High Resolution Satellite Imagery*. Tech. rep. DOI: 10.48550/arxiv.2107.12283.
- Sisay, G., G. Gitima, M. Mersha, and W. G. Alemu (2021). “Assessment of land use land cover dynamics and its drivers in Bechet Watershed Upper Blue Nile Basin, Ethiopia”. *Remote Sensing Applications: Society and Environment* 24, 100648. DOI: 10.1016/J.RSASE.2021.100648.
- Song, A., J. Choi, Y. Han, and Y. Kim (2018). “Change Detection in Hyperspectral Images Using Recurrent 3D Fully Convolutional Networks”. *Remote Sensing*, 22. DOI: 10.3390/rs10111827.
- Sonter, L. J., D. Herrera, D. J. Barrett, G. L. Galford, C. J. Moran, and B. S. Soares-Filho (2017). “Mining drives extensive deforestation in the Brazilian Amazon”. *Nature Communications* 2017 8:1 8.1, 1–7. DOI: 10.1038/s41467-017-00557-w.
- Spracklen, B. D., M. Kalamandeen, D. Galbraith, E. Gloor, D. V. Spracklen, M. C. Hansen, P. V. Potapov, R. Moore, M. Hancher, S. A. Turubanova, A. Tyukavina, D. Thau, S. V. Stehman, S. J. Goetz, T. R. Loveland, A. Kommareddy, A. Egorov, L. Chini, C. O. Justice, and J. R. G. Townshend (2015). “A Global Analysis of Deforestation in Moist Tropical Forest Protected Areas”. *PLOS ONE* 10.12, e0143886. DOI: 10.1371/JOURNAL.PONE.0143886.
- Stévant, T., G. Dauby, P. Lowry, A. Blach-Overgaard, V. Droissart, D. J. Harris, A. B. Mackinder, G. E. Schatz, B. Sonké, M. S. Sosef, J. C. Svenning, J. Wieringa, and T. L. Couvreur (2019). “A third of the tropical African flora is potentially threatened with

- extinction”. *Science Advances* 5.11. DOI: 10.1126/SCIADV.AAX9444/SUPPL{_}FILE/AAX9444{_}SM.PDF.
- Stickler, C., A. E. Duchelle, D. Nepstad, and J. P. Ardila (n.d.). *Subnational jurisdictional approaches Policy innovation and partnerships for change Chapter 12*. Tech. rep.
- SURFsara (2022). *SURFsara (The Netherlands) — ESCAPE*.
- Tadese, S., T. Soromessa, and T. Bekele (2021). “Analysis of the Current and Future Prediction of Land Use/Land Cover Change Using Remote Sensing and the CA-Markov Model in Majang Forest Biosphere Reserves of Gambella, Southwestern Ethiopia”. *Scientific World Journal* 2021. DOI: 10.1155/2021/6685045.
- Tano, A. M. (2012). *Crise Cacaoyère et Stratégies des Producteurs de la Sous-Préfecture de Méadji au Sud-Ouest Ivoirien*.
- Tasar, O., Y. Tarabalka, and P. Alliez (2019). “Incremental Learning for Semantic Segmentation of Large-Scale Remote Sensing Data”. *IEEE Journal of Selected Topics in Applied Earth Observations and Remote Sensing* 12.9, 3524–3537. DOI: 10.1109/JSTARS.2019.2925416.
- Tewabe, D., T. Fentahun, and F. Li (2020). “Assessing land use and land cover change detection using remote sensing in the Lake Tana Basin, Northwest Ethiopia”. *Cogent Environmental Science* 6.6. DOI: 10.1080/23311843.2020.1778998.
- Tracewski, L., L. Bastin, C. C. Fonte, and F. Group (2017). “Repurposing a deep learning network to filter and classify volunteered photographs for land cover and land use characterization”. *Geo-spatial Information Science* 20.3, 252–268. DOI: 10.1080/10095020.2017.1373955.
- Tsendbazar, N., M. Herold, L. Li, A. Tarko, S. de Bruin, D. Masiliunas, M. Lesiv, S. Fritz, M. Buchhorn, B. Smets, R. Van De Kerchove, and M. Duerauer (2021). “Towards operational validation of annual global land cover maps”. *Remote Sensing of Environment* 266, 112686. DOI: 10.1016/J.RSE.2021.112686.
- Tseng, G., H. Kerner, C. Nakalembe, and I. Becker-Reshef (2021). “Learning to predict crop type from heterogeneous sparse labels using meta-learning”. In: *Proceedings of the IEEE/CVF Conference on Computer Vision and Pattern Recognition (CVPR) Workshops*, 1111–1120. DOI: 10.5281/zenodo.4680394.
- Tuntiwachiratrakun, P. and P. Vateekul (2017). “Applying active learning strategy to classify large scale data with imbalanced classes”. *2016 International Conference on Control, Automation and Information Sciences, ICCAIS 2016*, 100–105. DOI: 10.1109/ICCAIS.2016.7822443.
- Tyukavina, A., M. C. Hansen, P. Potapov, D. Parker, C. Okpa, S. V. Stehman, I. Komareddy, and S. Turubanova (2018). “Congo Basin forest loss dominated by increasing smallholder clearing”. November.

- Uba, N. K. (2016). “Land Use and Land Cover Classification Using Deep Learning Techniques”. PhD thesis. ARIZONA STATE UNIVERSITY, 53.
- UNEP-WCMC (2020). *Cote d Ivoire - Country overview to aid implementation of the EU Timber Regulation (EUTR)*.
- UNEP-WCMC and IUCN (2022). *Protected Planet: The World Database on Protected Areas (WDPA) and World Database on Other Effective Area-based Conservation Measures (WD-OECM) [Online]*, November 2022, Cambridge, UK: UNEP-WCMC and IUCN.
- UNFCCC (2017). *UN Climate change: Annual Report 2017*. Tech. rep. Bonn: United Nations Framework Convention on Climate Change, 52.
- (2018). *The Katowice Climate Package: Making The Paris Agreement Work For All — UNFCCC*.
- (2021). *Nationally determined contributions under the Paris Agreement*. Tech. rep. Glasgow: United Nations.
- USDA (2017). *8-Day MODIS NDVI*.
- Verbesselt, J., R. Hyndman, G. Newnham, and D. Culvenor (2010a). “Detecting trend and seasonal changes in satellite image time series”. *Remote Sensing of Environment* 114.1, 106–115. DOI: 10.1016/j.rse.2009.08.014.
- (2010b). “Detecting trend and seasonal changes in satellite image time series”. *Remote Sensing of Environment* 114.1, 106–115. DOI: 10.1016/j.rse.2009.08.014.
- Verma, D. and A. Jana (2020). “LULC classification methodology based on simple Convolutional Neural Network to map complex urban forms at finer scale: Evidence from Mumbai”. DOI: 10.48550/arxiv.1909.09774.
- Vogelmann, J. E., G. Xian, C. Homer, and B. Tolck (2012). “Monitoring gradual ecosystem change using Landsat time series analyses: Case studies in selected forest and rangeland ecosystems”. *Remote Sensing of Environment* 122, 92–105. DOI: 10.1016/j.rse.2011.06.027.
- Wang, H., X. Zhao, X. Zhang, D. Wu, and X. Du (2019). “Long Time Series Land Cover Classification in China from 1982 to 2015 Based on Bi-LSTM Deep Learning”. *Remote Sensing* 11.14, 1639. DOI: 10.3390/rs11141639.
- Wang, K., D. Zhang, Y. Li, R. Zhang, and L. Lin (2017). “Cost-Effective Active Learning for Deep Image Classification”. *IEEE Transactions on Circuits and Systems for Video Technology* 27.12, 2591–2600. DOI: 10.1109/TCSVT.2016.2589879.
- Wang, Y., Z. Zhang, L. Feng, Y. Ma, and Q. Du (2021). “A new attention-based CNN approach for crop mapping using time series Sentinel-2 images”. *Computers and Electronics in Agriculture* 184, 106090. DOI: 10.1016/J.COMPAG.2021.106090.
- WCF (2015). “Wild Chimpanzee Foundation. Rapport de mission d’observation indépendante mandatee: Rapport 2: Blocs 18 et 6 - Novembre 2014/Juillet 2015.”

- World Resources Institute (2016). *INSIDER: Global Forest Watch and the Forest Resources Assessment, Explained in 5 Graphics* — World Resources Institute.
- WRI (2017). *Kenya GIS Data* — World Resources Institute.
- Wu, J., V. S. Sheng, J. Zhang, P. Zhao, and Z. Cui (2014). “Multi-label active learning for image classification”. *2014 IEEE International Conference on Image Processing, ICIP 2014*, 5227–5231. DOI: 10.1109/ICIP.2014.7026058.
- Wynants, M., C. Kelly, K. Mtei, L. Munishi, A. Patrick, A. Rabinovich, M. Nasser, D. Gilvear, N. Roberts, P. Boeckx, G. Wilson, W. H. Blake, and P. Ndakidemi (2019). “Drivers of increased soil erosion in East Africa’s agro-pastoral systems: changing interactions between the social, economic and natural domains”. *Regional Environmental Change* 19.7, 1909–1921. DOI: 10.1007/s10113-019-01520-9/FIGURES/2.
- Xu, Z., K. Guan, N. Casler, B. Peng, and S. Wang (2018). “A 3D convolutional neural network method for land cover classification using LiDAR and multi-temporal Landsat imagery”. *ISPRS Journal of Photogrammetry and Remote Sensing* 144, 423–434. DOI: 10.1016/j.isprsjprs.2018.08.005.
- Yahya, N., T. Bekele, O. Gardi, and J. Blaser (2020). “Forest cover dynamics and its drivers of the Arba Gugu forest in the Eastern highlands of Ethiopia during 1986 – 2015”. *Remote Sensing Applications: Society and Environment* 20, 100378. DOI: 10.1016/J.RSASE.2020.100378.
- Yanai, R. D., C. Wayson, D. Lee, A. B. Espejo, J. L. Campbell, M. B. Green, J. M. Zuskewitz, S. B. Yoffe, J. E. Aukema, A. J. Lister, J. W. Kirchner, and J. G. Gamarra (2020). “Improving uncertainty in forest carbon accounting for REDD+ mitigation efforts”. *Environmental Research Letters* 15.12, 124002. DOI: 10.1088/1748-9326/ABB96F.
- Yang, R., S. K. Singh, M. Tavakkoli, N. Amiri, Y. Yang, M. A. Karami, and R. Rai (2020). “CNN-LSTM deep learning architecture for computer vision-based modal frequency detection”. *Mechanical Systems and Signal Processing* 144, 106885. DOI: 10.1016/j.ymsp.2020.106885.
- Ye, S., J. Rogan, Z. Zhu, and J. R. Eastman (2021). “A near-real-time approach for monitoring forest disturbance using Landsat time series: stochastic continuous change detection”. *Remote Sensing of Environment* 252, 112167. DOI: 10.1016/J.RSE.2020.112167.
- Yuan, Q., H. Shen, T. Li, Z. Li, S. Li, Y. Jiang, H. Xu, W. Tan, Q. Yang, J. Wang, J. Gao, and L. Zhang (2020). “Deep learning in environmental remote sensing: Achievements and challenges”. *Remote Sensing of Environment* 241, 111716. DOI: 10.1016/j.rse.2020.111716.
- Zeng, Z., L. Estes, A. D. Ziegler, A. Chen, T. Searchinger, F. Hua, K. Guan, A. Jintrawet, and E. F. Wood (2018). “Highland cropland expansion and forest loss in Southeast Asia in the twenty-first century”. *Nature Geoscience* 2018 11:8 11.8, 556–562. DOI: 10.1038/s41561-018-0166-9.

- Zewdie, W. and E. Csaplovics (2017). “European Journal of Remote Sensing Remote Sensing based multi-temporal land cover classification and change detection in north-western Ethiopia”. *European Journal of Remote Sensing* 48.1, 121–139. DOI: 10.5721/EuJRS20154808.
- Zhang, C., I. Sargent, X. Pan, H. Li, A. Gardiner, J. Hare, and P. M. Atkinson (2019). “Joint Deep Learning for land cover and land use classification”. *Remote Sensing of Environment* 221.May 2018, 173–187. DOI: 10.1016/j.rse.2018.11.014.
- Zhang, X., L. Du, S. Tan, F. Wu, L. Zhu, Y. Zeng, and B. Wu (2021). “Land Use and Land Cover Mapping Using RapidEye Imagery Based on a Novel Band Attention Deep Learning Method in the Three Gorges Reservoir Area”. *Remote Sensing 2021, Vol. 13, Page 1225* 13.6, 1225. DOI: 10.3390/RS13061225.
- Zhao, B., B. Huang, and Y. Zhong (2017). “Transfer Learning with Fully Pretrained Deep Convolution Networks for Land-Use Classification”. *IEEE Geoscience and Remote Sensing Letters* 14.9, 1436–1440. DOI: 10.1109/LGRS.2017.2691013.
- Zhao, F., R. Sun, L. Zhong, R. Meng, C. Huang, X. Zeng, M. Wang, Y. Li, and Z. Wang (2022). “Monthly mapping of forest harvesting using dense time series Sentinel-1 SAR imagery and deep learning”. *Remote Sensing of Environment* 269, 112822. DOI: 10.1016/J.RSE.2021.112822.
- Zhao, W. and S. Du (2016). “Learning multiscale and deep representations for classifying remotely sensed imagery”. *ISPRS Journal of Photogrammetry and Remote Sensing* 113, 155–165. DOI: 10.1016/j.isprsjprs.2016.01.004.
- Zhao, Y., K. Zhang, Y. Fu, and H. Zhang (2012). “Examining Land-Use / Land-Cover Change in the Lake Dianchi Watershed of the Yunnan-Guizhou Plateau of Southwest China with Remote Sensing and GIS Techniques : 1974 – 2008”, 3843–3865. DOI: 10.3390/ijerph9113843.
- Zhong, L., L. Hu, and H. Zhou (2019). “Deep learning based multi-temporal crop classification”. *Remote Sensing of Environment* 221.December 2018, 430–443. DOI: 10.1016/j.rse.2018.11.032.
- Zhu, J., H. Chen, and W. Ye (2020). “A Hybrid CNN-LSTM Network for the Classification of Human Activities Based on Micro-Doppler Radar”. *IEEE Access* 8, 24713–24720. DOI: 10.1109/ACCESS.2020.2971064.
- Zhu, X. X., D. Tuia, L. Mou, G.-S. Xia, L. Zhang, F. Xu, and F. Fraundorfer (2017). “Deep Learning in Remote Sensing: A Comprehensive Review and List of Resources”. *IEEE Geoscience and Remote Sensing Magazine* 5.4, 8–36. DOI: 10.1109/MGRS.2017.2762307.

Acknowledgements

A PhD is a Journey with many facets. This journey would not have been possible without the contributions and support of the following people.

First and foremost, I'd like to thank my promotor, Martin Herold, for giving me the opportunity to work on this project with you, and for providing inspiration and guidance over the past four years. I appreciate that you were open to ideas from my side and from each other, and that I had a lot of freedom in developing and carrying out my research, as well as support in showcasing my research outside of the geoinformation science and remote sensing laboratory.

I would also like to thank my supervisors, Niki, Diego, Jan, and Christopher, for all of their help and advice throughout my Ph.D. journey. Niki, thank you for your invaluable advice, unwavering support, and patience throughout my Ph.D. studies. Your vast knowledge and wealth of experience on my Ph.D. research topic, particularly land-use and deforestation, have always inspired me in both my academic work and daily life. Diego and Jan, thank you for your technical assistance with my research. Your advice and support were extremely helpful in shaping my experiment methods and critiquing my results. What's more, Diego, you were always available for impromptu questions and discussions about work and life in general. Without your quick input and suggestions, I might not have considered some of the analyses present in the thesis today. Christopher, I appreciated your detailed feedback on my manuscripts and as well as your criticism of the importance of making the manuscript readable to a broader audience, including non-experts in remote sensing and deep learning.

To continue the round, I'd like to thank my co-authors Fabian Gieseke, Heiru Sebrala Ahmed, Atmadja Stibniati, Nandika Tsendbar, Mathieu Decuyper, Kalkidan Ayele Mulatu, Christopher Martius, and Yitebitu Moges for providing me with critical inputs and support in either of the Chapters in the PhD projects discussion cycles. There are never enough eyes to see all aspects of a project, and having support in the form I did was a major pillar in realizing all of my work during my PhD iteration.

A special thanks to my paranymphs, Daniela and Bart. Daniela, when I first came to Wageningen, you were always my first contact person for questions related to CIFOR and

life in Wageningen. You made me feel welcome. Bart thanks for all the chit-chat during the coffee breaks and the exchange on the research on near-real-time tracking of drivers of deforestation. Above all, thank you for agreeing to be my first point of contact and backup during my PhD defence.

I would also like to thank and acknowledge my opponents for selflessly investing the time and effort to assess this thesis and for their participation in the Ph.D. defence. My special thanks go to every colleague of the GRS group. Doing a PhD in this group has given me the gratification of working alongside a diverse research group. I am content with the activities outside academia, especially the warm receptions and Christmas dinners. I do recognize and appreciate the tea breaks and outings we had together. Thus, I would like to thank Aldo, Alex, Alexander, Arend, Arnan, Arnold, Arun, Benjamin B., Benjamin K., Carmelo, Charles, Chenglong, Christelle, Corne, Dainius, David, Deborah, Devis, Dilli, Elina, Elise, Erika R., Erika S., Federico, Frida, George, , Gonzalo, Gustavo, Harm, Hasib, Hiske, Hilmy, Ilan, Ioannis, Jaap-Willem, Jan C., Jens, Joao, Johannes, John, Jose, Judith, Julia, Jiayan, Jingye, Juul, Karimon, Karina, Lala, Laura, Layla, Lammert, Lili, Linlin, Lisa, Lukasz, Magdalena, Marcello, Marian, Martijn, Michiel, Milutin, Mirt-Andrei, Myke, Na, Nandika, Natalia, Ovidiu, Panpan, Patric, Paulo, Peter R., Peter V., Qijun, Quanxing, Ron, Sabina, Sebastian, Simon, Sytze, Sietse, Tom, Ximena, Yang, Yaqing, Yunyu, and anybody that I might not have mentioned here. To MSc students Elisha and Hugo, I learned a lot and enjoyed supervising your MSc research. Thanks for allowing me to share and exchange knowledge with you. Gerlinde, Antoinette, and Truus, many thanks for your pre-eminent support during the Ph.D. years.

Finally, I would like to thank my family for their encouragement and sempiternal support. My father, Thomas, and my mother, Avila, thank you for guiding me to shape my life with positivity and passion. Without you, I'd never be the person I am today. My siblings Pelegi, Samsoni, Majaliwa, Hezrom, Rahabu, Rachel, and Abeid, many thanks for always being there for me. I am fond of our funny or serious conversations online and in real life. You know me well, and I am very fortunate you are always available to help me when needed. My wife Janeth, we met on my very first day as a student at kitangiri secondary school, and we have been together since. You have been an indispensable best friend. Although not always physically together. Living far apart made us endure many ups and downs in our life adventures. But through all that, we learned to support and complement each other. Thank you for always being there for me and for supporting my work while living abroad. My kids Hellen, Hendrick, and Hollie, I love you. Thank you always for believing in me and taking care of your mom. Although I wasn't physically with you most of the time, it's the memory of all the funny moments, dances, talks, hugs, and kisses in video calls and when I am at home that keeps me going and smiling. I am thankful and blessed to have you as my family.

Asanteni sana.

About the author



Robert Masolele was born on 25 July 1987 in Geita, Tanzania. He grew up in Mwanza region, where he attended secondary education at Kitangiri secondary school. He later joined high school at Tarime secondary school in Mara District, where he majored in physics, chemistry, and biology with a minor in mathematics and general studies. Following his interest in nature, and the environment, in 2012, Robert moved to Morogoro region, Tanza-

nia, where he pursued his BSc in Forestry at Sokoine University of Agriculture. He became interested in various subjects, including silviculture, remote sensing and geoinformation science, forest engineering, forest inventory, forest management, biodiversity, and computer science. In 2015 while doing fieldwork on forest inventory with traditional tools, he realized that his work might have been a lot easier if he could do the same amount of work remotely and much faster. From that moment, he fell in love with the prospect of using remote sensing and computer algorithms for forest management and monitoring. In 2016, Robert started his MSc in Remote Sensing and Geoinformation Science at ITC Faculty Geo-Information Science and Earth Observation, University of Twente, the Netherlands, focusing on Natural resource management. For his MSc thesis, he used ALOS-2 PALSAR-2 L-band cross-polarised radar data to model above-ground biomass/carbon stock and carbon sequestration of tropical rainforest, Berkelah, Malaysia. After completing his MSc studies, Robert started his PhD research within the CIFOR global comparative study on REDD+ project of the Laboratory of geo-information science and remote sensing, Wageningen University, the Netherlands. His research focused on assessing land-use following tropical deforestation by combining remote sensing, deep learning, and cloud computing technologies. During his PhD, he enjoyed careful thinking about the highly mathematical parts of analyzing natural resource problems, particularly in tracking land-use change and dynamics using machine learning and deep learning algorithms. Following his PhD, Robert plans to continue his research with a Postdoctoral position at Wageningen University's

Radar group in the Laboratory of geo-information science and remote sensing. His research will focus on up-scaling the assessment of deforestation drivers at a global scale using deep learning and cloud computing, a knowledge gained during his PhD. He looks forward to more exciting research and more collaborations in the coming years.

Peer-reviewed Journal Publications

Masolele, R., V. D. Sy, M. Herold, D. M. Gonzalez, J. Verbesselt, F. Gieseke, A. Mullissa, and C. Martius (2021). “Spatial and temporal deep learning methods for deriving land-use following deforestation: A pan-tropical case study using Landsat time series”. *Remote Sensing of Environment* 264. DOI: 10.1016/j.rse.2021.112600.

Masolele, R. N., V. D. Sy, D. Marcos, J. Verbesselt, F. Gieseke, K. A. Mulatu, Y. Moges, H. Sebrala, C. Martius, and M. Herold (2022). “Using high-resolution imagery and deep learning to classify land-use following deforestation: a case study in Ethiopia”. *GIScience Remote Sensing* 59 (1), 1446–1472. DOI: 10.1080/15481603.2022.2115619.

Other Scientific Publications

Masolele, R. N., Y. A. Hussin, and D. E. H. Kloosterman (2018). *ALOS-2 PALSAR-2 L-band cross-polarized radar data analysis for modelling above-ground biomass/carbon stock and carbon sequestration of tropical rainforest, Berkelah, Malaysia.*

PE&RC Training and Education Statement

With the training and education activities listed below the PhD candidate has complied with the requirements set by the C.T. de Wit Graduate School for Production Ecology and Resource Conservation (PE&RC) which comprises of a minimum total of 32 ECTS (= 22 weeks of activities)



Writing of project proposal (4.5 ECTS)

- Assessment of land use change at national and subnational scales using remote sensing time series

Post-graduate courses (8.5 ECTS)

- Machine learning for spatial data; WUR-PE&RC (2019)
- Geocomputation using free and open source software; WUR-PE&RC (2019)
- Summer school ecosystem & land use change; KIT (2019)
- The OpenGeoHub Summer School; The OpenGeoHub Summer School (2020)

Invited review of (unpublished) journal manuscript (5 ECTS)

- Computers and Geosciences: Semi-supervised Label Propagation for Heterogeneous Remote Sensing Images Change Detection
- Ecological Informatics: Spatio-Temporal Stacked Neural Network for Plant Accession Classification from Time Series Image Sequences
- Method in ecology and evolution: Using deep convolutional neural networks to forecast spatial patterns of Amazonian deforestation
- Remote sensing of Environment: Harvesting the Landsat Archive using Deep Neural Networks: Comparison with traditional classifiers and multi-sensor benefits

- Remote sensing of Environment: Semantic segmentation of water bodies in very high-resolution satellite and aerial images

Competence strengthening / skills courses (4.8 ECTS)

- Scientific writing; WUR-WGS
- Scientific Integrity; WUR-WGS
- Project and Time Management; WUR-WGS
- Reviewing a Scientific Paper; WUR-WGS

PE&RC Seminars and the PE&RC weekend (1.5 ECTS)

- PE&RC first years edition (2019)
- PE&RC last years edition (2022)

Discussion groups / local seminars / other scientific meetings (6 ECTS)

- Webinar - Classifying direct drivers of forest loss with deep learning in Ethiopia. Organised by the Forest Resources Assessment Monitoring Directorate -Ethiopia (2022)
- Time series group meeting (2019-2021)
- Discussion Group – Climate – Forests - Food (2019)
- IKI-project meetings; IKI (2021-2022)

International symposia, workshops and conferences (4.7 ECTS)

- Living planet symposium; oral presentation (2022)
- ForestSAT; poster presentation (2022)

Lecturing / supervision of practical's / tutorials (2.1 ECTS)

- GRS-33806 Geo Scripting (2019)

Supervision of MSc students

- Mapping Natural and Plantation Forests in Africa: A case study of the Oil Palm in Ejisu-Juaben District of Ghana
- Flood Risk Mapping and Effects on livelihood in Ghana using Sentinel-1 data
- Assessing The Temporal Dynamics Of Drivers Of Deforestation With Deep Learning In Southern Nations, Nationalities, and Peoples' Region, Ethiopia

This research was carried out as part of CIFOR's Global Comparative Study on REDD+ (www.cifor.org/gcs). The research was mainly funded by the International Climate Initiative (IKI) of the German Federal Ministry for the Environment, Nature Conservation, Building and Nuclear Safety (BMUB) (Grant Agreement number 20.III.108). The other funding partners that have supported this research include the Norwegian Agency for Development Cooperation (Norad), and the CGIAR Research Program on Forests, Trees and Agroforestry (CRP-FTA) with financial support from the CGIAR Fund Donors. Also this research is funded by the European Commission Horizon Europe project "Open-Earth-Monitor" (Grant number 101059548), the European Commission H2020 REDD Copernicus project (Grant agreement number 821880), and the H2020 LANDSENSE project (Grant Agreement number 689812).

Financial support from Wageningen University for printing this thesis is gratefully acknowledged.

Cover design by Robert N. Masolele.

Printed by ProefschriftMaken.

